9-2006

Some Aspects of the Mechanical Response of PMR-15 Neat Resin at 288°C: Experiment and Modeling

Christina M. Falcone

SOME ASPECTS OF THE MECHANICAL RESPONSE OF PMR-15 NEAT RESIN AT 288^{o}C: EXPERIMENT AND MODELING

THESIS

Christina M. Falcone, 2nd Lt, USAF

AFIT/GAE/ENY/06-S03

DEPARTMENT OF THE AIR FORCE
AIR UNIVERSITY

AIR FORCE INSTITUTE OF TECHNOLOGY

Wright-Patterson Air Force Base, Ohio

The views expressed in this thesis are those of the author and do not reflect the official policy or position of the United States Air Force, Department of Defense, or the U.S. Government.

AFIT/GAE/ENY/06-S03

SOME ASPECTS OF THE MECHANICAL RESPONSE OF PMR-15 NEAT RESIN AT 288^{o}C: EXPERIMENT AND MODELING

THESIS

Presented to the Faculty

Department of Aeronautics and Astronautics

Graduate School of Engineering and Management

Air Force Institute of Technology

Air University

Air Education and Training Command

In Partial Fulfillment of the Requirements for the

Degree of Master of Science in Aeronautical Engineering

Christina M. Falcone, BS

2nd Lt, USAF

September 2006

AFIT/GAE/ENY/06-S03

SOME ASPECTS OF THE MECHANICAL RESPONSE OF PMR-15 NEAT RESIN AT 288^{o}C: EXPERIMENT AND MODELING

Christina M. Falcone, BS

2nd Lt, USAF

Approved:

/signed/	9/5/06
Dr. Marina Ruggles-Wrenn (Chairman)	Date
/signed/	9/1/06
Dr. Richard Hall (Member)	Date
/signed/	9/1/06
Dr. Greg Schoeppner (Member)	Date

Abstract

The mechanical response of PMR-15 neat resin was investigated at 288 °C. The effect of loading rate on monotonic stress-strain behavior was explored in monotonic tests at several constant stress rates. Considerable rate dependence was observed, especially on the unloading path. Effect of prior stress rate on creep behavior was evaluated in creep tests preceded by uninterrupted loading to a target stress where loading rate was changed from test to test. Creep response was dependent on the prior stress rate. Effect of loading history was studied in stepwise creep tests, where specimens were subjected to a constant stress rate loading followed by unloading to zero stress with intermittent creep periods during both loading and unloading. Comparison of creep strains accumulated during a stepwise creep test to those accumulated during creep preceded by uninterrupted loading indicate that the prior stress history affects the creep behavior. Negative creep as well as creep rate reversal was observed on the unloading path.

A nonlinear viscoelastic model (Schapery's formulation) was characterized using creep and recovery tests at 288 °C. The model was verified by comparing the predictions with experimental results obtained in monotonic loading/unloading tests and single-step as well as multi-step creep tests. The model qualitatively predicted creep response to single- and multi-step creep tests, including negative creep and creep rate reversal during unloading. However, predictions were not quantitatively accurate. The model was unable to accurately predict the recovery behavior and could not account for rate effects.

Acknowledgements

I would like to thank the following individuals for their assistance during the course of my work: my thesis advisor, Dr. Marina Ruggles-Wrenn, for always having an open door and providing constant guidance, Aaron Schinder for the efforts he put forth in creating and verifying Matlab code, Daniel Ryan for his flexibility in machining the specimens, Barry Page for his technical assistance with the lab equipment, Dr. Greg Schoeppner (AFRL/MLBCM), Dr. Charles Y-C Lee (AFOSR/NE), and Dr. Richard Hall (AFRL/MLBCM) for their sponsorship of my thesis, my fellow students for their companionship, my family for sustaining me, and to my husband for always supporting me.

Christina M. Falcone

Table of Contents

Page

List of Figures

Page

Page

Page

Page

List of Tables

Page

SOME ASPECTS OF THE MECHANICAL RESPONSE OF PMR-15 NEAT RESIN AT 288^{o}C: EXPERIMENT AND MODELING

I. Introduction

The aerospace industry's unrelenting drive for the advancement of aircraft performance simultaneously fuels the need for high performance structural materials. Composite materials stand at the forefront of this search as their high strength and stiffness to weight ratios offer numerous advantages over other materials. Composites materials are not a novel concept. Modern composite materials first played a substantial role in military applications with the inclusion of boron-reinforced epoxy composites in the skins of the U.S. Navy's F-14. While initially composite materials were only used in secondary structures, the evolution of aircraft design has already witnessed substantial advancements with the F-22 Raptor carrying 24% of its weight in thermoset composites.

Polymer matrix composites (PMCs) have been incorporated into aircraft structural components for many decades. In the 1980's, many low speed aircraft such as the Boeing 757 and McDonnell Douglas MD-80 series contained components made of epoxy resins reinforced with aramid, carbon, and E-glass fibers (9:36). While these composites met the requirements of the aforementioned aircraft, the epoxy resins were limited to operating temperatures below 130°C. Therefore, researchers sought out more aggressive

polymer systems that could withstand temperatures beyond that of the epoxy resins. The result was intense investigation of a group of polymers called polyimides which are recognized today as extremely stable and environmentally resistant polymer systems (30:477). Polyimides are appealing for their use as matrix resins for high-temperature composite applications due to their high toughness, high tensile strength, high modulus, and resistance to temperature and solvents (30:477). Current efforts focus on incorporating lightweight High Temperature Polymer Matrix Composites (HTPMCs) into engine or body parts of supersonic aircraft.

Prior to their use in advanced aerospace applications, however, the behavior of these advanced materials under a variety of loading conditions must be investigated and a predictive model must be developed and validated. Furthermore, the use of a composite material requires the ability to predict not only the composite's behavior, but the behavior of its constituents. For composites utilized primarily at high temperatures, it is therefore necessary to develop a predictive model for the behavior of the matrix resin at such temperatures in effort to predict the overall behavior of the composite itself. The present effort investigates the mechanical response of PMR-15, a polyimide neat resin. This research will focus on the use of an existing model to determine if it can be used to predict the behavior of the polymer neat resin. This task is a critical step in advancing the predictive model framework and use of HTPMCs.

The following sections will provide a detailed explanation of this research. First, a background of composite materials with a focus on polymers will be presented. This section will also provide a thorough discussion of the expected mechanical behavior of polymer materials in addition to the modeling efforts that have been developed for

predicting this sort of behavior. Next, an explanation of the material being tested and the experimental setup and procedures used for testing will be described. The presentation of experimental results and model capabilities will follow. Finally, recommendations for future efforts and conclusions will be provided.

II. Background

This section provides a general overview of polymer matrix composites (PMCs) including a description of polymers and their specific use as neat resins in composite materials. The use of PMCs in various aerospace applications will also be presented. Next, the basic concepts of viscoelastic theory used to describe the behavior of polymers will be reviewed. The corresponding constitutive equations used to describe materials which undergo viscoelastic behavior are presented, including both the linear and non-linear formulations. Finally, a summary of previous efforts involving PMR-15 and the modeling of high-temperature polymer deformations will be given and the objective of this research will be stated.

Polymer Matrix Composites

A composite, by definition, is a "material system consisting of two or more phases on a macroscopic scale, whose mechanical performance and properties are designed to be superior to those of the constituent materials acting independently" (5:1). In polymer matrix composites (PMCs), one phase of the composite is a polymeric material. PMCs are generally used for structural purposes in engineering applications. They may assume a variety of forms depending on the reinforcement phase distributed throughout the matrix. Continuous-fiber reinforced, particulate-reinforced, and even nanoparticle filled materials may be classified as PMCs (3:4). In high-performance structural applications, PMCs typically consist of micron-diameter fibers bound in a polymer resin material. The fibers are responsible for the stiffness and strength properties of the composites whereas

the matrix provides protection and support for the fibers. In lower performance composites, it is possible for the matrix to be the main load bearing constituent for the material. It is necessary to gain an understanding of the polymers used as matrices in PMCs before undertaking a review of their role in aerospace applications.

Polymers

The word polymer literally means "many parts". In fact, a polymer is a "macromolecule that contains many groups of atoms, called monomeric units" covalently bonded together (21:1). Polymers are usually classified into three groups based upon their thermomechanical properties. These groups are as follows: thermoplastics, elastomers, and thermosets.

Thermoplastics, often simply referred to as plastics, become fluid when heated and can be easily processed using techniques such as injection molding and extrusion (21:6, 14:10). Their structure can be either linear or branched. Thermoplastics can be further divided into two classifications: amorphous and crystalline. These divisions are based upon the manner in which the plastic is arranged upon cooling. Most thermoplastics do not crystallize upon cooling as this requires reorganization of their highly coiled macromolecules which become entangled in the liquid state (14:10). Those that are capable of some crystallization usually have both organized and amorphous regions. These crystalline polymers are characterized by their melting temperature, T_m. Most plastics, however, are incapable of crystallization upon cooling and assume a random structure even upon annealing. These amorphous polymers are characterized by their glass transition temperature, T_g, at which they transform suddenly from a "glassy" hard

state to a “rubbery” soft state. Below their T_g, amorphous polymers are “frozen” in position, but beyond this temperature limit they can move freely (14:10).

Elastomers, or rubbery polymers as they are commonly referred to, are cross-linked polymers that can be easily deformed many times beyond their original length. However, these polymers rapidly recover their original dimensions upon release of the applied force. Examples of common elastomers include rubber and neoprene.

Thermoset polymers are the most predominant types of matrix systems (5:33). The structure of these rigid polymers is populated with a high degree of cross-linking during the curing process. As a result, thermosets cannot be reshaped after their original formation and decompose thermally at high temperatures (5:33, 14:11). The most commonly used types of thermosets include unsaturated polyesters, epoxies, vinylesters, and polyimides (5:33). While epoxies generally have better mechanical properties than the other thermoset polymers, polyimides are recognized for their abilities to survive higher temperatures.

Aerospace Applications

Applications of PMCs are often categorized based upon the operating temperature or environment to which they are exposed. PMCs used in aerospace vehicles are likely to be exposed to the most demanding conditions of all applications. Extreme temperatures encountered in these applications may range from -150°C to 550°C (3:6). PMCs may be subjected to rapid heating conditions, exposure to pollutants in the environment, solar radiation, and numerous other environmental factors (3:6). PMCs are desirable because they provide a lightweight and high-strength solution to material demands.

The need for high temperature polymer matrix resins to be used in PMCs has been evident for many decades. A new class of polyimides, Polymerization of Monomeric Reactants (PMR), was born out of the need for a high temperature resistant polymer matrix resin that could surpass the performance of the widely used epoxy resins in aerospace applications (20). Epoxy resins, although frequently used in missile and aircraft structures, could not sustain temperatures above 200°C. Furthermore, these resin systems were highly affected by environmental factors such as moisture which further degraded their capabilities. These downfalls led to intensive research over the years for polymers with better elevated temperature properties and more environmental resistance than existing resins. In the mid-1970's, NASA Lewis Research Center developed PMR-15, a neat matrix resin which offered stable performance at high temperatures in addition to low cost and ease in processing (16).

PMR-15 is one of the most sought after thermosetting polyimide resins for high-temperature polymer-matrix composite applications (17:2979). PMR-15 polyimide composites have a glass transition temperature of 348°C. Therefore, the long-term use temperature of PMR-15 composites is 288°C (composite materials must be used at temperatures well below the T_g of the matrix) (6). In comparison to other resins of its type, "PMR-15 displays the best overall balance of processing, behavior, oxidative stability, and retention of mechanical properties" at high temperatures (17:2979). Since PMR-15's adoption into the commercial world, its processing materials, molding powders, chopped-fiber-molding compounds, and variations of PMR resin are readily available from major aerospace composite material suppliers (20). PMR-15 has gained wide acceptance in the engineering community. It is now being used to fabricate various

engine components ranging from small compression molded bearings to large structural autoclave-molded engine ducts used on the F404 engine for the U.S. Navy F-18A Hornet (20). Additional examples of engine applications include gear box covers, transmission housings, external exit flaps, and parts in numerous General Electric engines such as inlet particle separators, vent tubes, fan stators, and core cowls (20). Today, PMR-15 has been recognized as the leading polymer matrix resin for carbon-fiber-reinforced composites used in aircraft engine components.

The amount of polymer matrix composites used in fighter vehicles has continuously increased over the last 30 years. For example, in the 1970s fighter aircraft such as the F-14, F-15, and F-111 had 2 to 4 percent by weight carbon-epoxy composites (3:11). By the 1990s, these numbers grew to 15 to 30 percent in aircraft such as the A-6, AV-8, F-18, and F-22 by weight (3:11). Typical uses of PMCs have been horizontal and vertical stabilizers, fuselage sections, and wing skins. Similar trends are noticeable in rotor aircraft. Whereas PMCs were commonly used for rotor blades and fuel tanks in the 1970s, the V-22's entire airframe is composed of PMCs (3:11). The use of lightweight polymer composites has increased the structural capability of aircraft while reducing weight, resulting in better performance. As applications continue to mature, the use of PMCs will likely be extended to entire aircraft and their support structures.

Linear Viscoelastic Theory

Viscoelastic Behavior

Polymers exhibit unique behavior under applied loads in comparison to other matrix materials such as metals or ceramics. The behavior of a material is often characterized as either an elastic solid or a viscous fluid. In the first case, forces acting on a material create some deformation which is immediately reversible upon removal of the force (22). Most materials which exhibit this behavior are linear elastic in that an increase in stress produces an equivalent increase in strain (22). For example, metals typically exhibit nearly linear elastic behavior below their yield point. On the contrary, a viscous liquid has no definite shape and flows irreversibly under the action of external forces.

Most materials behave elastically under small stresses (8:2). However, once the stress exceeds the elastic limit the behavior is no longer elastic and the strain does not completely disappear after removal of the load (8:2). The permanent strain that remains after the removal of the load is known as plastic strain (8:2). Polymers are unique in that they fit into an intermediate regime displaying the qualities of both an elastic solid and a viscous fluid at different times and temperatures. Upon loading, they exhibit an initial elastic behavior followed by a continuous increase in strain at a decreasing rate. After removal of the load, they undergo an initial elastic recovery of strain followed by a continuous decrease in strain. This type of material response, which exhibits both solid and liquid behavior, is termed viscoelasticity (8:3). Another significant characteristic of viscoelastic materials is dependency on time. Different loading rates used to achieve a

certain stress level affect the amount of strain accumulated by a material. Therefore, these materials are also called time-dependent materials (8:2).

Phenomenological Aspects

The viscoelastic behavior of materials is often studied with three types of experiments to include creep and recovery, relaxation, and constant stress or strain rate tests. Creep is defined as the time-dependent change in strain under constant stress (28:55). The response to creep is divided into three different phases: 1) primary creep 2) secondary creep and 3) tertiary creep as shown in Figure 1. In primary creep, the creep strain increases at a decreasing rate. During secondary creep, the creep strain rate is nearly constant. In the final phase, tertiary creep, the creep strain rate is increasing and continues until it terminates in fracture. Generally, polymers do not enter into the tertiary phase and only enter secondary creep if the minimum creep rate is attained (8:3).

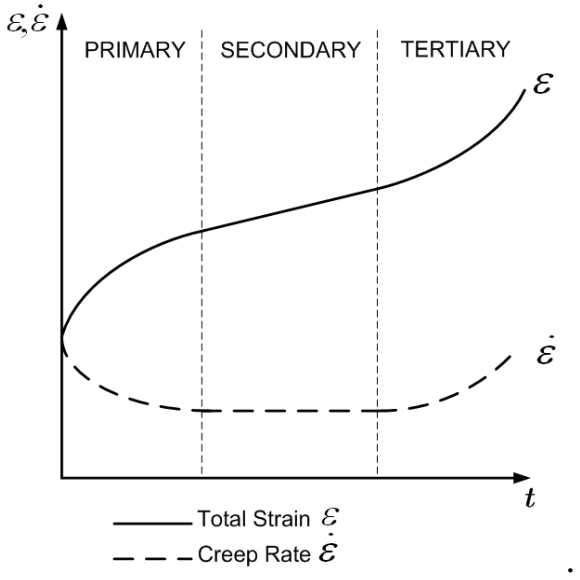

Figure 1: Primary, Secondary, and Tertiary Creep

Following removal of the load, recovery of strain occurs at a continually decreasing rate. For most polymers, a large portion of the time-dependent creep strain will be removed during recovery (8:3). Some polymers may even exhibit full recovery if sufficient time is allowed (8:3). Recovery, like creep, is a non-linear process in which the rate is dependent on time. An example creep-recovery test is shown in Figure 2 below. For non-linear viscoelastic materials, such as polymers, a step input in stress causes an instantaneous increase in strain followed by a non-linear accumulation of strain throughout the creep period. Similarly, removal of the load causes an instantaneous decrease in strain with a continual non-linear decrease in strain.

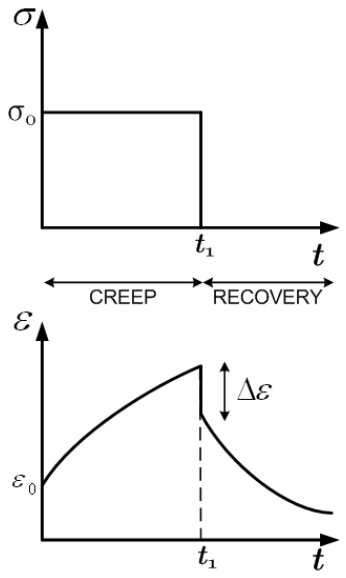

Figure 2: Creep-Recovery Test

Relaxation is defined as the gradual decrease in stress under a constant strain as shown in Figure 3. The initial stress is proportional to the applied strain and decreases

with time. Amorphous polymers at high temperatures may achieve complete relaxation where the stress eventually decays to zero.

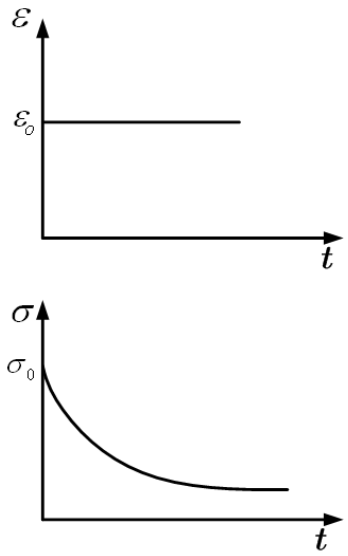

Figure 3: Relaxation Test

Linearity

A material may be considered linear viscoelastic if it complies with the requirements of proportionality and the Boltzmann linear superposition principle (8:5, 22). The proportionality requirement is stated in the following equation:

$$\varepsilon[c\sigma(t)] = c\varepsilon[\sigma(t)] \tag{1}$$

where c is a constant, ε is the strain output, and σ is the stress input. This implies that a stress input of the scalar value $c\sigma(t)$ will produce a strain output equivalent to that produced by the input $\sigma(t)$ multiplied by the constant c (8:6, 22). The second requirement is expressed as follows:

$$\varepsilon\left[\sigma_1(t-t_1)+\sigma_2(t-t_2)\right]=\varepsilon[\sigma_1(t-t_1)]+\varepsilon[\sigma_2(t-t_2)] \quad (2)$$

This principle implies that if a stress, σ_1, is applied at a time, t_1, and an additional stress, σ_2, is applied at a later time, t_2, than the strain output at some time t ($t > t_2$) will be equal to the summation of the strain outputs from each stress acting independently (8:6, 22). Figure 4 illustrates each of the principles of linearity. In the superposition portion, Figure 4 (b), segment 1 denotes the strain due to application of stress σ_1, segment 2 denotes the strain due to application of stress σ_2, and segment 3 represents the strain resulting from the summation of stress σ_1 and stress σ_2.

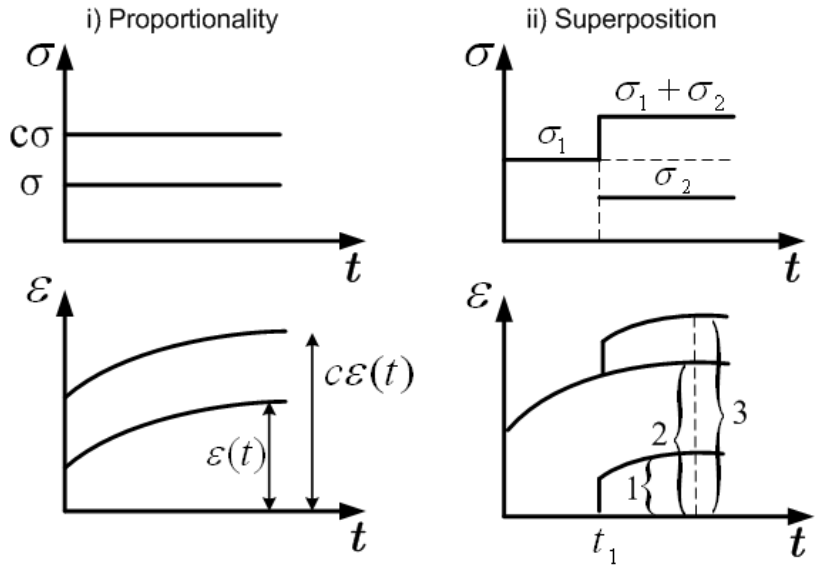

a) **b)**

Figure 4: Principles of Linearity

The determination of linearity from empirical data may be accomplished by the formulation of isochronous stress strain curves from creep tests conducted over the stress range of interest (22). The strain values for different stress levels may be selected at various times throughout each individual creep test. These values are plotted for each chosen time on a stress strain graph. If the material's behavior is within the linear region, the curves will remain parallel; however, if the material response becomes nonlinear as the stress values increase, the curves become nonparallel. An example of this method is shown in the results section for the PMR-15 neat resin.

Mathematical Representations

Two important material properties can be defined for a viscoelastic material subjected to creep and relaxation tests. Creep compliance, *J(t)*, is the creep strain per unit of applied stress. For linear viscoelastic materials, the creep compliance is expressed as follows:

$$J(t) = \frac{\varepsilon(t)}{\sigma_0} \tag{3}$$

The logarithm of creep compliance as a function of the logarithm of time is shown graphically in Figure 5. During the glassy phase, *J(t)* has an order of magnitude of ~10^{-9} Pa^{-1} (22). During the rubbery phase, *J(t)* has an order of magnitude of ~10^{-5} Pa^{-1} (22). The retardation time, or characteristic time, is the value in the viscoelastic region labeled as the logarithm of τ'. This time marks the inflection from rising to falling slope of the creep compliance.

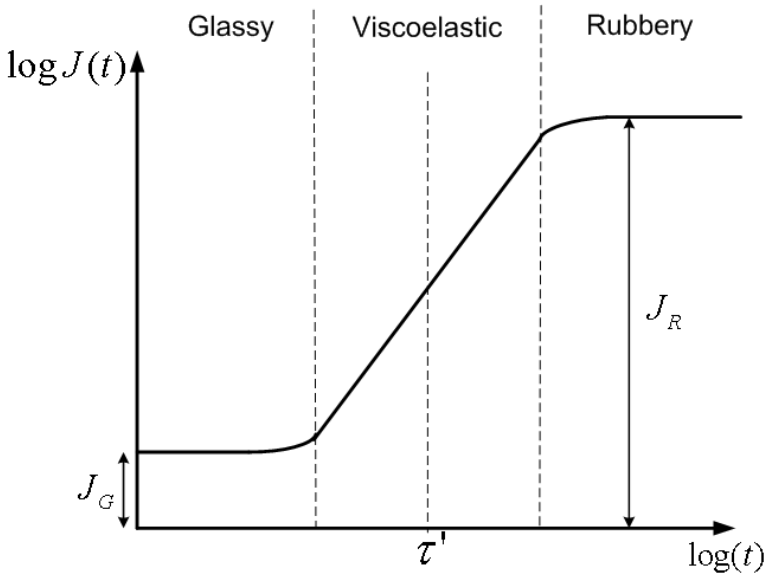

Figure 5: Creep Compliance

During creep testing, a polymer initially exhibits "glassy compliance" in which the elastic deformation is a result of bond deformation (22). Eventually the compliance rises to equilibrium and exhibits "rubbery compliance" as a result of molecular mobility (8).

Similarly, the relaxation modulus, *G(t)*, is defined as the relaxation stress per unit of applied strain. For linear viscoelastic materials, the relaxation modulus is expressed as follows:

$$G(t) = \frac{\sigma(t)}{\varepsilon_0} \tag{4}$$

The logarithm of relaxation modulus as a function of the logarithm of time is shown graphically in Figure 6. During the glassy phase, *G(t)* has an order of magnitude of ~10^9 Pa which decreases to a value of ~10^5 Pa during the rubbery phase (22). Polymers initially exhibit "glassy compliance" during a relaxation test; however, molecular mobility is the mechanism that generally prevails and is reached very quickly (22).

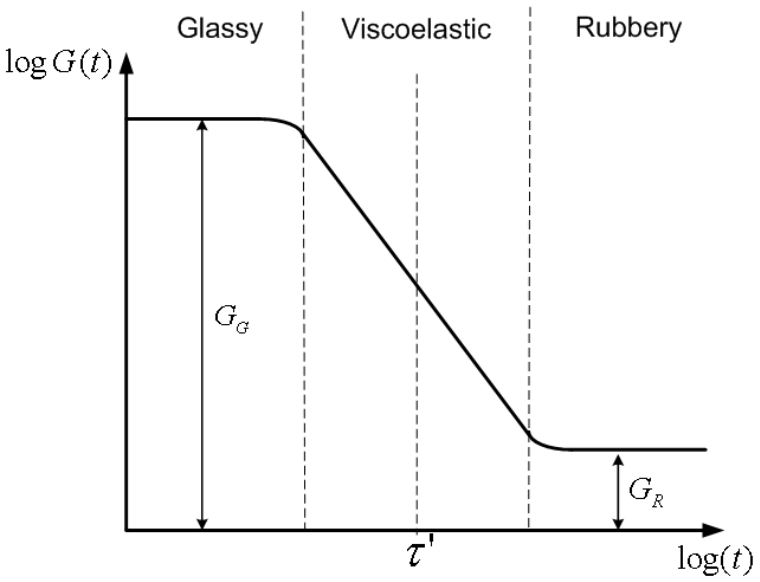

Figure 6: Relaxation Modulus

The relationship between the creep compliance and relaxation modulus for linear viscoelastic materials is expressed in the following equations:

$$G_G = \frac{1}{J_G} \qquad G_R = \frac{1}{J_R} \tag{5}$$

It is important to note that the characteristic time, or relaxation time, for relaxation response is different than that from the creep response because relaxation achieves equilibrium much faster (22).

Integral Representation of Linear Viscoelasticity

An integral representation or hereditary integral exists that is capable of describing creep strains due to an arbitrary stress input for linear viscoelastic behavior. This integral representation of viscoelasticity is capable of incorporating the entire history of stress

input into the predictive equation. This integral representation involves the use of Boltzmann's Superposition principle described earlier.

Using the unit step function $H(t)$, a step input of constant stress σ_0 applied at t = 0 and the corresponding strain response may be expressed as the following:

$$\sigma = \sigma_0 H(t) \tag{6}$$

$$\varepsilon(t) = \sigma_0 J(t) H(t) \tag{7}$$

If a new stress input σ_1 is applied not at t = 0 but at some later time, ξ_1, Eq. 6 and Eq. 7 would become the following:

$$\sigma = \sigma_1 H(t - \xi_1) \tag{8}$$

$$\varepsilon(t) = \sigma_1 J(t - \xi_1) H(t - \xi_1) \tag{9}$$

According to Boltzmann's superposition principle, if the stresses σ_0 and σ_1 were applied at their respective times, t_0 and ξ_1, the resulting strain output becomes the following:

$$\varepsilon(t) = \sigma_0 J(t) H(t) + \sigma_1 J(t - \xi_1) H(t - \xi_1) \tag{10}$$

If an arbitrary stress input is represented as the sum of a series of constant stress inputs, as shown in Figure 7, the stress input and associated strain response may be represented as:

$$\sigma(t) = \sum_{i=1}^{N} \Delta\sigma_i H(t - \xi_i) \tag{11}$$

$$\varepsilon(t) = \sum_{i=1}^{N} \Delta\sigma_i J(t - \xi_i) H(t - \xi_i) \tag{12}$$

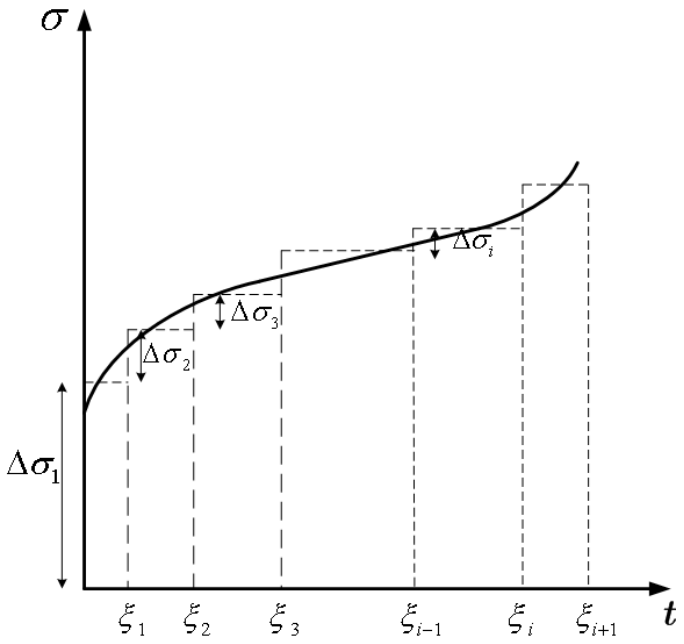

Figure 7: Arbitrary Stress Input

As the number of steps becomes infinite, the summation may be replaced by integration and Eq. 12 becomes:

$$\varepsilon(t) = \int_0^t J(t-\xi)\frac{\partial\sigma(\xi)}{\partial\xi}\partial\xi \tag{13}$$

Further manipulation to include integration by parts, allows Eq. 13 to be written in the following form:

$$\varepsilon(t) = J_0\sigma(t) - \int_0^t \frac{\partial J(t-\xi)}{\partial\xi}\sigma(\xi)\partial\xi \tag{14}$$

This equation may be further reduced to:

$$\varepsilon(t) = J_0\sigma(t) + \int_0^t \phi(t-\xi)\frac{\partial\sigma(\xi)}{\partial\xi}\partial\xi \tag{15}$$

if the compliance is separated into the initial time independent elastic compliance, J_0, and the time-dependent creep function, $\varphi(t)$ (23:84). This same process may be repeated for a relaxation test in which an arbitrary strain is the input and stress is the response.

Time-Temperature Equivalence

The concept of time-temperature equivalence was introduced to allow linear viscoelastic models to provide more accurate predictions. Empirical observations reveal that the deformation of materials, polymers in particular, often depends on external parameters such as temperature or prior aging. By plotting data on a logarithmic scale, however, it is easily shown that often the same process is occurring at various temperatures. As a result, a shift function is introduced to allow for consideration of these effects. This scaling of time to compare similar behavior is termed time-temperature dependence (22).

The time-temperature dependence concept is demonstrated in Figure 8. In this example, the curves have identical shapes but differ by a horizontal shift factor, a_T, for various temperatures.

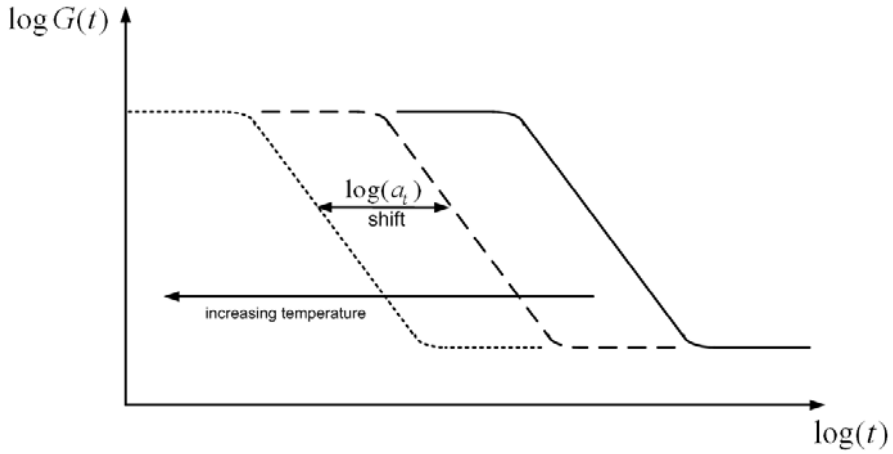

Figure 8: Dependence of Stress Relaxation Modulus on Time and Temperature

The time-temperature dependence is described as follows:

$$\log(t_0) - \log(t) = \log(a_T) \tag{16}$$

where t_0 is the time corresponding to the master temperature T_0 and t is the time corresponding to some other temperature T. The horizontal shift is then given:

$$a_T = \frac{t_0}{t} \tag{17}$$

and the behavior at temperature T is described as the behavior occurring at T_0 except at time $t = \frac{t_0}{a_T}$. Because the temperature is also a function of time, this expression must be rewritten as the following:

$$dt_T = \frac{dt_0}{a_T(T(t_0))} \qquad \text{or} \qquad t_T = \int_0^{t_0} \frac{dt_0'}{a_T(T(t_0'))} \tag{18}$$

A material that exhibits time-temperature equivalence is known as a thermorheollogically simple material (22). Williams, Landel, and Ferry developed a commonly used equation for determination of the shift factor, known as the WLF equation:

$$\log(a_T) = \frac{-C_1(T - T_{ref})}{C_2 + (T - T_{ref})} \tag{19}$$

where C_1 = 17.4 and C_2 = 51.6. This equation is often used for amorphous polymers with $T_{ref} = T_g$ and T in the nearby region of T_g (21:65, 22, 28:109).

Linear Viscoelastic Models

Rheological Models

The linear viscoelastic behavior of materials may be represented by models which describe stress-strain relations with time. These models are composed of two basic elements, the linear spring and the linear viscous dashpot.

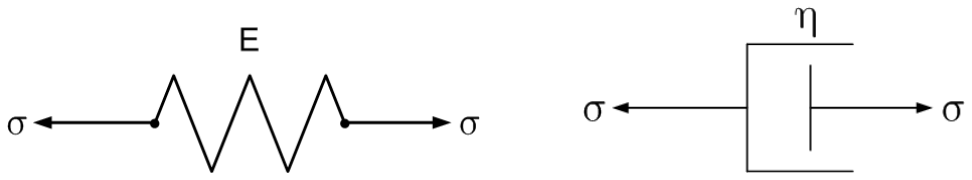

a) **b)**

Figure 9: a) Linear Spring and b) Linear Viscous Dashpot

The linear spring, shown in Figure 9 a), results in an instantaneous strain, ε_o, after application of an instantaneous stress, σ_o, represented by the equation:

$$\sigma_e = E\varepsilon_e \tag{20}$$

where *E* is the linear spring constant or the Young's modulus. The behavior predicted by the linear spring is shown in Figure 10.

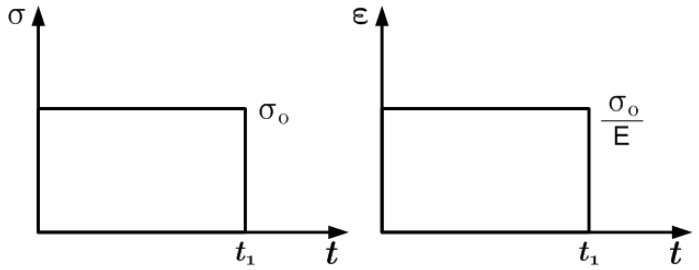

Figure 10: Linear Spring Behavior

The linear viscous dashpot is represented by the equation:

$$\sigma_v = \eta \frac{d\varepsilon}{dt} = \eta \dot{\varepsilon}_e \tag{21}$$

where η is the coefficient of viscosity. Figure 11 depicts the behavior predicted by a linear viscous dashpot. As shown in Figure 11 a), a step input of constant stress results in a time dependent increase in strain. However, a step input of constant strain, as in Figure 11 b), results in an infinite spike in stress followed by an immediate decrease to zero stress at time t = (0^+). The stress then remains zero for the remainder of time. The spike in stress to an infinite value, represented by the Dirac delta function, is physically unrealistic.

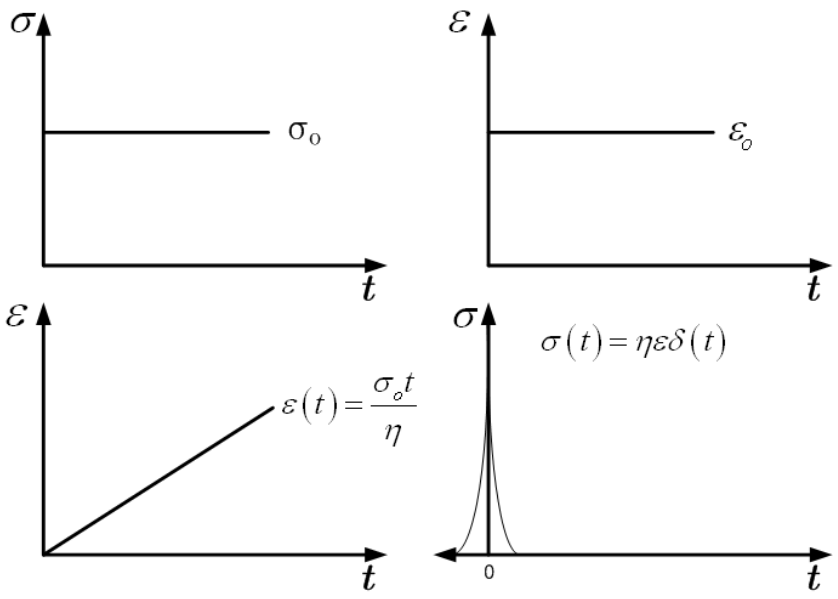

a) **b)**

Figure 11: a) Creep and b) Relaxation predicted by Linear Viscous Dashpot

Various combinations of the linear spring and linear viscous dashpot elements are used in rheological models. Three popular models include the Maxwell Model, the Kelvin-Voigt Model, and the Standard Linear Solid.

Maxwell Model

The Maxwell model consists of a spring and a dashpot arranged in series as shown in Figure 12.

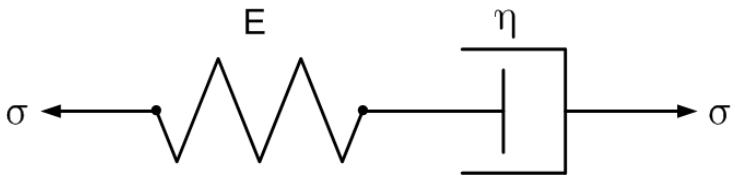

Figure 12: Maxwell Model

Because the elements are arranged in series, the total stress and total strain of the model are represented by the following equations:

$$\text{Total Stress: } \sigma = \sigma_e = \sigma_v \tag{22}$$

$$\text{Total Strain: } \varepsilon = \varepsilon_e + \varepsilon_v \tag{23}$$

where the subscript *e* denotes the elastic spring element and the subscript *v* denotes the viscous dashpot element. The total strain rate of the model is then represented as the following:

$$\text{Total Strain Rate: } \dot{\varepsilon} = \dot{\varepsilon}_e + \dot{\varepsilon}_v \tag{24}$$

By introducing the spring strain rate, obtained by taking the time derivate of Eq. 20, and the viscous damper strain rate, expressed in Eq. 21, into the total strain rate, the total strain rate for the Maxwell model becomes the following:

$$\dot{\varepsilon} = \dot{\varepsilon}_e + \dot{\varepsilon}_v = \frac{\dot{\sigma}_e}{E} + \frac{\sigma_v}{\eta} \tag{25}$$

Further consideration of the stress equivalence for the model, described in Eq. 22, allows simplification to the following relation:

$$\dot{\varepsilon} = \frac{\dot{\sigma}}{E} + \frac{\sigma}{\eta} \tag{26}$$

During creep, the specimen is subject to a constant stress input and as a result $\dot{\sigma} = 0$. By integrating with respect to time and using the initial condition $\sigma = \sigma_0$ at $t = t_0$, the strain response due to creep as predicted by the Maxwell model is expressed as:

$$\varepsilon = \frac{\sigma_o}{\eta} t + \frac{\sigma_o}{E} \tag{27}$$

where $\frac{\sigma_o}{E}$ is the constant of integration determined from initial conditions. It is now possible to examine the ability of the Maxwell model to predict material behavior for creep, a step increase in stress, and relaxation, a step increase in strain. The Maxwell model accurately predicts an instantaneous increase in strain upon application of a step increase in stress. However, it predicts a linear increase in strain over time which is not correct. In addition, the model only allows for recovery of the elastic component of strain and predicts a permanent strain due to the viscous component of the model. Creep strain as a function of time, as predicted by the Maxwell Model, is shown in Figure 13 a).

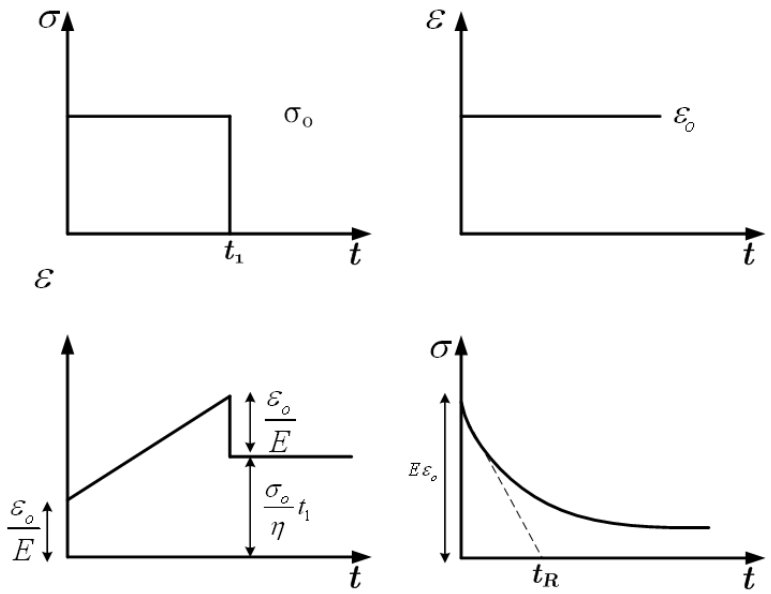

a) **b)**

Figure 13: a) Creep and b) Relaxation predicted by Maxwell Model

In the case of relaxation, the specimen is subject to a constant strain input and $\dot{\varepsilon} = 0$. Eq. 26 becomes $0 = \frac{\dot{\sigma}}{E} + \frac{\sigma}{\eta}$. Both sides of the equation are multiplied by η and an integration factor of $e^{\frac{E}{\eta}t}$ is used. By integrating with respect to time, the prediction of stress response during relaxation by the Maxwell model is represented by the following equation:

$$\sigma(t) = -\frac{\sigma_o E}{\eta} t + \sigma_o \tag{28}$$

where σ_o is the constant of integration determined from initial conditions. Relaxation stress as a function of time, as predicted by the Maxwell Model, is shown in Figure 13 b). The Maxwell Model accurately predicts relaxation. As depicted in Figure 13, the Maxwell model allows for definition of a relaxation time as follows:

$$t_R = \frac{\eta}{E} \tag{29}$$

During relaxation stress rapidly decreases for times $t < t_R$ with the majority of relaxation occurring before t_R.

Kelvin-Voigt Model

Similar to the Maxwell model, the Kelvin-Voigt model also consists of a spring and a dashpot; however, they are arranged in a parallel as shown in Figure 14.

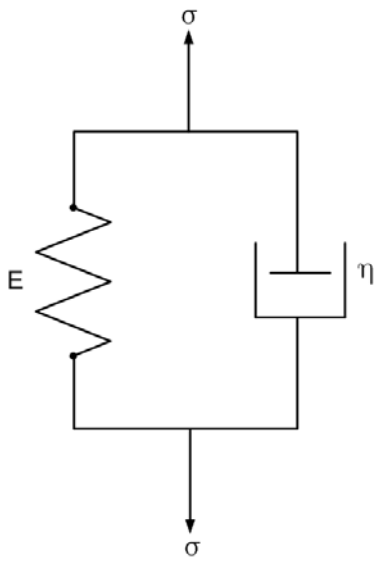

Figure 14: Kelvin-Voigt Model

The parallel configuration of the spring and dashpot elements in the Kelvin-Voigt model result in the following total stress and total strain equations:

$$\text{Total Strain:} \quad \varepsilon = \varepsilon_e = \varepsilon_v \tag{30}$$

$$\text{Total Stress:} \quad \sigma = \sigma_e + \sigma_v \tag{31}$$

where the subscript *e* denotes the elastic spring element and the subscript *v* denotes the viscous dashpot element. The total strain rate of the model is then represented by the following:

$$\dot{\varepsilon} = \dot{\varepsilon}_e = \dot{\varepsilon}_v \tag{32}$$

The stress strain relations for the Maxwell model are derived by considering the total stress (Eq. 31), the linear spring strain rate (Eq. 20), the viscous damper strain rate, (Eq. 21), and the total strain rate (Eq. 32) as follows:

$$\sigma = \sigma_e + \sigma_v = E\varepsilon_e + \eta\dot{\varepsilon}_v = E\varepsilon + \eta\dot{\varepsilon} \tag{33}$$

Both sides of Eq. 33 are divided by η to provide the following relation.

$$\frac{\sigma}{\eta} = \frac{E\varepsilon}{\eta} + \dot{\varepsilon} \tag{34}$$

Integration is completed using an integration factor of $e^{\frac{E}{\eta}t}$. The prediction of strain response during creep by the Kelvin Voigt model is represented by the following equation:

$$\varepsilon(t) = \frac{\sigma_0}{E}(1 - e^{-\frac{E}{\eta}t}) \tag{35}$$

In order to develop the strain response during recovery, it is necessary to adapt an alternate method for depicting creep using the Boltzmann superposition principle. The loading history may be thought of as two different steps in stress followed by periods of creep depicted by segment 1) and 2) in Figure 15. Segment 1 illustrates loading as a step increase in stress to σ_o at time t = 0 followed by creep at σ_o. Segment 2 depicts unloading of the stress at time t_1 which is equivalent to applying a stress ($-\sigma_o$) at time $t = t_1$. Finally, recovery at zero stress is equivalent to creep at ($-\sigma_o$) at time > t_1.

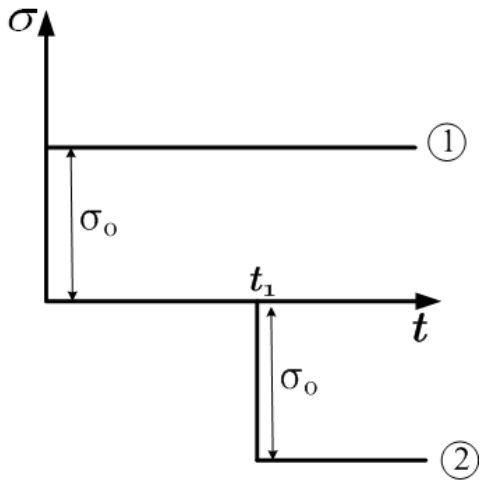

Figure 15: Creep Input for Recovery Prediction by Kelvin-Voigt Model

Using Eq. 35, the strain response for both segment 1) and segment 2) can be shown in Eq. 36 and 37, respectively:

$$\varepsilon(t) = \frac{\sigma_0}{E}(1 - e^{-\frac{E}{\eta}t}) \tag{36}$$

$$\varepsilon(t) = -\frac{\sigma_0}{E}(1 - e^{-\frac{E}{\eta}(t-t_1)}) \tag{37}$$

The summation of Eq. 36 and Eq. 37 provides the strain response during recovery ($t > t_1$) by the Maxwell model:

$$\varepsilon(t) = \frac{\sigma_0}{E} e^{-\frac{E}{\eta}t}[e^{\frac{Et_1}{\eta}} - 1] \tag{38}$$

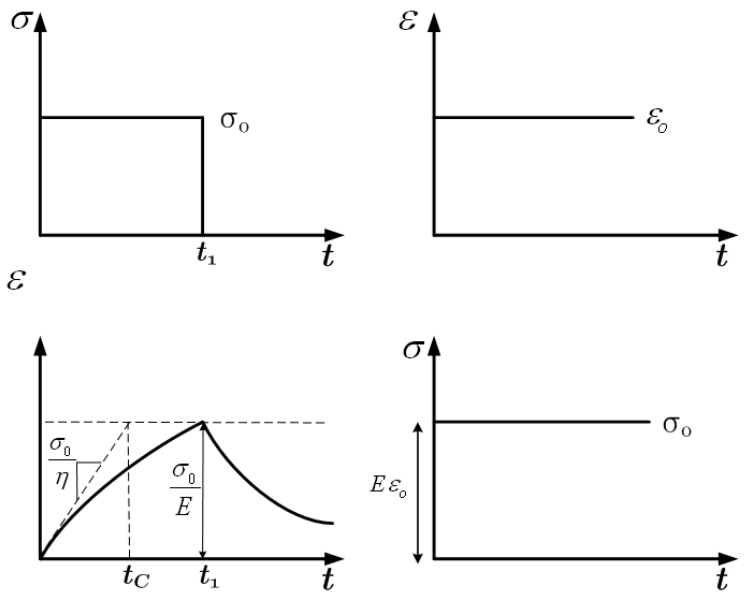

a) **b)**

Figure 16: a) Creep and b) Relaxation predicted by Kelvin-Voigt Model

The Kelvin Voigt model accurately predicts the shape of the strain response during creep. The strain is increasing at an initial rate of $\frac{\sigma_o}{\eta}$. It continues to increase at a decreasing rate. The bulk of the creep strain is accumulated before the retardation time t_c which is defined as follows:

$$t_C = \frac{\eta}{E} \tag{39}$$

In the Kelvin-Voigt model, stress is initially carried by the viscous element and gradually transmitted to the elastic element which eventually dominates at infinite time. This behavior is described as delayed elasticity.

In the case of relaxation, the specimen is subject to a constant strain input and $\dot{\varepsilon} = 0$. Equation 34 becomes $\frac{\sigma}{\eta} = \frac{E\varepsilon}{\eta}$. Both sides of the equation are multiplied by η and the Kelvin-Voigt model simply reduces to Hooke's Law. Therefore, because a constant strain input produces a constant stress input, the Kelvin-Voigt model is incapable of predicting relaxation behavior.

Table 1 illustrates the abilities of the Maxwell and Kelvin Voigt models to accurately predict the behavior associated with most viscoelastic materials. Those characteristics which are achieved with each model are marked with an X. The Maxwell model describes the time-independent strain on loading and unloading as well as the relaxation behavior. The Kelvin-Voigt model describes the delayed elasticity and recovery of the creep. Neither model is independently capable of predicting the desired behavior.

Table 1: Ability of Maxwell and Kelvin-Voigt Models to Represent Viscoelastic Behavior

Model	Instantaneous increase in strain on loading	Delayed elasticity	Instantaneous decrease in strain on unloading	Time Dependent Recovery	Relaxation
Maxwell	X		X		X
Kelvin Voigt		X		X	

Standard Linear Solid

Numerous multi-element models exist that provide greater accuracy in predicting the behavior of a viscoelastic material. One such model is the Standard Liner Solid (SLS). The SLS consists of a spring element acting in series with the Kelvin Voigt model as depicted in Figure 17.

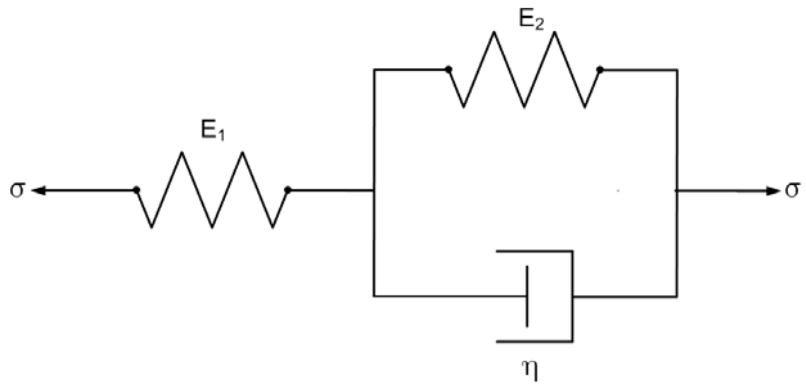

Figure 17: Standard Linear Solid (SLS) Model

When determining the governing equations for the SLS model, it is useful to view it as a combination of two elements. The first element is the spring with modulus of elasticity of E_1. Its governing equation is as follows:

$$\sigma_{E1} = E_1 \varepsilon_{E1} \tag{40}$$

The second element is the parallel combination of spring and dashpot referred to as the Kelvin element represented by the following equations:

$$\text{Spring equation } \sigma_{E2} = E_2 \varepsilon_{E2} \tag{41}$$

$$\text{Dashpot equation } \sigma_{\eta} = \eta \dot{\varepsilon}_{\eta} \tag{42}$$

Total stress equation $\sigma_k = \sigma_{E2} + \sigma_\eta$ (43)

Total strain equation $\varepsilon_k = \varepsilon_{E2} = \varepsilon_\eta$ (44)

The total stress and total strain equations for the entire model are expressed:

Total Stress: $\sigma = \sigma_{E1} = \sigma_k$ (45)

Total Strain: $\varepsilon = \varepsilon_{E1} + \varepsilon_k$ (46)

The total strain rate of the model is then represented by the following:

Total Strain Rate: $\dot{\varepsilon} = \dot{\varepsilon}_{E1} + \dot{\varepsilon}_k$ (47)

Using the equations for each element, Eq. 40-44, and substituting them into the total strain rate equation for the two elements connected in series, Eq. 47, the following relationship is determined:

$$\dot{\varepsilon} + \frac{E_2}{\eta}\varepsilon = \frac{\dot{\sigma}}{E_1} + (1 + \frac{E_2}{E_1})\frac{\sigma}{\eta} \tag{48}$$

With an integration factor $e^{\frac{E_2}{\eta}t}$ and initial conditions of $\sigma = \sigma_0$ and $\varepsilon = \frac{\sigma_0}{E_1}$ at $t = t_0$, the strain response due to creep as predicted by the SLS model is expressed as:

$$\varepsilon(t) = \sigma_0\left(\frac{E_1 + E_2}{E_1 E_2}\right) - \frac{\sigma_0}{E_2}e^{-\frac{E_2}{\eta}t} \tag{49}$$

The recovery equation for the SLS model is developed by applying the Boltzmann superposition principle as done for the Kelvin Voigt model and depicted in Figure 15. As a result, the strain response during recovery ($t > t_1$) for the SLS model becomes:

$$\varepsilon(t) = \frac{\sigma_0}{E_2}e^{-\frac{E_2}{\eta}t}[e^{\frac{E_2 t_1}{\eta}} - 1] \tag{50}$$

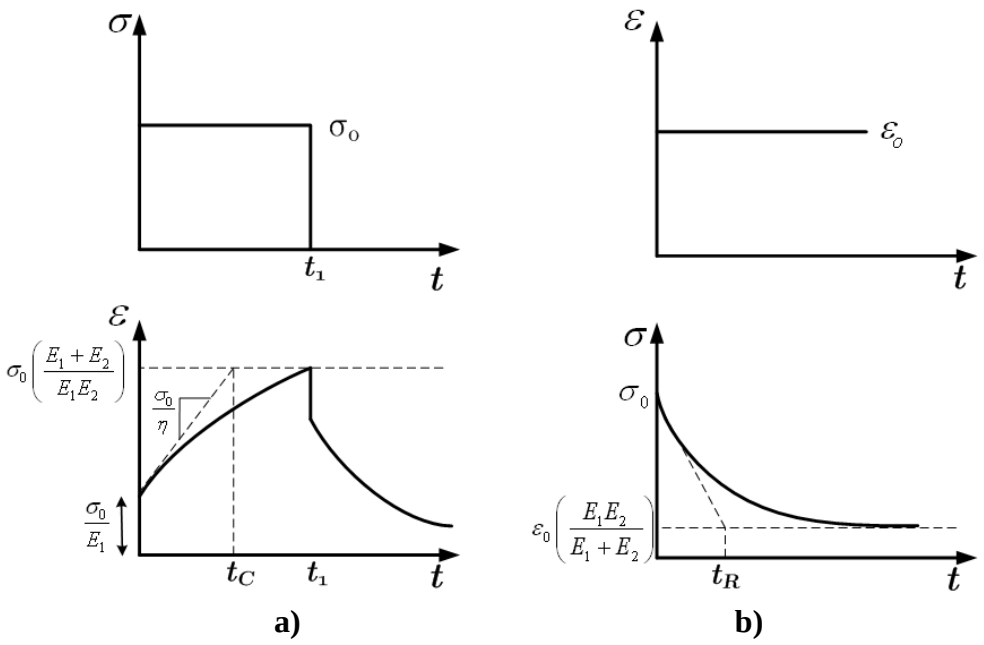

Figure 18: a) Creep and b) Relaxation predicted by the Standard Linear Solid Model

For relaxation, the input is constant strain input and $\dot{\varepsilon} = 0$. Eq. 48 reduces to $\frac{E_2}{\eta}\varepsilon = \frac{\dot{\sigma}}{E_1} + (1+\frac{E_2}{E_1})\frac{\sigma}{\eta}$. An integration factor of $e^{\frac{E_1+E_2}{\eta}t}$ is applied to this equation. By integrating with respect to time, the prediction of stress response during relaxation by the SLS model is represented by the following equation:

$$\sigma(t) = \left(\frac{E_1E_2}{E_1+E_2}\right)\varepsilon_0 + \left(\sigma_0 - \left(\frac{E_1E_2}{E_1+E_2}\right)\varepsilon_0\right)e^{-\left(\frac{E_1+E_2}{\eta}\right)t} \tag{51}$$

The SLS is capable of providing an approximate representation of polymer behavior in the viscoelastic range as shown in Figure 18. It is capable of modeling time-independent strain on loading and unloading, delayed elasticity, time dependent recovery, and relaxation. While the Standard Linear Solid model does predict this general behavior; it

is important to note that it is incapable of describing the behavior of many viscoelastic materials over a large number of variables. Therefore, more complex models have been proposed to provide greater accuracy.

Nonlinear Viscoelastic Theory

The aforementioned theories provide an accurate representation of linear viscoelastic material behavior if the stresses and strains are small (24:295). However, this linear range is often only a small portion of the total material response before failure (24:295). Therefore, further considerations are necessary to incorporate non-linear behavior into predictive models. For non-linear materials, the creep compliance, *J(t)*, and the relaxation modulus, *G(t)*, are no longer a function of time alone. As shown in the relations below, they become functions of stress and strain, respectively.

$$J(t,\sigma) = \frac{\varepsilon(t)}{\sigma} \tag{52}$$

$$G(t,\varepsilon) = \frac{\sigma(t)}{\varepsilon} \tag{53}$$

As a result, the Boltzmann superposition principle does not directly apply for the development of constitutive equations relating the stress strain behavior of materials. However, the Boltzmann superposition principle is often used as a preliminary basis for developing relations that are capable of predicting the behavior of non-linear materials (24:296).

Lederman made two important observations from the plots of creep compliance (relaxation modulus) as a function of time obtained for certain textile fibers. First, the

creep compliance at various stress levels overlapped for small values of time near the origin (22). This was an indication of an instantaneous elastic deformation in non-linear materials. Secondly, delayed creep and recovery was a unique function of stress for any given load (22). This led to the development of the Modified Superposition Principle (MSP), an extension of the integral formulation for nonlinear materials. Leaderman proposed the following equation to predict the strain behavior of non-linear materials as a function of time, *t*, and creep stress, σ :

$$\varepsilon(t) = \frac{\sigma}{E} + \int_{-\infty}^{t} \frac{df(\sigma)}{\partial \xi} J(t-\xi)\partial\xi \tag{54}$$

Note that the Modified Superposition Principle is very similar to the integral formulation developed for linear viscoelastic materials with the exception of the function of stress in the second term.

Pipkin and Rogers extended the integral formulation for non-linear viscoelastic materials by introducing a non-linear creep function for the prediction of strain (19:60, 22). This function is given as the following:

$$C(t,\sigma) = \frac{d\varepsilon(t,\sigma)}{d\sigma} \tag{55}$$

The prediction of strain, according to Pipkin and Rogers, is then expressed as:

$$\varepsilon(t,\sigma) = \int_{-\infty}^{t} \frac{d\sigma(\tau)}{d\tau} C[\sigma(\tau), t-\tau]d\tau \tag{56}$$

Pipkin and Rogers used the same approach for the prediction of stress during a stress-relaxation test by introducing a non-linear relaxation modulus.

Schapery advanced the prediction schemes for non-linear viscoelastic materials even further by incorporating a concept based on time-temperature equivalence into the

Modified Superposition Principle (24:296). Schapery's model consists of constitutive equations which include material constants determined from empirical data. Schapery defined creep compliance as the summation of initial elastic compliance and secondary transient compliance, the first and second term respectively in the equation below:

$$J(t) = \frac{\varepsilon(t)}{\sigma} = D_0 + \Delta D(t) \tag{57}$$

Accordingly, the creep strain for a case of uniaxial loading is expressed as follows:

$$\varepsilon(t) = g_0 D_0 \sigma(t) + g_1 \int_{0-}^{t} \Delta D(\psi - \psi') \frac{d}{d\tau}\left[g_2 \sigma(\tau)\right] \partial\tau \tag{58}$$

$$\psi(t) = \int_0^t \frac{dt'}{a_0[\sigma(t')]} \qquad \psi'(\tau) = \int_0^\tau \frac{dt'}{a_0[\sigma(t')]} \tag{59}$$

where g_0, g_1, g_2, a_0 are material constants that depend on stress level and ψ is the reduced time (18:246, 24:297). The reduced time defined by Schapery is based upon the concept of time-temperature equivalence. However, time-temperature equivalence introduces a horizontal shift, a_T, dependent on temperature whereas the horizontal shift used in Schapery's model, a_σ, is dependent on stress. It is convenient to recognize that if $g_0 = g_1 = g_2 = a_\sigma = 1$, Eq. 58 becomes the strain response for a linear material as previously shown by the Boltzmann Superposition principle (24:297).

Schapery's model is capable of predicting the strain response when stress is applied through stepwise loading. For example, in a uniaxial two-step loading condition, the applied stress is given as follows:

$$\sigma(t) = \begin{cases} \sigma_a, & 0 < t < t_a \\ \sigma_b, & t_a < t < t_b \end{cases} \tag{60}$$

Therefore, the stress input may be rewritten as:

$$\sigma(t) = [H(t) - H(t - t_a)]\sigma_a + [H(t - t_a) - H(t - t_b]\sigma_b \tag{61}$$

where $H(t)$ is defined as the unit step function. By substituting the input stress of Eq. 61 into Eq. 58, the strain response due to the first loading step, σ_a, is expressed as follows:

$$\varepsilon_c(t) = \left[g_0^a D(0) + g_1^a g_2^a \Delta D_0 \frac{t}{a_\sigma^a} \right] \sigma_a, \quad 0 < t < t_a \tag{62}$$

While the response to the second loading step becomes the following:

$$\varepsilon_c(t) = g_0^b D(0)\sigma_b + g_1^b \left[g_2^a \sigma_a \Delta D\left(\frac{t_a}{a_\sigma^a} - \frac{t - t_a}{a_\sigma^b} \right) + (g_2^b \sigma_b - g_2^a \sigma_a)\Delta D\left(\frac{t - t_a}{a_\sigma^b} \right) \right], \; t_a < t < t_b \tag{63}$$

where the superscripts in Eq. 62 and 63 represent the constants corresponding to the stress level (18:247). For example, $g_0^a = g_0(\sigma_a)$. These formulations may be extended for additional step inputs of constant stress.

If a creep-recovery test is performed as shown in Figure 2, the stress input is reduced to:

$$\sigma(t) = [H(t) - H(t - t_1)]\sigma_0 \tag{64}$$

Substituting this expression into Eq. 58 results in the following equations for strain response during creep and recovery respectively:

$$\varepsilon_c(t) = g_0 D(0)\sigma_0 + g_1 g_2 \Delta D_0 \frac{t}{a_0}\sigma_0, \quad 0 < t < t_1 \tag{65}$$

$$\varepsilon_r(t) = g_2[\Delta D(\psi) - \Delta D(\psi - \psi_1)]\sigma_0, \quad t > t_1 \tag{66}$$

$$\text{where} \quad \psi_1 = \frac{t_1}{a_0} \text{ and } \psi = \frac{t_1}{a_0} + (t - t_1) \tag{67}$$

These equations may be further broken down into the instantaneous increase in strain upon addition of the load, ε_0; the final strain value at the end of the creep period, ε_1; and strain at the beginning of recovery, ε_1', resulting from the instantaneous decrease in strain upon removal of the load. These relations are defined by extracting the appropriate terms from Eqs. 65 and 66 as follows:

$$\varepsilon_0 = g_0 D(0)\sigma_0 \tag{68}$$

$$\varepsilon_1 = g_0 D(0)\sigma_0 + g_1 g_2 \Delta D_0 \frac{t}{a_\sigma}\sigma_0 \tag{69}$$

$$\varepsilon_1' = g_2 \Delta D(\psi_1)\sigma_0, \quad t > t_1 \tag{70}$$

Figure 19 is useful in gaining a visual understanding of these variables and the behavior associated with non-linear viscoelasticity.

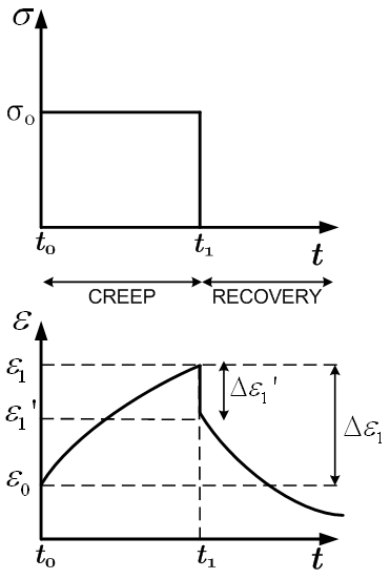

Figure 19: Creep and Recovery Test Notation for Schapery's Model

Recognizing that for many engineering polymers compliance can be represented by a power law, Schapery proposed that the transient component of creep compliance, the second term in Eq. 57, be represented by a power law as well:

$$\Delta D(\psi) = C(\psi)^n \tag{71}$$

where the constants C and n are independent of stress (18:9, 24:32). Utilizing this relation the expressions for creep and recovery strain, Eq. 65 and Eq. 66, become the following:

$$\varepsilon_c(t) = \left[g_0 D(0) + C g_1 g_2 \left(\frac{t}{a_0} \right)^n \right] \sigma_0 \tag{72}$$

$$\varepsilon_r(t) = \frac{\Delta\varepsilon_1}{g_1} [(1+\lambda a_0)^n - (\lambda a_0)^n] \tag{73}$$

where $\Delta\varepsilon_1$ is the total amount of strain accumulated during the creep process defined as follows:

$$\Delta\varepsilon_1 = \varepsilon_1 - \varepsilon_0 = C g_1 g_2 \frac{t_1^n}{a_\sigma^n} \sigma_0 \tag{74}$$

and λ is the non-dimensional reduced time as shown by the following:

$$\lambda = \frac{(t - t_1)}{t_1} \tag{75}$$

The uniaxial constitutive equations capable of predicting the behavior of non-linear viscoelastic materials as developed by Schapery are represented by Eq. 72 and 73. It is possible to apply a characterization scheme to empirical creep and recovery data to determine the parameters *C, n, D(0)* and g_0, g_1, g_2, a_σ as functions of stress for a given

material. Characterization of Schapery's model for the PMR-15 neat resin is presented in the results portion of the paper.

Previous Efforts

Schapery's model is a well-established method for predicting the behavior of non-linear viscoelastic materials. At the onset of studies utilizing Schapery's model to predict material behavior of this nature, Lou and Schapery were successful in characterizing the constitutive equations for a non-linear fiber reinforced plastic. The results of this effort, shown in Figure 20, illustrate the greatly increased capability to predict material behavior when using Schapery's model versus the Modified Superposition Principle introduced by Leaderman (13:221). This research also confirmed the validity of the power-law representation for compliance (13:221).

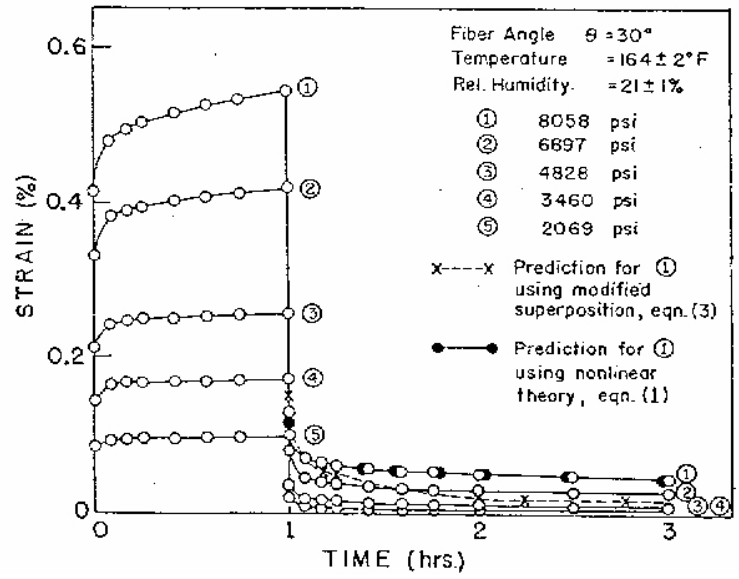

Figure 20: Lou and Schapery: Viscoelastic Characterization (13:221)

Peretz and Weitsman (18) conducted a similar experimentation on FM-73 adhesive in an isothermal environment. However, after characterization of Schapery's model using creep and recovery data, the theory was used to predict the response under two-step loading and hysteresis response under cyclic constant stress rate tests. The two-step loading tests consisted of the application of stress to a value of approximately 50% of the ultimate tensile stress, followed by partial removal of the load to produce different levels of reduced stress. Results of the model verification revealed that the model was capable of predicting creep and recovery strain (18:258). Peretz and Weitsman emphasized that the "discrepancy between experimental results and the prediction of non-linear theory fall within the scatter ranges" of creep data used to develop the characterization scheme (18:257).

In both works previously described, "mechanical conditioning" of the specimen was done to reduce the effects of crack and damage growth prior to model characterization (13:220, 18:246). This was done by loading and unloading the specimen to a percentage of the ultimate tensile strength until stress-strain repeatability was observed (13:246). The need for this pre-conditioning of the sample materials was indicative of future work that would focus on the inclusion of a damage function into Schapery's model.

Smith and Weitsman modeled the mechanical response of a swirl-mat composite composed of randomly oriented strands of E-glass fibers embedded in a urethane matrix (26:301). The model predicted single-step creep and recovery using the process set forth in Schapery's model but also incorporated continuum damage and permanent deformation features which were necessary to represent the behavior of the composite.

The continuum damage theory accounted for severe microcracking under increasing loads in addition to overall reduction in stiffness (26:301). Model predictions were compared to experimental results of multi-step creep and recovery tests. The above process incorporated prediction methodology for material behavior within the viscoelastic regime, damage due to severe microcracking, and permanent strains upon load removal. The results revealed that it is possible to maintain the creep expression based upon power law, developed by Schapery, while introducing enhancements for additional behaviors.

Numerous other investigations have successfully captured the non-linear viscoelastic behavior of materials using variants of Schapery's model. These include efforts by Elahi and Weitsman on the mechanical response of P4 Chopped Glass/Urethane Resin Composite (7) and Jerina et al on the characterization of random fiber composites (10). In recent efforts, Balaconis characterized Schapery's model for BMI-5250-4 neat resin and concluded that the model performed well when the stress levels applied were in the range used for model characterization (2). In addition, when the prior stress rate was comparable to that used in model characterization experiments, the model was capable of predicting stepwise creep behavior (2).

Since its development, much research has been done on PMR-15 although most of it was focused on the thermo-oxidative stability and effects of aging (17, 27). As a result, most of these efforts do not pertain directly to this investigation. However, Marais and Villotreix did complete analysis and modeling of the creep behavior of the PMR-15 neat resin in the linear region. The model employed in this effort incorporated the retardation time concept with a four element rheological model, known as Burgers model (15).

Burgers model connects Maxwell and Kelvin models in series. The model was capable of predicting the creep compliance of PMR-15 for short loading times for the temperature range considered. The WLF equation was applied and predictions were extended to temperatures beyond those used in the model formulation; however, the predictions deviated significantly from experimental data (15). Westberry conducted an experimental investigation of the rate-dependent behavior and short-term creep of PMR-15 (29). Results revealed that rate dependence was not significant at elevated temperatures when conducting a simple tensile test. However, when examining the effect of prior stress rate on creep behavior proceeded by uninterrupted loading, significant rate dependence was observed.

Thesis Objective

The objective of this thesis is to characterize a nonlinear viscoelastic model based on Schapery's formulation using creep and recovery tests of PMR-15 neat resin at 288 °C. The model will be used to predict the experimental results obtained under single step test as well as multi-step creep test histories. The constitutive model predictions will be compared to experimental results to reveal the ability of the model to represent the material behavior while identifying any limitations of the model.

Further experimental investigation will be conducted to verify previous work involving the rate dependent and history dependent behavior of PMR-15. Effect of loading rate on monotonic stress-strain behavior will be explored in monotonic tests at several constant stress rates at 288 °C. Effect of prior stress rate on creep behavior will

be explored in creep tests preceded by uninterrupted loading to a target stress where loading rate will be changed from test to test. The ability of the model to take into account variation in stress rates and prior loading history will be explored.

III. Material and Specimen

This section will discuss in detail the material under investigation. The actual test specimens will then be discussed, including processing of the material, specimen shape and tabbing of the specimens.

Specimen Development

Processing

The PMR-15 neat resin panels were provided by the Air Force Research Laboratory's Materials and Manufacturing Directorate. A high purity PMR-15 imidized foam, commercially available from Cytec Industries, Inc, was crushed into powder with a hydraulic press (29:10). Neat resin panels were compression molded from the PMR-15 powder with a heat press. Prior to machining the specimens, the C-scans of all panels were examined and any defects were noted. To discern the impact of these defects, the behavior of certain specimens with defects were compared to those without. The mechanical testing of the various specimens revealed that no recognizable pattern was observed between the various qualities of specimens as reflected in the C-scans.

Specimen Geometry

A reduced gage section or dog bone shape was chosen for test specimens to ensure gage section failures during testing. Test specimens were machined from the PMR-15 neat resin panels at the Air Force Institute of Technology Machine Shop by two different methods. The first method involved a water-jet machine in which a highly pressurized

mixture of water and abrasive cuts the specimens. In the second method, specimens were cut using a diamond-saw. While the water-jet process required less time in machining the specimen, the diamond-grinding produced fewer defects. While defects in the grip section would not affect results, those occurring in the gage section were unacceptable. Specimens with machining defects in the gage section were not used in this investigation.

The thicknesses of the specimens were dictated by the panels from which they were cut. The average thickness of panels used was 3.81 mm while the range of thicknesses encountered in the specimens tested were from 3.29 to 4.46 mm. The specimen gage length was 17 mm, fully enabling placement of the extensometer rods with a 12.7 mm gage length. The specimens were stored at room temperature in the laboratory air. The specimen geometry is shown in Figure 21.

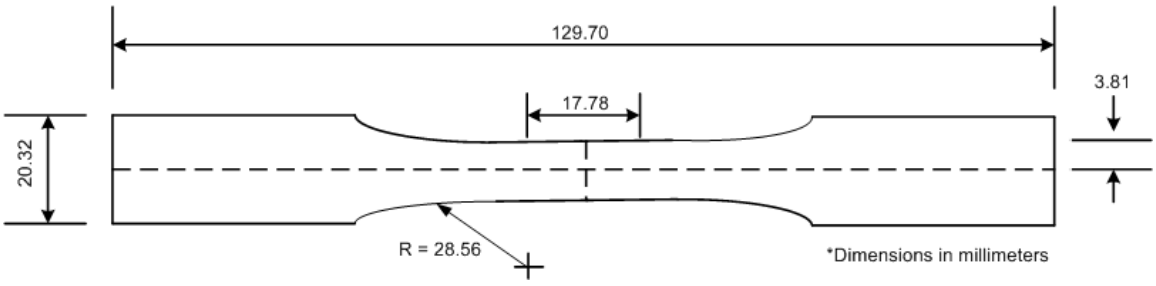

Figure 21: Test Specimen Geometry

Specimen Tabbing

All PMR-15 neat resin test specimens were tabbed using a glass fabric/epoxy material. The purpose of the tabs is to evenly transfer the load from the gripping wedge surface to the test specimen and to protect the gripping surface of the polymer. The glass fabric/epoxy material is chosen because it is a compliant material capable of providing

the desired load transfer. In addition, this material absorbs the surface damage inflicted by the hydraulic wedge grips. To apply the tabs to the specimen, the grip surface area of the specimen was cleaned free of debris. The tabs were then coated with an M-Bond Catalyst. After ample time for the catalyst to set in, 4 to 6 drops of M-Bond 200 Adhesive were applied to the tab. The tabs were placed onto the specimen and continuous pressure was applied for at least one minute to allow a strong bond to form. A tabbed specimen is shown in Figure 22.

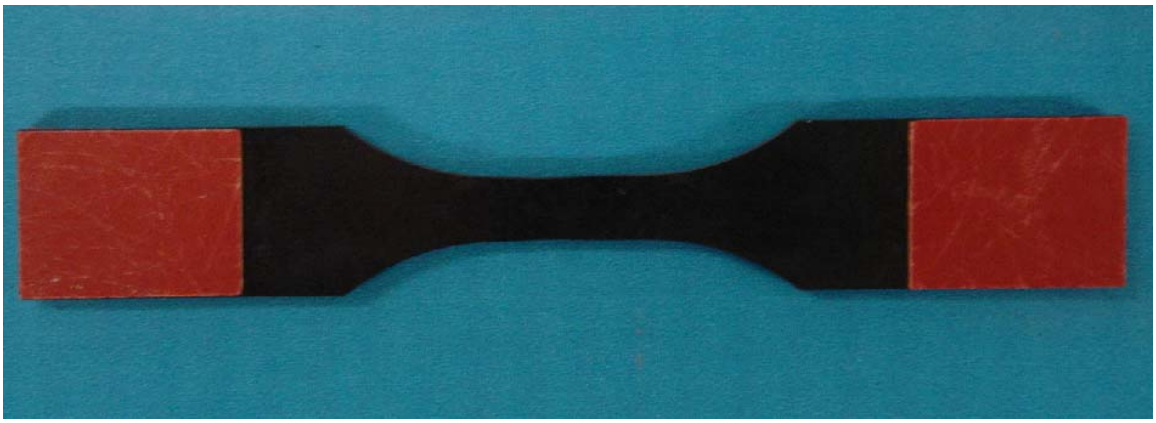

Figure 22: Tabbed PMR-15 Specimen

IV. Experimental Setup and Testing Procedures

This section describes the equipment setup and associated testing procedures used throughout experimentation.

Test Equipment

The mechanical apparatus necessary for testing included the servo hydraulic machine equipped with a chilled water system, the extensometer, the computer software, and the high temperature equipment.

Servo Hydraulic Machine

A vertically configured 810 Material Test Systems (MTS) servo hydraulic machine was utilized for all tests. The machine capacity was 13.3 kN (3 kips) whereas the maximum load reached during all testing of the PMR-15 resin was 0.8 kN (0.2 kips). The hydraulic machine employed MTS 647.02B hydraulic wedge grips capable of applying a pressure of up to 21 MPa at each end of the specimen. The grip pressure throughout testing of the PMR-15 neat resin was set to 2.76 MPa. Each grip included a pair of flat wedges coated with surf alloy to provide additional friction at the gripping surface. The purpose of the coating is to prevent the specimen from slipping throughout mechanical testing. Additionally, each wedge was equipped with an inlet and outlet to allow cooling water to pass through the grips during testing to prevent overheating of the grips region. The cooling water was supplied by a NESLAB model HX-75 chilled water

system. The chiller regulated the temperature of the cooling water and maintained it between 9 and 24^{o}C. This system was used during elevated temperature tests. Finally, an anti-rotation device was fitted onto the machine actuator to maintain purely tensile loading. Figure 23 depicts the test setup with the servo hydraulic machine, the furnace, and the extensometer assembly.

Figure 23: 3 KIP MTS Hydraulic Machine

Extensometer

An MTS model 632.53E-14 Axial Extensometer for High-Temperature Testing was used for strain measurement. The extensometer includes two 3.5 mm diameter alumina extension rods and has a gauge length of 12.7 mm (0.5 in). Each extensometer rod end

has a conical point which allows it to maintain contact with a dimpled specimen. For this reason, two indentations were placed on each specimen with the standard dimpling tool provided by MTS, shown in Figure 24.

Figure 24: MTS Dimpling Tool

The extensometer tips are placed into the dimples on the specimen to ensures that no slipping of the extensometer occurs during testing. The use temperature for the extensometer is up to 650 ^{o}C without air cooling or up to 1200 ^{o}C with air cooling. It is capable of measuring strains in the range of -10 % to +20%. The extensometer, with the extension rod contacting the specimen, is held in place by a spring-loaded assembly which places a 3 N contact force per rod onto the specimen. The extensometer assembly also includes a heat shield to protect the extensometer from the test conditions. The extensometer assembly is shown in Figure 25.

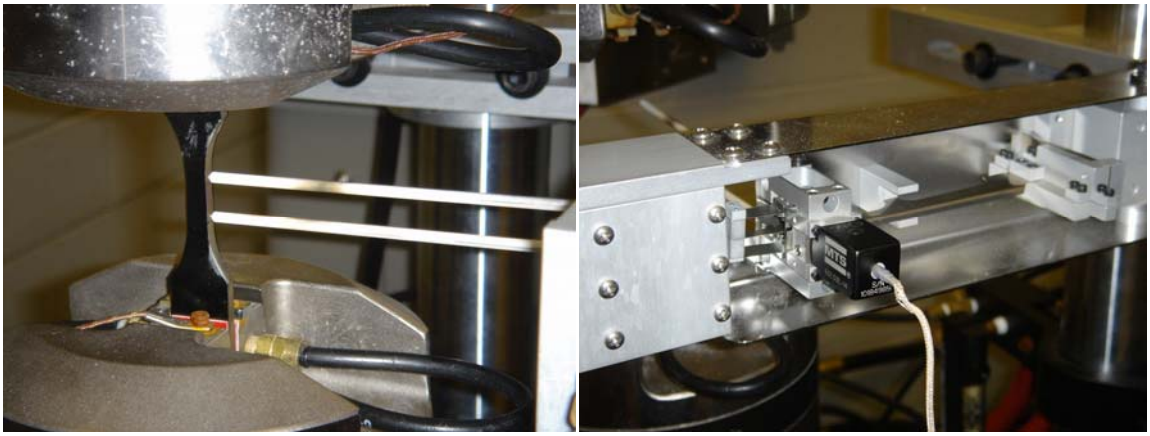

Figure 25: MTS High Temperature Axial Extensometer Assembly

Computer Software

The MTS Teststar II digital controller was used for input signal generation and data acquisition. The MTS Station Builder application was used to create a configuration file specific to the performance of the PMR-15 neat resin. This application allocates controller resources, specifically the input of the appropriate tuning parameters for a material. The MTS Station Manager application was used to perform routine test operations such as controlling hydraulic power, setting station interlock limits, manually controlling the force or displacement, monitoring the input and output signals from the controller, and running tests. As a subprogram of the Station Manager, the MultiPurpose Testware (MPT) application was used to build test procedures by defining activities and assigning triggering relationships between them. Such activities include loading the specimen, heating the test specimen, maintaining a particular force level, and acquiring data. The construction of various programs within the MPT software allowed for automated testing and data acquisition. Figure 26 shows an example of an MPT test program used during a creep test.

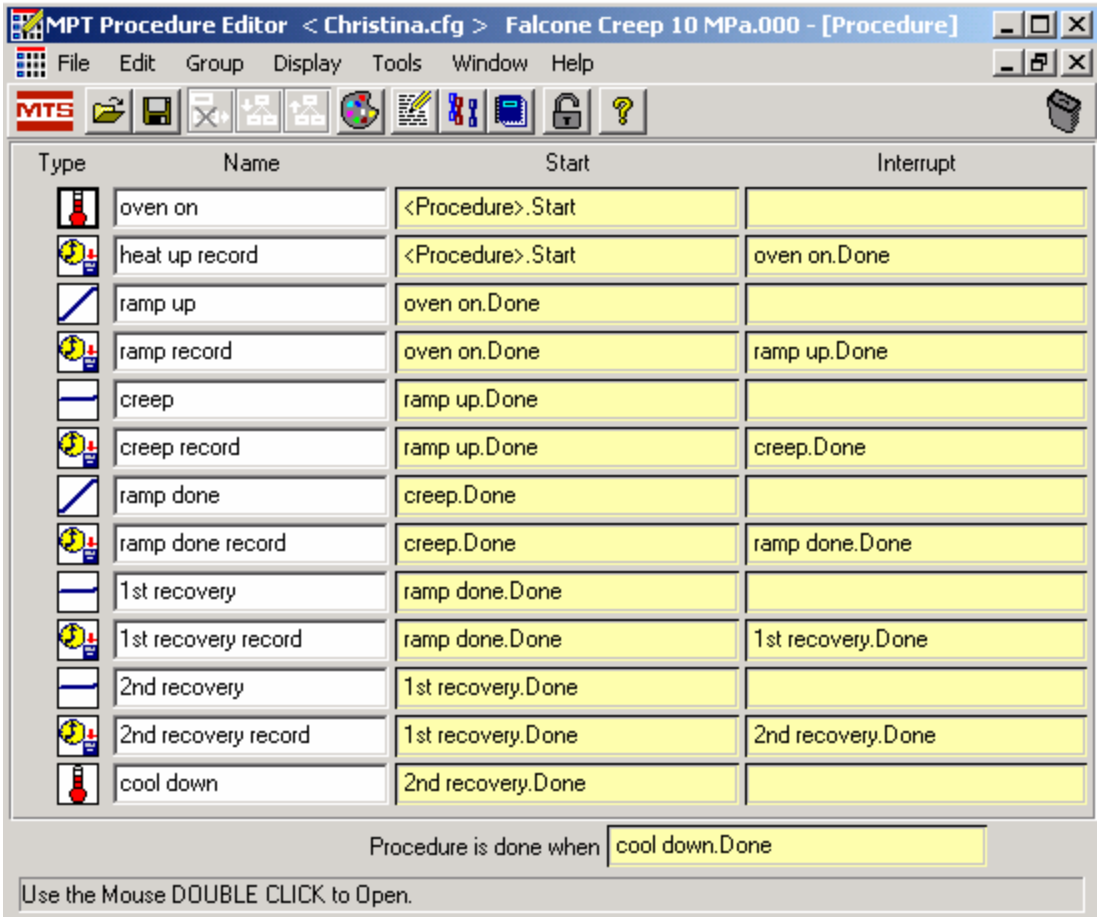

Figure 26: MPT Creep Test Procedure

The following signals were recorded during each test: time (s), command temperature (^{o}C), displacement (mm), force command (N), force (N), and strain (m/m). It was important to compare the force command with the actual force applied throughout each phase of the test to ensure the test was accurately executed. The frequency of data acquisition was dependent on the test history and the resultant deformation in the specimen. During the heating phase, in which the temperature of the test specimen was elevated from 23 to 288 ^{o}C, it was unnecessary to collect a large number of data points as

the primary interest was the overall thermal expansion of the material after reaching the target temperature. On the contrary, during a loading phase when the stress applied to the specimen was increased from zero to the target creep stress, the material deformation was of primary interest and the frequency of data collection was increased. In this case, the data collection frequency was also dependent on the loading rate. For example, a loading rate of 3 MPa/s required data collection at a much higher frequency than that of 0.01 MPa/s because the changes in stress and strain were much more gradual in the latter case. It was also important to avoid collecting data at an excessive rate as this caused great difficulty in transferring data to a program for interpretation. The data acquisition frequency used for various activities throughout testing is shown in Table 2.

Table 2: Data Collection Frequencies used for Various Testing Activities

Activity	**Data Collection Frequency (time between data points)**
Heat up to Use Temperature of 288 ^{o}C	1 min
Load/Unload Rate = 3 MPa/s	0.01 s
Load/Unload Rate = 1 MPa/s	0.01 s
Load/Unload Rate = 0.01 MPa/s	1 s
Creep	1 s
Recover for < 3 h	1 s
Recover for > 3 h	3 s

High Temperature Equipment

An MTS 653 Furnace was used for elevated temperature tests. The furnace has a center split design and an operating range of 100 to 1400 ^{o}C. The furnace could be opened and shifted away from the test area during specimen and extensometer setup and closed around the specimen for testing. Each furnace half contained a silicon carbide heating element surrounded by silica foam. The insulation material was carved to allow for a close fit around the specimen and extensometer rods. A 19 mm portion of the test specimen is encased by the furnace and held at the test temperature. The temperature is controlled by an MTS 409.83 Temperature Controller Unit. This unit displays the temperature of each furnace half and the current input temperature. A feedback loop between the controller and a S-type thermocouple located in the right furnace half maintained the furnace temperature throughout testing. Variation in temperature between the right and left halves of the furnaces was limited to 5 ^{o}C. Figure 27 shows the temperature controller and the right portion of the furnace in place next to the specimen and the extensometer.

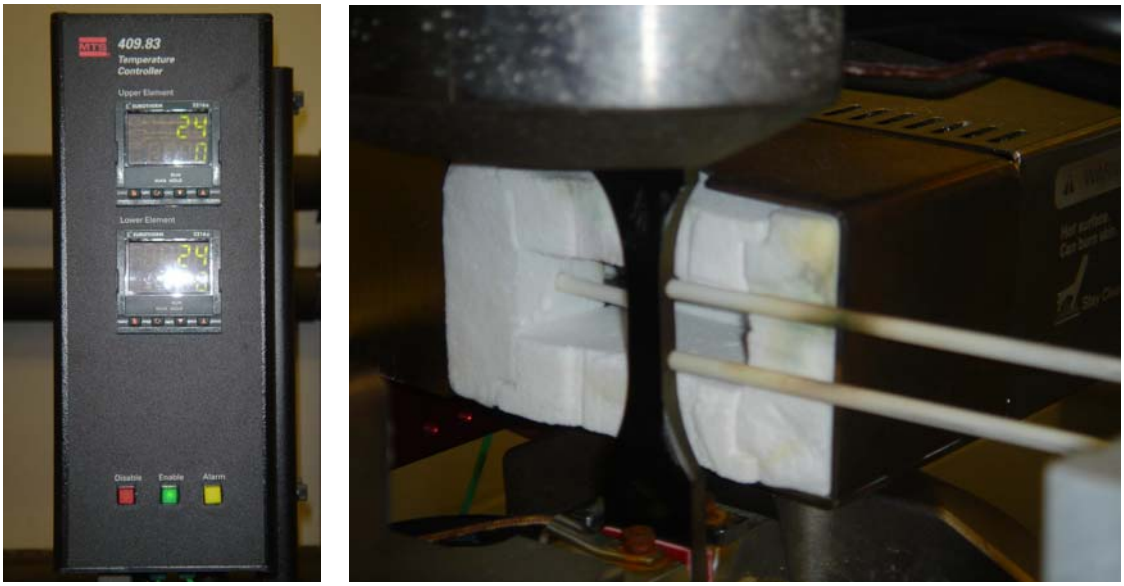

Figure 27: Temperature Controller and Right Portion of Furnace

Experimental Procedures

Test Temperature

Temperature calibration was performed to determine the input temperature needed to produce the desired specimen temperature of 288 ^{o}C. Two K-type thermocouples were fixed onto a PMR-15 neat resin specimen. The thermocouples were secured with Kapton tape and wire to ensure contact between the thermocouples and the specimen throughout calibration. The specimen was carefully situated in the machine grips with the thermocouple wires exiting the oven through the openings allowed for the extensometer rods. The thermocouples were then connected to an Omega Engineering, Inc. OMNI-CAL-SA-110 portable, two-channel temperature sensor to monitor the specimen temperature in both locations. The oven temperature was elevated to 150 ^{o}C at a rate of

1.5 ^{o}C/min and manually increased thereafter. The manual increases were accompanied by intermittent dwelling periods of 10 min to allow the specimen to soak at the higher temperatures. This was necessary to ensure that the target temperature was not inadvertently exceeded. A set point of 253 ^{o}C was determined, which produced the desired specimen temperature of 288 ^{o}C. After reaching the target temperature, the oven was allowed to dwell for 2.5 h to ensure that the specimen temperature had thermally equilibrated. During this period, the temperature readings between the top and bottom thermocouples were within ± 4^{o}C of the desired temperature.

Test Procedures

Numerous preparatory steps were completed prior to all testing. First, the Function Generator application was used to cycle the actuator in displacement control for at least 30 min. This was necessary to allow the machine to properly warm up. Next, the specimen gage section width and thickness were measured and recorded. These dimensions were used to calculate the load levels corresponding to the desired stress levels used throughout testing. The MPT test procedure was then updated to reflect these load values. The dimples were then added to the specimen. The technique for dimpling the specimen included marking the extensometer contact points on the specimen and gently tapping the indentations into the specimen with the dimpling tool and a hammer. Next, the grip pressure was set at the appropriate value and the temperature controller enabled. The specimens were aligned in the machine utilizing the guides on the rear of the grip area. The load cell was then brought to the zero displacement level and the top portion of the specimen was locked into the grip. After zeroing out the load cell and

switching to force control, the bottom portion of the specimen was gripped. The extensometer was then mounted and the oven was closed around the specimen. The interlocks were then set to disable the hydraulic power if displacement and/or force exceeded expected limits. Finally, the displacement and strain channels were zeroed out before beginning the test. The machine was kept in force control at zero force at the onset of testing to ensure that the specimen was allowed to freely expand during the heat up phase. Finally, the test description, specimen label, procedure name, specimen dimensions, and the force values used throughout the test were recorded prior to beginning the test.

Test Descriptions

All testing of the PMR-15 specimens was conducted at the temperature of 288^{o}C in laboratory environments. Therefore, the first step in every test procedure was to heat the specimen up to the elevated temperature. This was achieved at a rate of 2^{o}C/s. In addition, each specimen was allowed to soak at the target temperature for 30 min prior to testing. This was necessary to ensure that the specimen was in thermal equilibrium and that all thermal expansion had ceased.

Monotonic Tension Tests

Three monotonic tensile tests to failure were performed on PMR-15 specimens. The first tensile test was performed in displacement control at a rate of 0.025 mm/s on a specimen with no dimples. This test was important because further testing on dimpled specimens revealed that the fracture typically originated from one of the dimple

locations. The extensometer was not used and strain data was not collected for this case as the dimples are necessary to maintain appropriate extensometer contact. The subsequent tensile tests were performed in stress control at rates of 1 MPa/s and 0.01 MPa/s. The main focus of the tensile tests was to determine an ultimate tensile strength from which the stress levels in creep tests could be determined.

Creep and Recovery Tests

Two creep tests were performed in stress control at load up rates of 1 MPa/s and 0.01 MPa/s. The specimens were loaded to creep stress level at the constant stress rate, held at the creep stress for a duration of 6 h, unloaded to zero stress at the same constant stress rate, and allowed to recover for 18 h after removal of the load. The creep stress level, 20 MPa, corresponded to 44% of the maximum tensile stress reached by the undimpled specimen in the tensile test described above. These tests allowed for the comparison of ε_{load}, the strain accumulated during load up to the creep stress level; ε_{creep}, the strain accumulated during the creep period; ε_{unload}, the strain removed during unloading; ε_{rec}, the amount of strain recovered at zero stress; and ε_{p}, the permanent strain remaining after recovery was saturated. In addition, the loading and unloading moduli were compared to determine if significant damage was inflicted to the material during the creep period.

Monotonic Load and Unload followed by Recovery

Two monotonic load and unload tests were performed in load control at rates of 1 MPa/s and 0.01 MPa/s followed by recovery at zero stress for 12 h. The maximum stress

level reached was 20 MPa. The loading and unloading moduli, the recovery strain, and the permanent strain remaining after recovery were compared for each rate.

Stepwise Creep Test

The stepwise creep test is schematically depicted in Figure 28. This test involved monotonic loading and unloading at constant stress rates with intermittent creep periods of 1 hour duration. Two stepwise creep tests were performed in load control at rates of 1 MPa/s and 0.01 MPa/s. Creep periods were introduced at 15 and 20 MPa. After the final unloading to zero stress, the specimen was allowed to recover for 12 h. The results of this test demonstrate the effect of prior stress history on creep and recovery behavior.

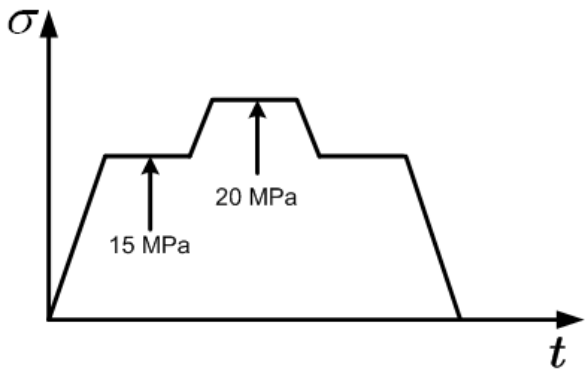

Figure 28: Stress as a function of time for stepwise creep test

Model Characterization Tests

Numerous creep-recovery tests were employed to characterize the nonlinear viscoelastic behavior of PMR-15 using Schapery's model. The goal of these tests was to subject the specimen to an instantaneous increase in stress followed by creep at various

stress levels. Similarly, the removal of the load would occur instantaneously. Following unloading, the specimen is allowed to recover at zero stress for some duration of time. A schematic of the creep and recovery tests used in model characterization is presented in Figure 29.

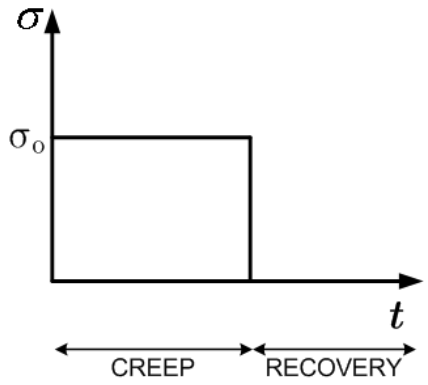

Figure 29: Stress as a function of time for creep and recovery tests used in model characterization tests

The loading and unloading of the applied stress cannot be accomplished in a step-wise manner. The stress rate of 3 MPa/s was used to limit the loading/unloading time to less than 15 s. The creep stress level corresponded to percentages of the maximum tensile stress of 45 MPa reached by the undimpled specimen in the tensile test. The percentages were $\approx$11, 22, 33, 44, and 55 percent. Each creep and recovery test was conducted three times.

All testing is summarized in Table 3. Once again, each test was conducted at a temperature of 288 ^{o}C.

Table 3: Test Types and Test Specifications Summary

Test Type	Load/Unload Rate (MPa/s)	Stress Level (MPa)	% of UTS	Creep Time (h)	Recovery Time (h)
Monotonic Tension	0.025 mm/s	--	--	--	--
Monotonic Tension	1	--	--	--	--
Monotonic Tension	0.01	--	--	--	--
Creep – Recovery	1	20	~ 44	6	18
Creep – Recovery	0.01	20	~ 44	6	18
Monotonic Load/Unload	1	20	~ 44	--	12
Monotonic Load/Unload	0.01	20	~ 44	--	12
Stepwise Creep	1	15,20,15	~33,44,33	1	12
Stepwise Creep	0.01	15,20,15	~33,44,33	1	12
Model Characterization*	3	5	~11	0.5	1.5
Model Characterization*	3	10	~22	0.5	5
Model Characterization*	3	15	~33	0.5	5
Model Characterization*	3	20	~44	0.5	5
Model Characterization*	3	25	~55	0.5	5

* Each model characterization test was triplicated.

V. Results and Discussion

Thermal Strain

All tests were conducted at a temperature of 288 ^{o}C and the thermal stain value, ε_{th}, was recorded for each test specimen. The coefficient of thermal expansion, α, could then be determined from the following relationship:

$$\varepsilon_{th} = \alpha \cdot \Delta T \tag{76}$$

where ΔT is the temperature change in ^{o}C. The temperature change was determined as the difference between the final specimen temperature of 288 ^{o}C and the initial specimen temperature of 23 ^{o}C, which was the nominal ambient room temperature in all tests. These results are presented in Table 4. The average value for the coefficient of thermal expansion was 51.50 x 10^{-6}/ ^{o}C and the associated standard deviation was 2.82 x 10^{-6}. The average values of coefficient of thermal expansion for each panel used throughout testing were well within a standard deviation from the total average. Specimen F-1 was omitted from these calculations due to the fact that it was not dimpled and strain data was not collected from this test.

Table 4: Linear Coefficient of Thermal Expansion

Specimen Number	Panel Number	Test Type	ε_{th} (m/m)	α ($10^{-6}/^{o}C$)
F-1	1	Monotonic Tension	N/A*	N/A*
F-2	1	Monotonic Tension	0.01430	53.97
F-3	1	Monotonic Tension	0.01394	52.60
F-4	1	Model Characterization	0.01550	58.48
F-5	1	Model Characterization	0.01512	57.06
F-6	1	Model Characterization	0.01449	54.68
F-7	1	Model Characterization	0.01351	50.98
F-8	1	Model Characterization	0.01358	51.23
F-9	1	Model Characterization	0.01412	53.28
F-10	1	Model Characterization	0.01446	54.57
F-11	1	Model Characterization	0.01348	50.87
F-12	1	Model Characterization	0.01339	50.52
F-13	1	Model Characterization	0.01325	49.99
F-14	1	Model Characterization	0.01317	49.71
F-15	12	Model Characterization	0.01495	56.42
F-16	12	Model Characterization	0.01340	50.57
F-17	12	Model Characterization	0.01396	52.67
F-18	12	Model Characterization	0.01401	52.85
F-19	13	Model Characterization	0.01313	49.56
F-20	1	Model Characterization	0.01336	50.42
F-21	2	Model Characterization	0.01231	46.44
F-22	2	Model Characterization	0.01367	51.58
F-23	2	Model Characterization	0.01323	49.91
F-24	2	Model Characterization	0.01333	50.32
F-25	2	Monotonic Load/Unload	0.01313	49.53
F-26	2	Monotonic Load/Unload	0.01355	51.13
F-27	2	Creep – Recovery	0.01292	48.75
F-28	2	Creep – Recovery	0.01307	49.30
F-29	2	Stepwise Creep	0.01245	47.00
F-30	2	Stepwise Creep	0.01191	44.95

* specimen was undimpled

Monotonic Behavior

Three monotonic tensile tests to failure were performed on PMR-15 specimens to determine preliminary values of the ultimate tensile strength (UTS) and modulus of elasticity at the use temperature. In addition, the effect of stress rate on each of these properties was evaluated. The monotonic tensile test results are summarized in Table 5.

Table 5: Monotonic Tensile Test Results

Specimen Number	Panel Number	Loading Rate	UTS (MPa)	E (GPa)	ε_f (%)	Time to Failure (min)
F-1	1	0.025 mm/s	48.48	N/A*	N/A*	16
F-2	1	1 MPa/s	30.49	1.42	3.65	0.53
F-3	1	0.01 MPa/s	30.38	1.42	6.13	51

* specimen was undimpled, no strain data was recorded

The first tensile test, performed in displacement control at a rate of 0.025 mm/s on a specimen without dimples, produced an UTS of 48.48 MPa. The subsequent tensile tests, performed in load control at rates of 1 MPa/s and 0.01 MPa/s, produced UTS values of 30.49 MPa and 30.38 MPa, respectively. The value of the UTS at room temperature was not measured in this experiment; however, the room-temperature UTS value provided by Cytec Industries Inc. is 38.6 MPa. It is apparent that the introduction of dimples into the virgin specimens resulted in a 37% decrease in the ultimate tensile strength. This is due to the fact that the dimples act as crack starters. However, it is important to recognize that the UTS measurement is not the primary focus of this research, while accurate strain measurements were of greater concern and more importance. Therefore, dimples were

introduced to all remaining specimens to ensure that the extensometer remained in contact with the material.

The modulus of elasticity was 1.42 GPa, for both tests performed in load control with loading rates of 1 MPa/s and 0.01 MPa/s. This modulus was determined by calculating the slope of the stress-strain curve in the linear region. In comparison, the modulus of elasticity at room temperature provided by Cytec Industries was 3.9 GPa. These observations reveal that the modulus of elasticity decreases by 64% as the temperature increases from 23 to 288 ^{o}C. Similarly, the average value of the failure strain, ε_f, was 4.89% for the tensile tests conducted at 288 ^{o}C whereas the failure strain at room temperature provided by Cytec Industries was 1.5%. The dependence of the modulus, E, and failure strain, ε_f, on temperature is anticipated for a polymeric material. As temperature rises, polymers' behavior changes from glass-like to rubber-like. At lower temperatures, the stiffness is dependent on stored elastic energy and the deformation is associated with small molecule displacements. The molecular chains have an increased flexibility at higher temperatures due to increased free volume.

The stress-strain curves obtained for the PMR-15 neat resin at 288 ^{o}C are shown in Figure 30. Both curves display nearly linear elastic behavior near the origin and are practically indistinguishable in that range. The approximate departure from linearity occurs at a stress of approximately 8 MPa and strain of 0.5%. After transition to the inelastic region, the stress-strain curves obtained at each loading rate become noticeably different. The strain values at corresponding stress levels for tests performed at different loading rates are compared to assess the rate dependence. Figure 30 reveals that the

strain value corresponding to 30 MPa is 3.65% for the stress rate of 1 MPa/s and 6.13% for the rate of 0.01 MPa/s. The slower stress rate of 0.01 MPa/s causes a 68% increase in ε_f compared to that achieved at a rate of 1 MPa/s. As expected, the effect of stress rate on Young's modulus was negligible as shown by the overlapping curves in the initial loading portion of Figure 30.

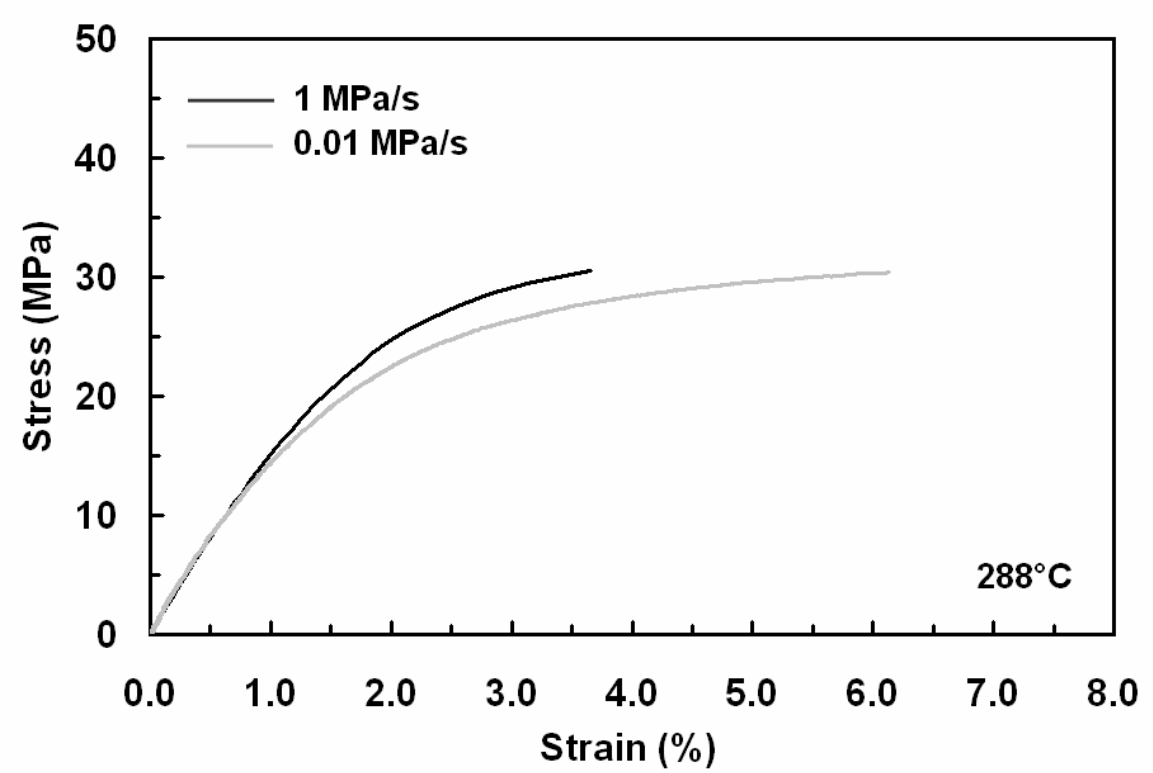

Figure 30: Tensile stress-strain curves for PMR-15 neat resin at 288 ^{o}C

Effect of Prior Stress Rate on Creep and Recovery Behavior

Two creep and recovery tests were performed in load control with loading/unloading magnitudes of 1 MPa/s and 0.01 MPa/s. In these tests, the stress was increased monotonically to the creep stress level at the aforementioned rates and then held constant for a period of 6 h (21,600 s). The specimen was then unloaded to zero load at the same stress rate and allowed to recover for a period of 18 h (64,800 s). These tests reveal the effect of loading/unloading stress rate on creep and recovery behavior. Results are summarized in Table 6.

Table 6: Effect of Prior Stress Rate on Creep and Recovery Response

Loading Rate (MPa/s)	ε_{load} **(%)**	ε_{creep} **(%)**	ε_{unload} **(%)**	ε_{rec} **(%)**	ε_{p} **(%)**
1	1.30	6.67	1.55	2.19	4.20
0.01	1.82	4.28	1.17	1.40	3.53

As seen in Table 6, a decrease in the loading rate by two orders of magnitude results in a 40% increase in strain accumulated during the load up period, ε_{load}. These results are congruent with those obtained in the monotonic tensile tests which revealed that a slower monotonic loading rate to a desired stress level results in a larger accumulation of strain. Next it is important to examine the influence of prior stress rate on creep strain accumulation, ε_{creep}. Creep strain accumulations of 6.67 and 4.28% were obtained in tests conducted with prior stress rates of 1 MPa/s and 0.01 MPa/s, respectively. Results in Figure 31 demonstrate that the creep behavior was considerably influenced by the prior stress rate. Westberry conducted a similar investigation to examine the influence of prior

stress rate on creep strain at 25 MPa (29:27). Creep strain accumulations of 2.83, 2.06, and 1.45% were obtained in tests conducted with prior stress rates of 0.75, 0.075, and 0.0075 MPa/s, respectively. These results support Westberry's qualitative findings on PMR-15 which revealed that "creep strain accumulation increases nonlinearly with increasing prior stress rate" (29:27). Discrepancies in quantitative results may be attributed to the fact that the specimens used for testing in each case were cut from panels manufactured at different times. These panels were likely formed from different batches of PMR-15 resin. In addition, the panels were subjected to different post-cure heat treatments that may have influenced the material properties.

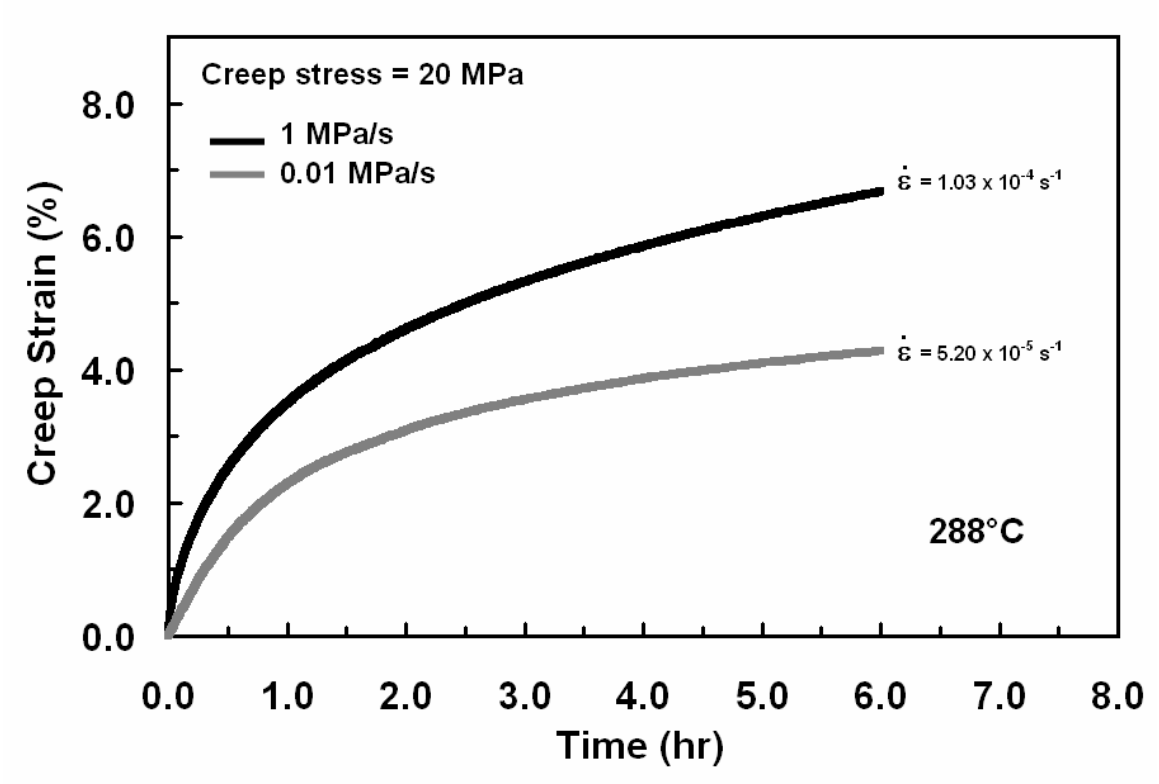

Figure 31: Effect of prior stress rates of 1 MPa/s and 0.01 MPa/s on 6 hour creep strain as a function of time

In order to determine the creep phases that PMR-15 undergoes, the creep rate is determined as a function of time. Comparison of results in Figure 32 with the creep phases depicted in Figure 1 reveals that PMR-15 neat resin tested at 288 ^{o}C, with a prior loading rate of 1 MPa/s, exhibits primary and secondary creep. Primary creep occurs over the first 5 h of the creep test. This is evident as the creep strain rate is decreasing throughout this period. During the secondary creep phase the creep strain rate is nearly constant. Similar analysis of the creep behavior associated with a prior loading rate of 0.01 MPa/s reveals that it transitions to secondary creep phase at approximately 4 h.

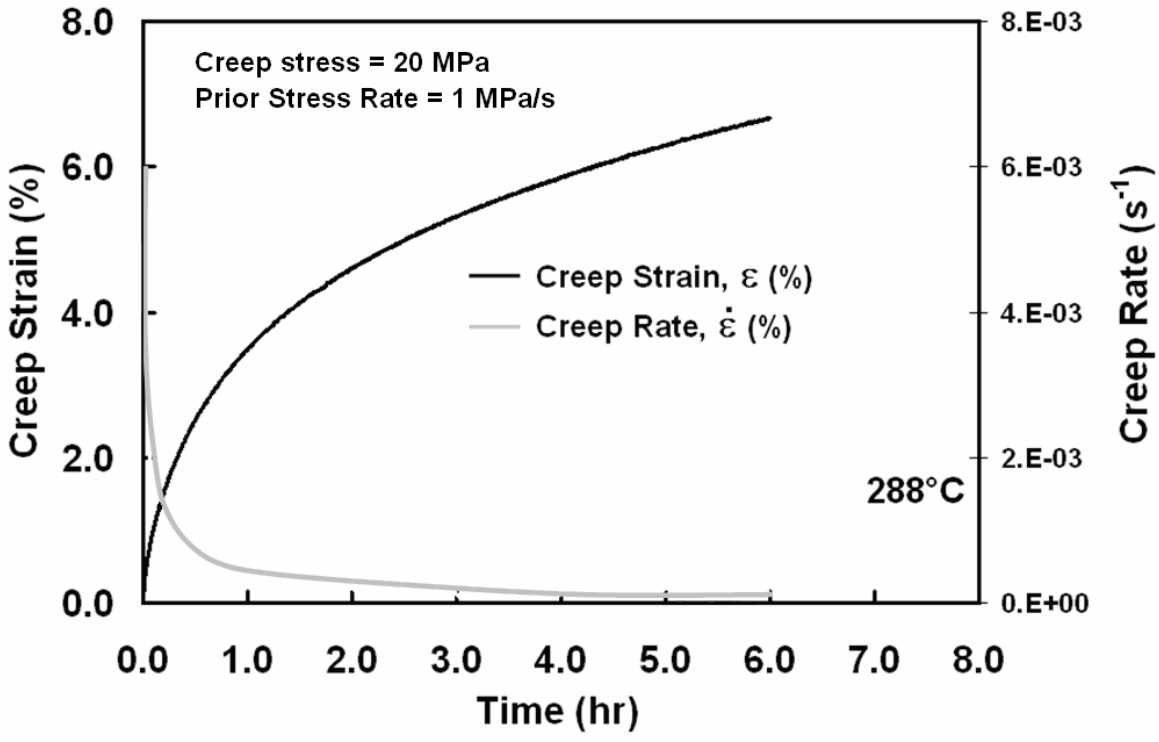

Figure 32: Creep Strain and Creep Rate as a function of time for 6 hour creep test with prior loading of 1 MPa/s

The secondary creep strain rates are calculated by examining a portion of the creep strain vs. time curve and plotting a best-fit linear trend line through the data. As shown in Figure 33, the tests with different prior stress rates achieved secondary creep rates that varied by an order of magnitude with the higher prior stress rate resulting in larger creep rate. Westberry reported that creep tests conducted with varying prior stress rates resulted in secondary creep rates of the same order of magnitude (29:28).

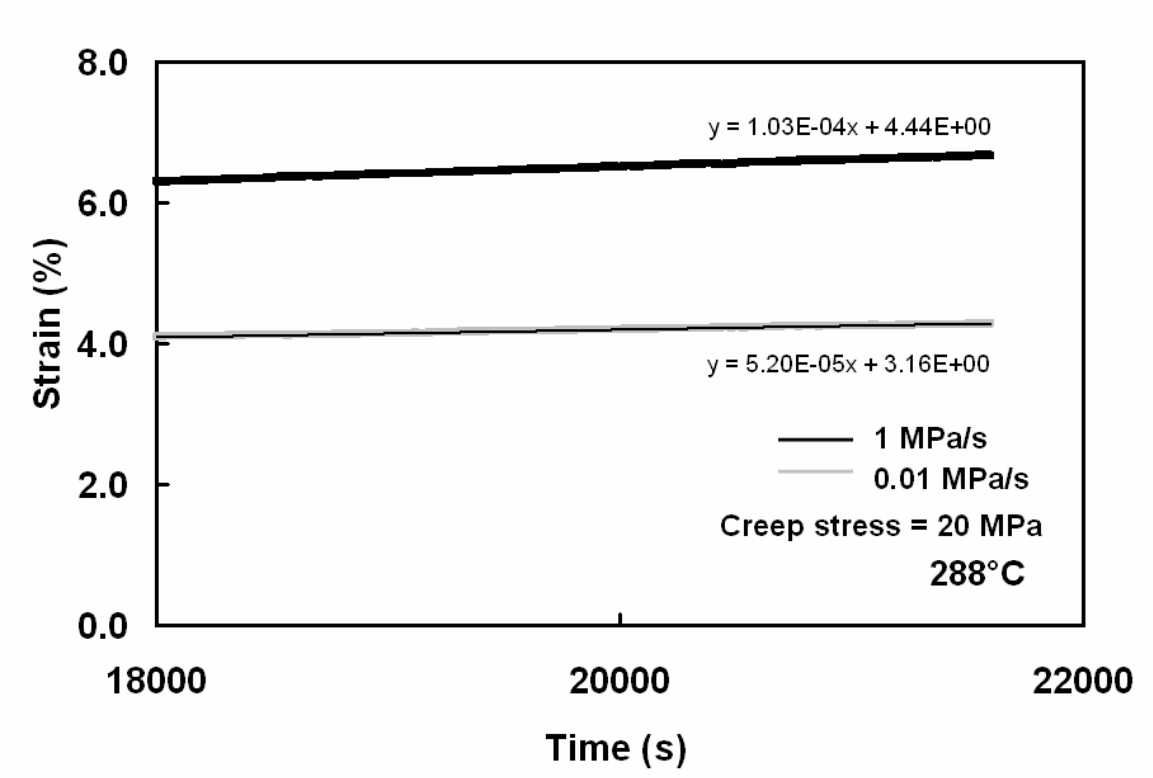

Figure 33: Portions of creep strain as a function of time used to determine the secondary creep rates.

After completion of the creep tests, the specimens were unloaded to zero stress and allowed to recover for 12 h. The strain removed during unloading, ε_{unload}, does not indicate a strong dependency on the unloading rate. For the 1 MPa/s case, the amount of strain removed during unloading was more than the amount of strain originally accumulated during loading. However, for the 0.01 MP/s case, the amount of strain removed during unloading was less than that gained during loading.

Finally, it is possible to examine ε_{rec}, the amount of strain recovered at zero stress; and ε_p, the permanent strain remaining after recovery for each stress rate. The value of ε_{rec} was measured as 2.19% for the faster prior stress rate and 1.40% for the slower rate; however, it is necessary to evaluate these values with consideration of the strain values at the initiation of the recovery period. For that reason, the recovery strain is presented as a percentage of initial strain at the beginning of the recovery phase. The recovery phase begins after complete removal of the applied stress during unloading.

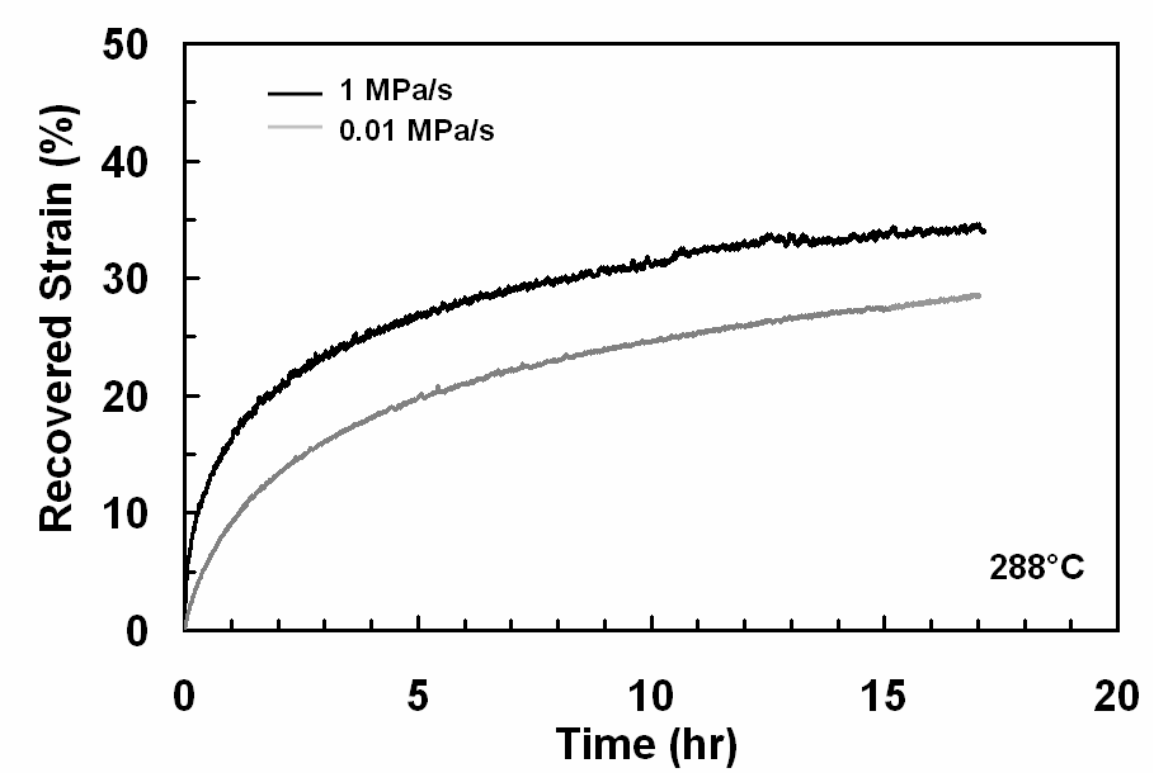

Figure 34: Recovered strain shown as percentage of the initial strain value at beginning of recovery period following creep at 20 MPa for various prior stress rates.

Figure 34 shows that the specimen subjected to a higher prior stress rate recovers a greater percentage of the strain measured immediately after unloading. Both specimens fail to achieve full recovery (100%) and a permanent strain, ε_p, remains after 18 h of recovery. The actual recovery curves are presented in Figure 35. It is apparent that recovery has nearly saturated after 18 h, as the recovery curves approach asymptotic values. As a result, allowing more time would not result in significant additional recovery.

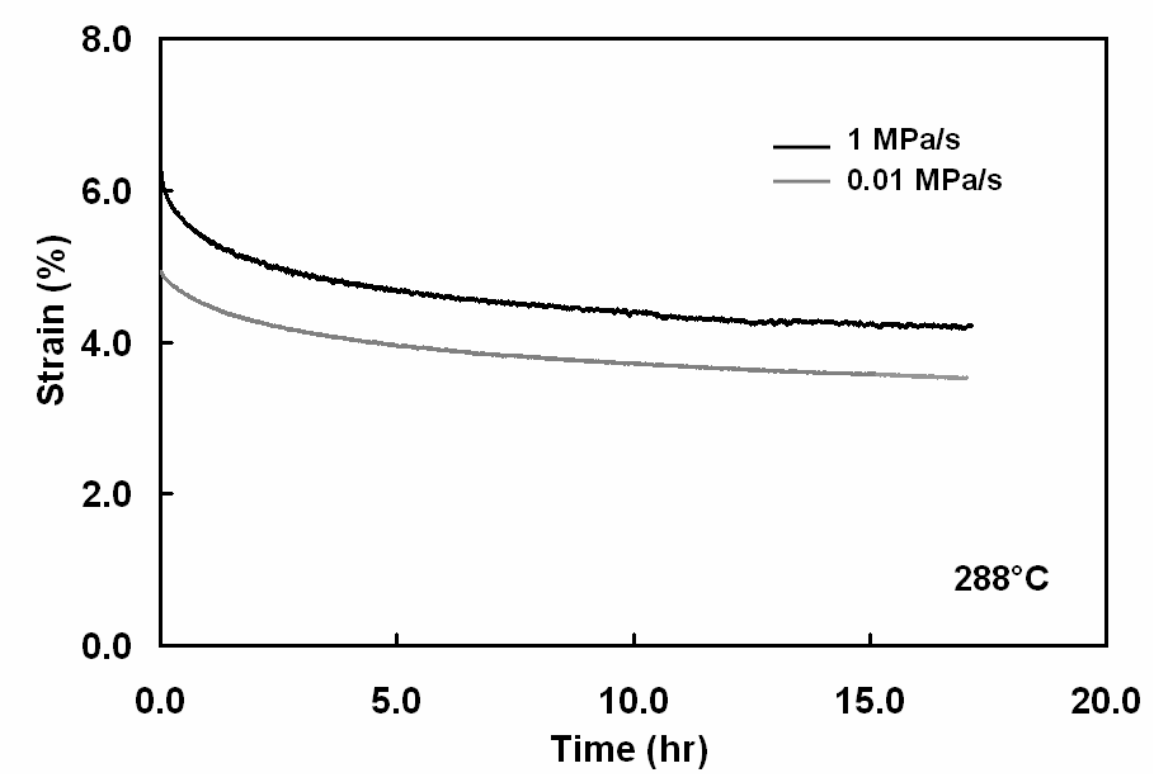

Figure 35: Recovery at zero stress following creep at 20 MPa for various prior stress rates.

The loading and unloading moduli obtained at each rate were compared as an additional means for accounting for the permanent strain. As shown in Table 7, the loading moduli are 37% and 59% greater than the unloading moduli for the 1 MPa/s and 0.01 MPA/s loading rates, respectively. Therefore, the 6 h creep test at 20 MPa causes a considerable reduction in stiffness, indicating that damage had developed in the material.

Table 7: Creep Test Loading and Unloading Moduli

Loading Rate (MPa/s)	Loading Moduli (GPa)	Unloading Moduli (GPa)
1	1.59	1.16
0.01	1.10	0.69

The results of the creep and recovery tests conducted on PMR-15 at 288^{o}C indicate that stress rate has a varying effect on the strain accumulation throughout each segment of the test. The amount of strain accumulated during loading, ε_{load}, was influenced by the load up rate, with greater strain resulting from the slower rate. The creep behavior at 20 MPa depended on the prior stress rate. The amount of strain recovered during unloading was negligibly influenced by the stress rate. The magnitude of the percent change in strain recovered at zero stress increased with increasing magnitude of prior stress rate.

Monotonic Loading and Unloading followed by Recovery

The effect of stress rate on monotonic loading, unloading, and recovery behavior was studied by loading the specimen to 20 MPa, unloading the specimen to zero stress, and holding the specimen at zero stress level for 12 h. This test was performed using stress rates of 1 MPa/s and 0.01 MPa/s at 288 ^{o}C.

The stress-strain curves obtained on the loading and unloading paths for rates of 1 MPa/s and 0.01 MPa/s are compared in Figure 36 and Figure 37. It should be noted that the modulus values presented in these figures were calculated as the slope of the stress-strain curves within the linear ranges. For the faster stress rate, shown in Figure 36, the

stress-strain curve remained nearly linear until approximately 3 MPa. Past this stress level the slope of the curve slowly decreases until the maximum stress level of 20 MPa is reached. During unloading, the stress-strain curve is initially non-linear but follows a nearly linear path as the stress level decreases from 13 MPa to zero stress.

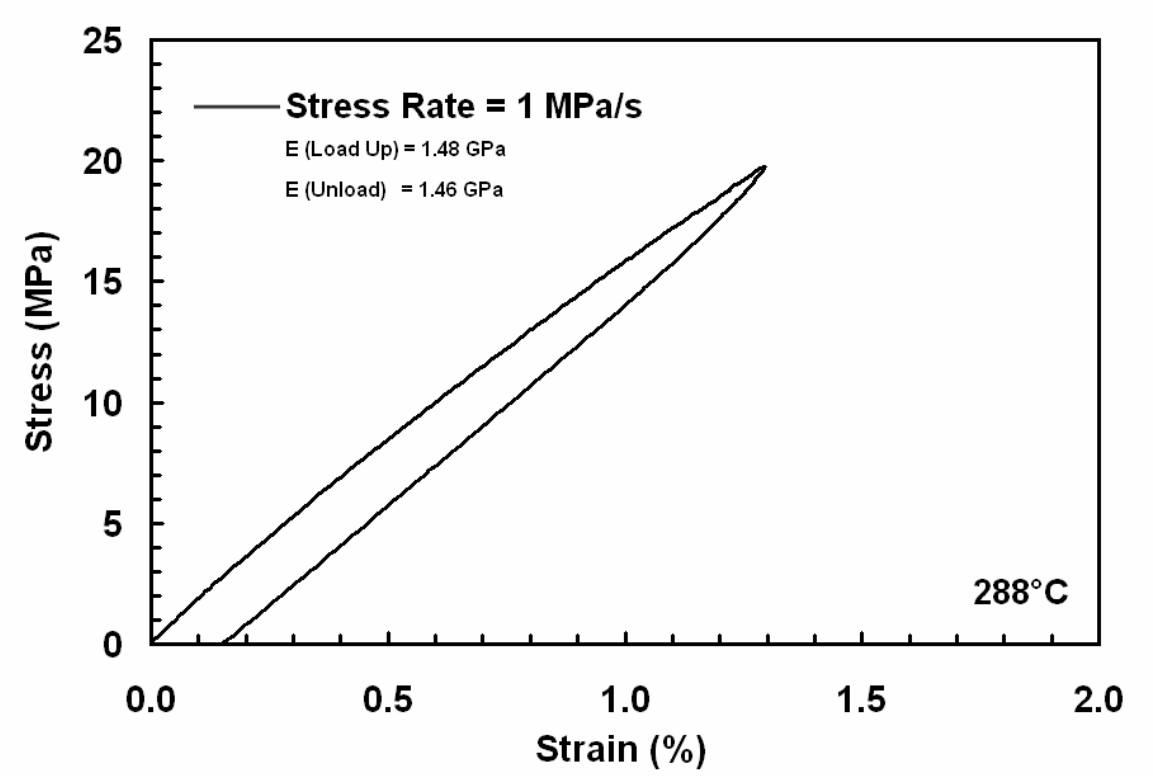

Figure 36: Loading and unloading of PMR-15 neat resin at 288 ^{o}C at a rate of 1 MPa/s

For the slower prior stress rate, shown in Figure 37, the stress-strain curve displayed an extremely small linear range up to approximately 2 MPa. Thereafter, the increase in stress resulted in a non-linear increase in strain. Upon unloading, as the stress was decreasing the strain continued to accumulate. An additional 0.5% of strain was accumulated during unloading from 20 MPa to 16 MPa. After the stress reached

approximately 15 MPa, the strain level began to decrease. A linear unloading path is not reached until very small stress levels (less than 4 MPa). This curved unloading is a distinguishable feature observed at the slower stress rate.

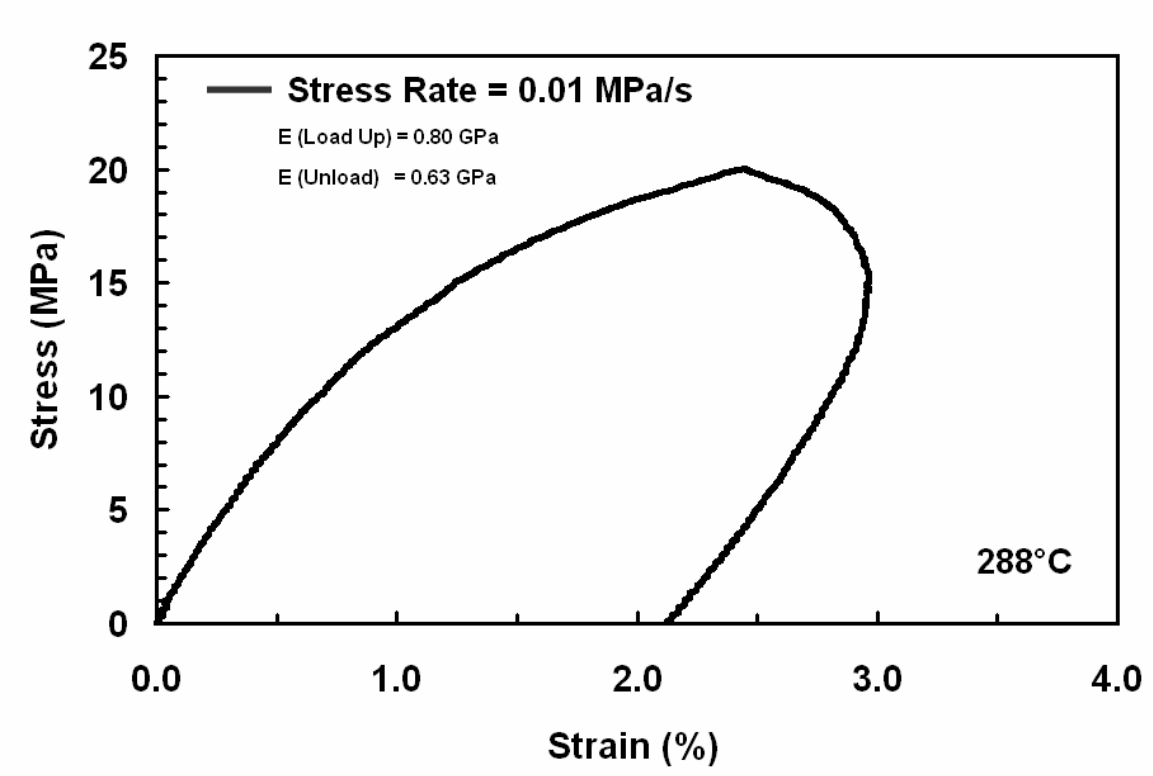

Figure 37: Loading and Unloading of PMR-15 neat resin at 288 ^{o}C at a rate of 0.01 MPa/s

While the loading and unloading to 20 MPa is completed in a time span of 42 s for the faster rate, the slower rate requires 4000 s (1.11 h) to complete this process. The loading and unloading moduli for each test are displayed in Table 8. For the 1 MPa/s rate, the loading modulus is approximately one percent greater than unloading modulus. The 0.01 MPa/s stress rate exhibits a 27% decrease in modulus from loading to unloading.

Table 8: Monotonic Loading and Unloading Moduli

Loading Rate (MPa/s)	Loading Moduli (GPa)	Unloading Moduli (GPa)
1	1.48	1.46
0.01	0.80	0.63

The strain measured immediately at the end of the unloading was 0.17% for the faster stress rate and 2.12% for the slower stress rate. The results of the recovery tests are shown in Figure 38. Again, the recovery strain is presented as a percent of the initial strain measured immediately after unloading. Due to the small value of that initial strain, full recovery (100%) is achieved within 1 hour of the recovery period in the test with prior stress rate magnitude of 1 MPa/s. The test conducted with a slower prior stress rate achieves 35% recovery after 12 h. A permanent strain of 1.37% exists after the 12 hour recovery. As shown in Figure 38, after the 12 hour recovery period, the recovery is nearly saturated as the curve approaches a horizontal asymptote.

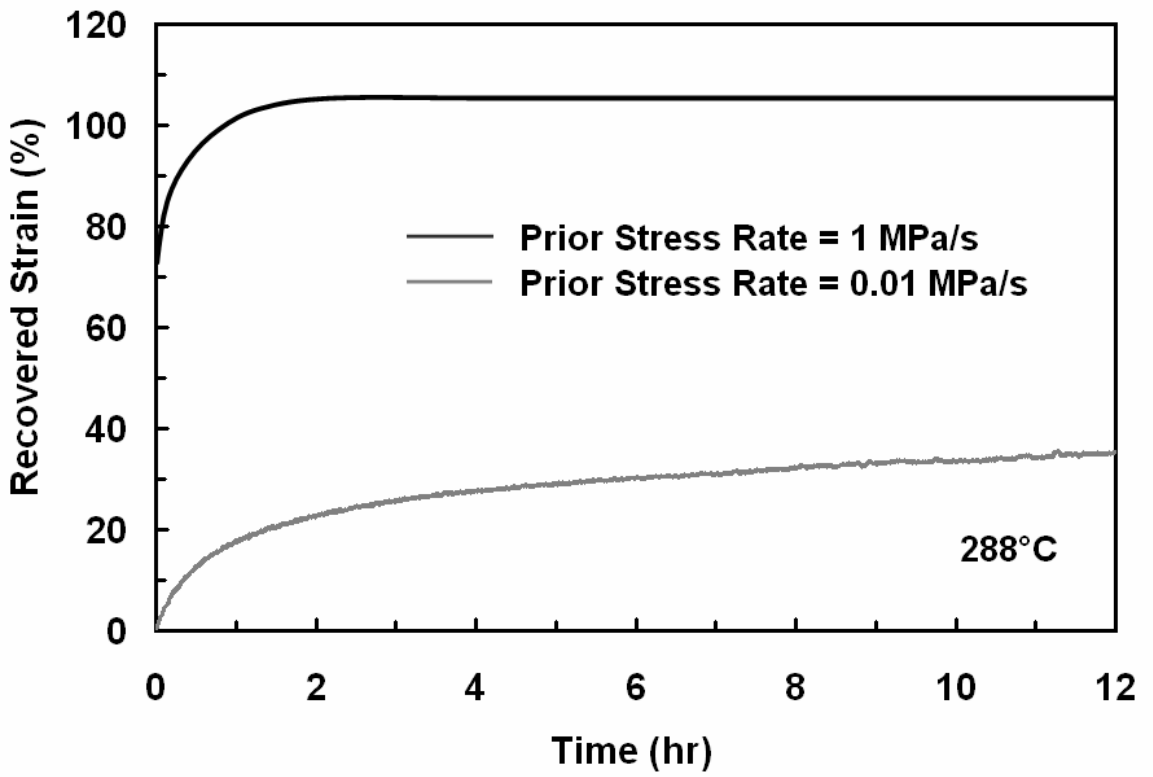

Figure 38: Recovered strain shown as percentage of the initial strain at beginning of recovery period following monotonic loading and unloading to 20 MPa at various stress rates.

Stepwise Creep Test and Recovery

The objective of the stepwise creep test was to demonstrate the effect of prior stress history on the mechanical behavior of PMR-15. The stepwise creep test subjected the specimen to creep at two different stress levels for periods of one hour. The stress levels were 15 and 20 MPa; creep periods were introduced during both loading and unloading at the 15 MPa level. Following the stepwise creep test, the specimen was allowed to recover at zero stress for a period of 12 h. This test was conducted using stress rates of 1 MPa/s and 0.01 MPa/s.

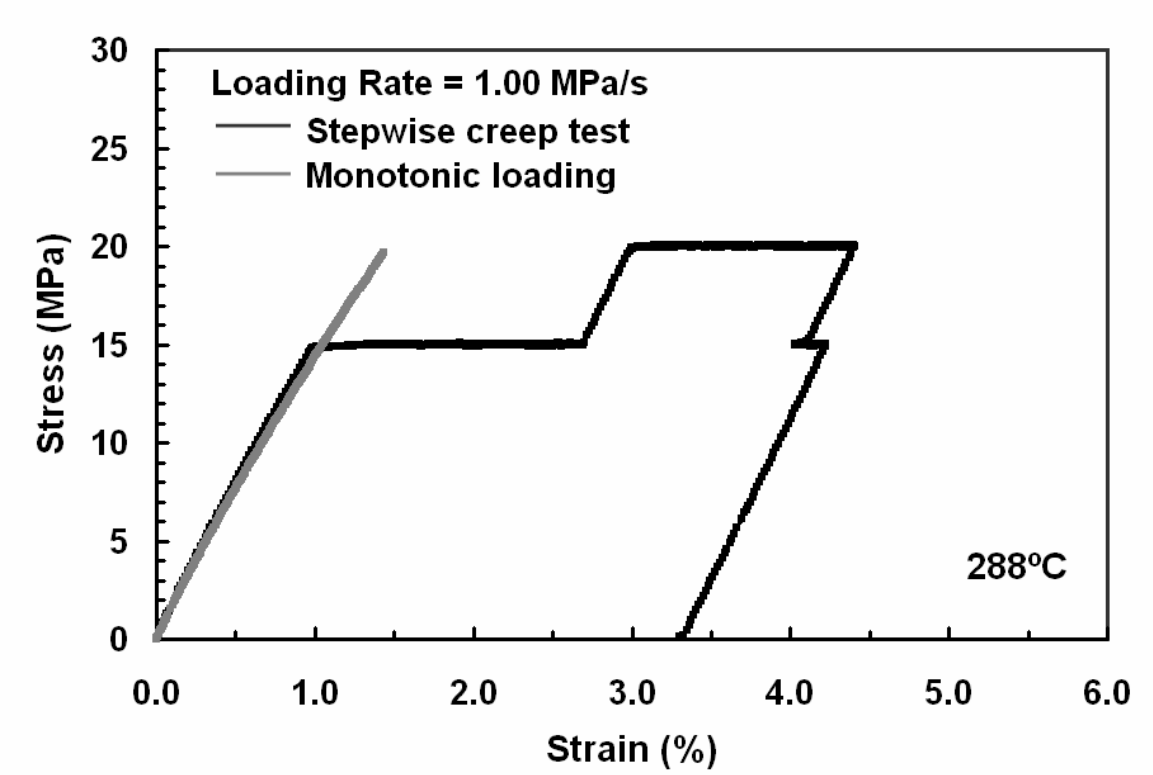

Figure 39: Stress-strain response in a stepwise creep test with loading and unloading stress rate magnitude of 1 MPa/s and 1 hr creep periods compared to uninterrupted monotonic tensile stress-strain curve

The stress-strain curve resulting from the stepwise creep test with a loading rate magnitude of 1 MPa/s is presented in Figure 39. The grey line in this figure depicts the stress-strain curve obtained in the monotonic loading test conducted with the same stress rate. The overlapping of the grey and black curves demonstrates that the specimen behaves as expected during the first loading portion of the stepwise test. The modulus of elasticity and stress-strain curve are consistent with the previously observed behavior of PMR-15. Examination of the stepwise creep test reveals that positive strain accumulation, or positive creep, takes places for the entirety of the creep periods on the loading path. However, during the third creep period (i.e 15 MPa creep test on the

unloading path), the amount of strain initially decreases, then increases, resulting in reversal of the creep rate. The initial behavior exhibited by PMR-15 is known as negative creep. After the negative creep was observed, creep rate reversal took place and positive creep was observed.

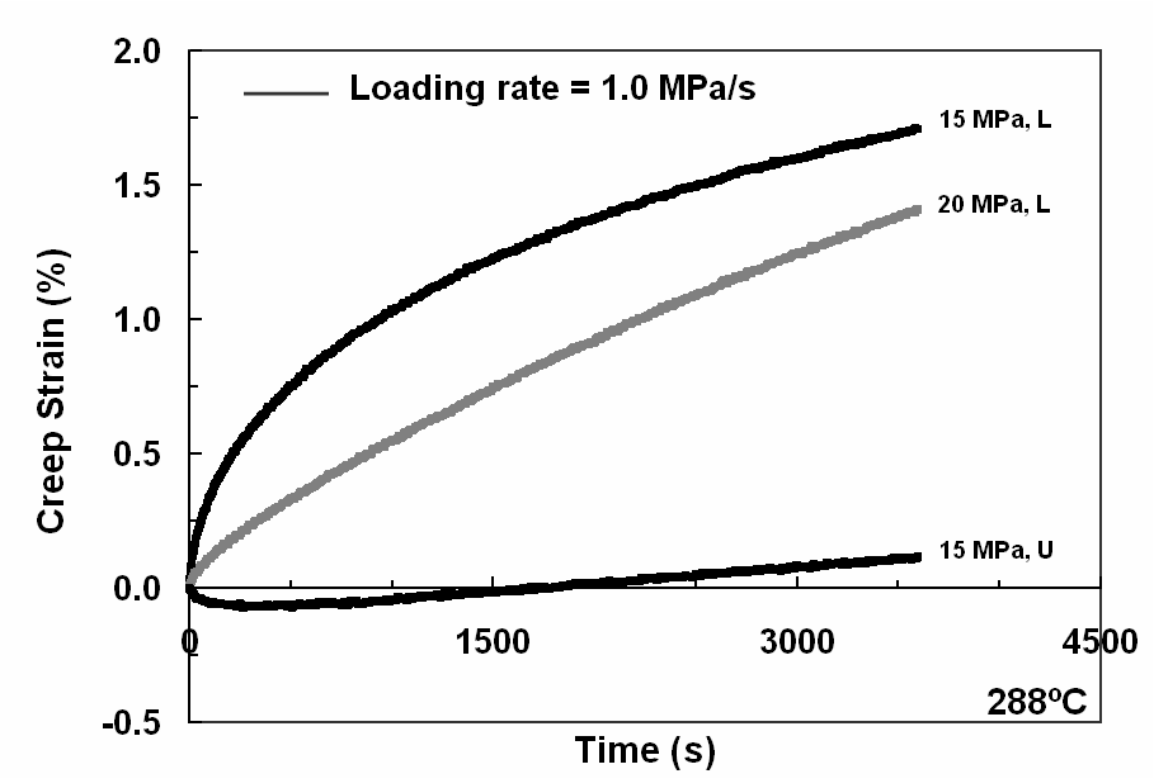

Figure 40: Creep strain as a function of time for the stepwise creep test conducted with a loading rate of 1.0 MPa/s. L=Loading. U=Unloading.

The creep strain produced during each creep period, including negative creep, is also presented as a function of time in Figure 40. It is important to note that accumulated creep strain for each creep period actually decreases with each additional step. While the creep strain of 1.73% was produced during the first creep period at 15 MPa, a smaller strain of 1.42% was accumulated during the next creep period conducted at a higher

stress of 20 MPa. The third creep period at 15 MPa on the unloading path resulted in only 0.12% additional strain. In addition, the negative creep is apparent during the third creep period. While the amount of strain decrease during negative creep is relatively small in comparison to the other creep strains, the creep rate reversal behavior is extremely significant. The negative creep behavior of PMR-15 was previously reported by Westberry (29:31). Westberry observed negative creep behavior on multiple unloading steps in which the amount of negative strain increased as the creep stress decreased (29:31). The phenomena of negative creep has been observed in other materials including BMI 5250-4 neat resin (2:57), Nylon 66 (12:313), and Poly (ether imide) or PEI (12:313). The creep rate reversal phenomenon observed in PMR-15 was previously reported in some instances of unloading during a stepwise creep test by Westberry (29:41). In addition, Khan observed similar rate reversal behavior at low stress levels for an amorphous polymer known as polycarbonate (11:81-82).

The creep strain as a function of time for the stepwise creep test conducted with a loading rate of 0.01 MPa/s is presented in Figure 41. Positive creep is observed during each creep period following the slower loading and unloading rate. In this case, creep strain accumulation increases as creep strain increases from 15 to 20 MPa. The third creep at 15 MPa during unloading produces the smallest creep strain accumulation. The first creep period at 15 MPa produced creep strain of 0.84%, the second creep period at 20 MPa produced creep strain of 1.36%, and the 15 MPa creep period during unloading generated creep strain of 0.33%.

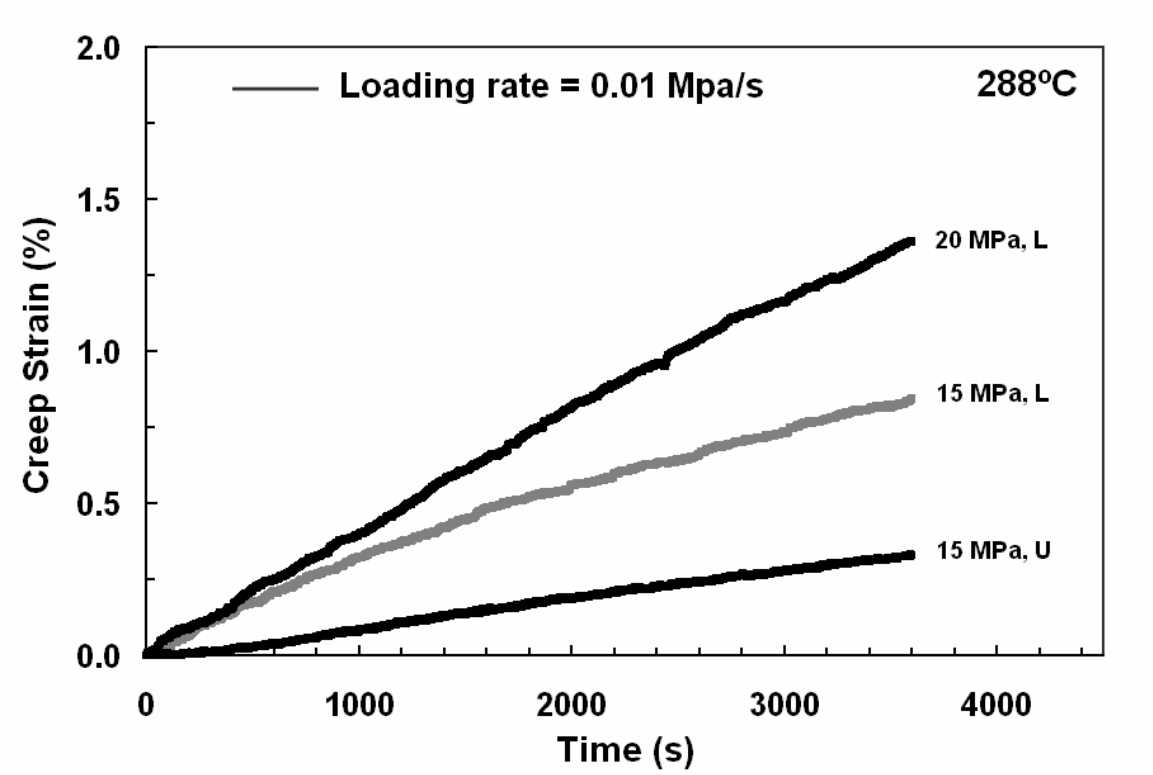

Figure 41: Creep strain as a function of time for the stepwise creep test conducted with a loading rate of 0.01 MPa/s. L=Loading. U=Unloading.

The creep strain accumulated at 20 MPa during the stepwise creep test was compared to that accumulated during creep at the same stress level preceded by uninterrupted loading at the same loading rate. Comparisons of the creep response were made for the prior loading rate of 1 MPa/s as shown in Figure 42. The creep behavior of the PMR-15 neat resin is dependent on stress history. Strain accumulated in the creep test preceded by uninterrupted loading was approximately 2.5 times that accumulated at 20 MPa in the stepwise creep test. In addition, the shapes of the creep curves are notably different for each loading case. The curve resulting from the stepwise creep test approaches secondary creep whereas the creep preceded by uninterrupted loading clearly remains in the primary creep regime.

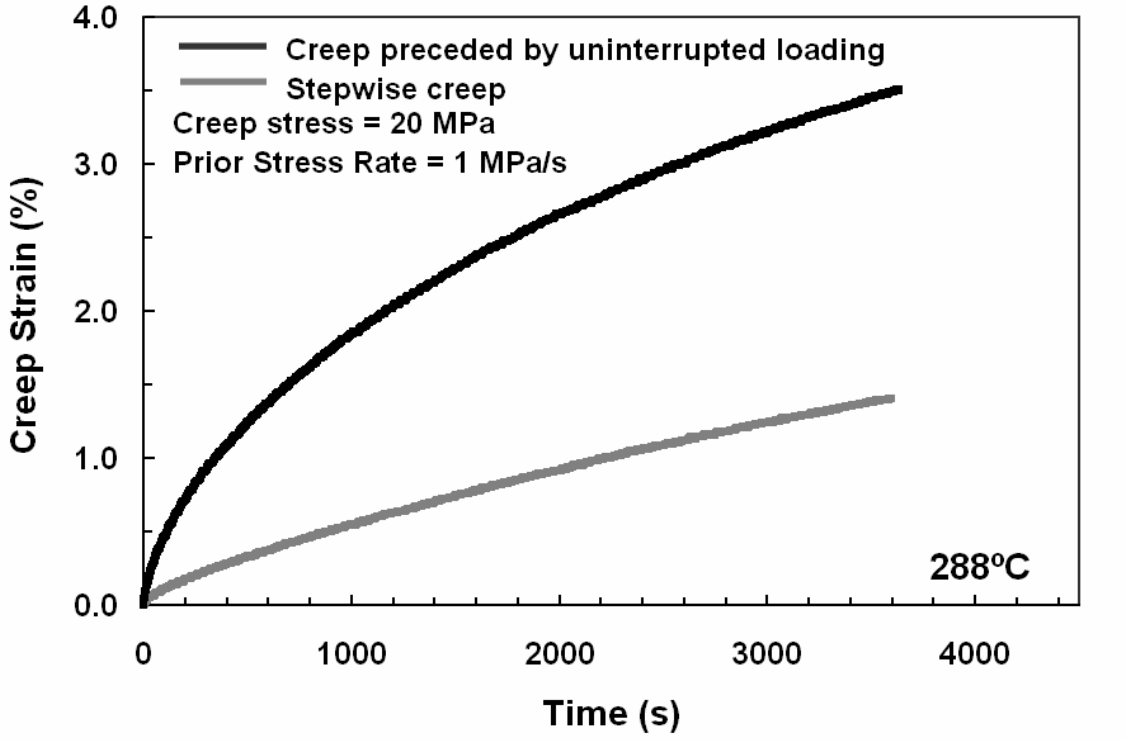

Figure 42: Creep strain as a function of time obtained at 20 MPa in the stepwise creep test and a creep test preceded by uninterrupted loading at a stress rate of 1 MPa/s. Mechanical strains at the beginning of the creep test are 3.04% (stepwise) and 1.30% (uninterrupted loading).

Recovery behavior obtained in a creep and recovery test was compared to that obtained following a stepwise creep and recovery test. While the creep and recovery test produced greater creep strain, it also allowed for greater recovery at zero stress as shown in Figure 43. Dependency on prior history is again evident in the recovery behavior of PMR-15.

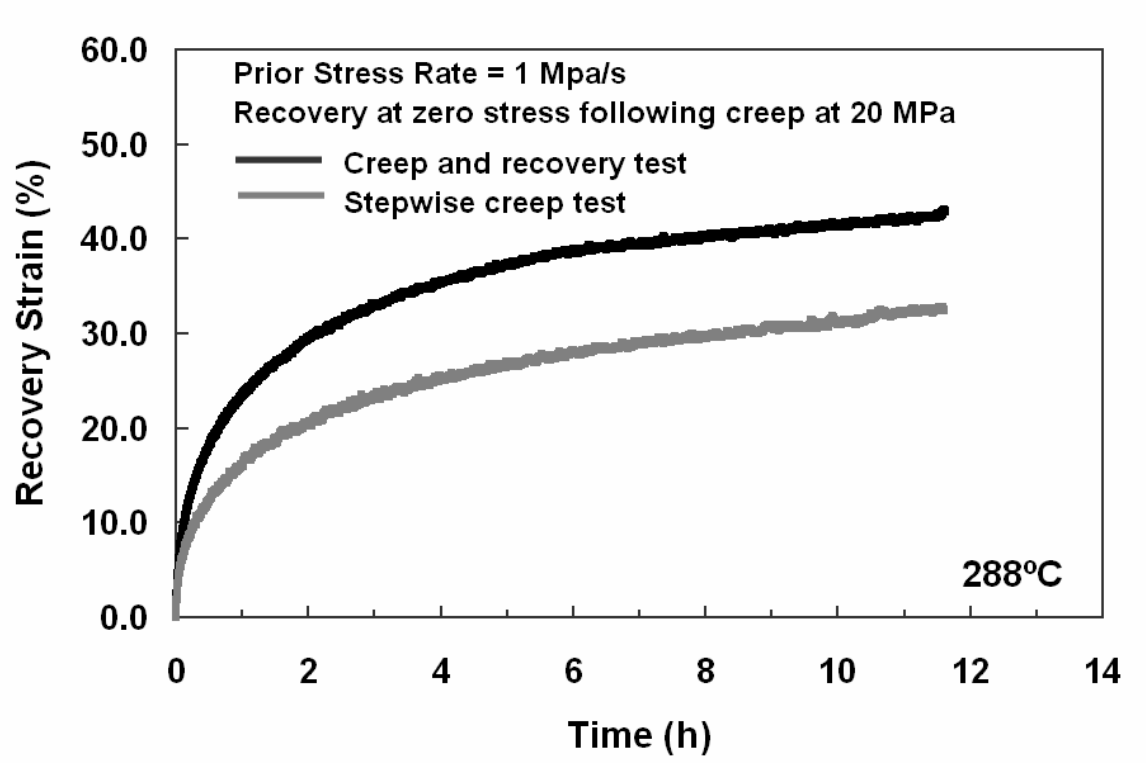

Figure 43: Recovery at zero stress following creep at 20 MPa in a creep and recovery test preceded by uninterrupted loading and a stepwise creep test. Recovered strain is presented as a percentage of the initial strain measured immediately after reaching zero stress.

Viscoelastic Model

Numerous creep-recovery tests were employed to characterize the nonlinear viscoelastic model developed by Schapery. After characterization, the ability of the model to predict material behavior was examined. The creep and recovery durations for each characterization test are presented in Table 9. The tests were repeated three times for each creep stress. The schematic depicting the creep and recovery test notation for Schapery's Model is again shown in Figure 44 (presented again for convenience).

Table 9: Model Characterization Test Specifications

Load/Unload Rate (MPa/s)	Stress Level (MPa)	% of UTS	Creep Time (h)	Recovery Time (h)
3	5	~11	0.5	1.5
3	10	~22	0.5	5
3	15	~33	0.5	5
3	20	~44	0.5	5
3	25	~55	0.5	5

* Each model characterization test was triplicated.

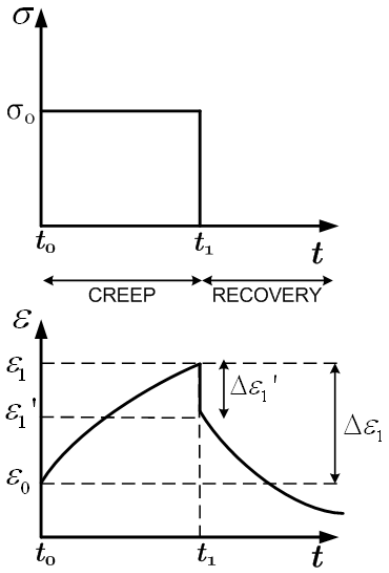

Figure 44: Creep and Recovery Test Notation for Schapery's Model

The constitutive equations capable of describing the behavior of non-linear viscoelastic materials subjected to a single step input under uniaxial loading are as follows:

$$\varepsilon_c(t) = \left[g_0 D(0) + C g_1 g_2 \left(\frac{t}{a_0} \right)^n \right] \sigma_0 \tag{77}$$

$$\varepsilon_r(t) = \frac{\Delta\varepsilon_1}{g_1} [(1+\lambda a_0)^n - (\lambda a_0)^n] \tag{78}$$

where $\Delta\varepsilon_1$ is the total amount of strain accumulated during the creep process defined as follows:

$$\Delta\varepsilon_1 = \varepsilon_1 - \varepsilon_0 = C g_1 g_2 \frac{t_1^n}{a_\sigma^n} \sigma_0 \tag{79}$$

A characterization scheme was applied to empirical creep and recovery data to determine the parameters *C, n, D(0)* and g_0, g_1, g_2, a_σ as functions of stress for the PMR-15 neat resin.

Linearity Region

The first step in the model characterization was to determine the region in which the behavior was linear viscoelastic. This is necessary in order to determine the threshold stress level above which the constants g_0, g_1, g_2, a_σ are no longer equal to one but are dependent on the stress level. The threshold stress was determined by examining isochronous stress strain curves obtained from results of creep tests conducted over the stress range of 5 to 25 MPa at increments of 5 MPa. As shown in Figure 45, the strain values at various times throughout each individual creep test were plotted for each stress

level. The times selected ranged from 250 s to 1700 s. The isochronous stress strain curves of PMR-15 neat resin reveal linear behavior for stresses below 10 MPa.

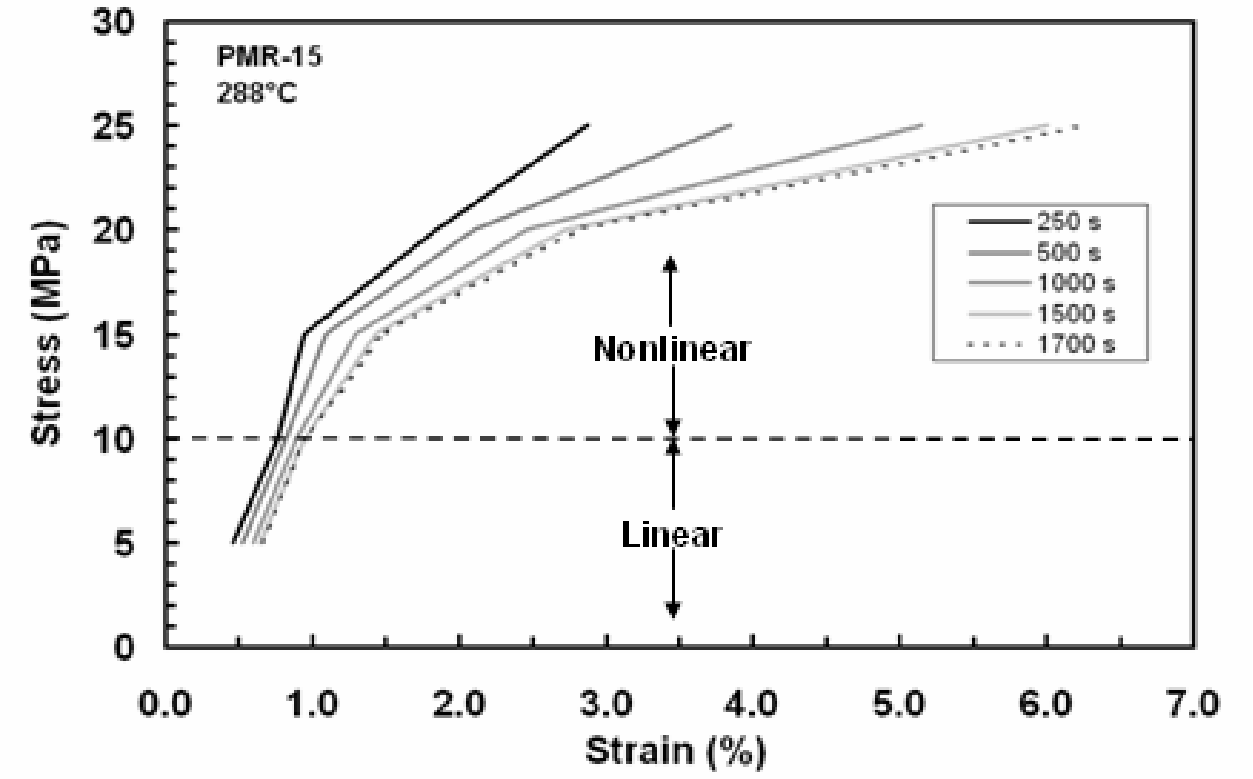

Figure 45: Isochronous stress-strain curves of PMR-15 neat resin indicate region of linear viscoelastic behavior

Panel-to-Panel Variability

As previously described, the goal of the creep-recovery characterization tests was to subject the specimen to an instantaneous increase in stress followed by creep at various stress levels. Ideally, the removal of the load would also occur instantaneously. Because it is not possible to conduct the loading and unloading in a stepwise manner, a loading and unloading rate of 3 MPa/s was used to limit the loading/unloading time to less than

15 s. During the ramp-up and ramp-down portions of the characterization tests, the Young's modulus was calculated and compared for various specimens. It was apparent that the modulus values obtained for specimens cut from the same panel were considerably different from those obtained for specimens cut from different panels. The average value of modulus of elasticity during loading was 1.65 GPa with a standard deviation of 0.16 GPa. The modulus values during loading and unloading for various specimens are presented in

Table 10.

Table 10: Modulus During Loading and Unloading for Various Specimens

Specimen Number	Panel Number	$E_{loading}$ (GPa)	E/E_{avg}	$E_{unloading}$ (GPa)
F-4	1	1.66	1.0052	1.62
F-5	1	1.61	0.9749	1.72
F-6	1	1.68	1.0173	1.68
F-7	1	1.78	1.0779	1.68
F-8	1	1.67	1.0112	1.42
F-9	1	1.64	0.9931	1.71
F-10	1	1.69	1.0234	1.72
F-11	1	1.76	1.0657	1.78
F-12	1	1.82	1.1021	1.89
F-13	1	1.53	0.9265	1.53
F-14	1	1.56	0.9446	1.53
F-15	12	1.29	0.7811	N/A
F-16	12	1.63	0.9870	1.38
F-17	12	1.43	0.8659	N/A
F-18	12	1.61	0.9749	1.58
F-19	13	1.45	0.8780	1.23
F-20	1	1.88	1.1384	1.81
F-21	2	2.06	1.2474	1.55
F-22	2	1.7	1.0294	1.59
F-23	2	1.65	0.9991	1.38
F-24	2	1.58	0.9567	1.33

The specimens cut from panels 12 and 13 exhibited significantly lower stiffness than those cut from panels 1 and 2. Note that specimens F-15 and F-17 failed during the creep period and therefore did not produce the required data for the model characterization. In order to account for panel-to-panel variability and reduce the effects of data scatter in the remaining specimens, the creep and recovery strains were adjusted using the following equation:

$$\varepsilon_{adj} = \frac{E_{loading}}{E_{avg}} \varepsilon \tag{80}$$

Three creep and recovery tests were conducted at each stress level of 5, 10, 15, 20 and 25 MPa. The strain values recorded during the creep period for each stress level were averaged. The creep strain as a function of time for various stress levels is presented in Figure 46. The heavy lines represent the average values while the shaded areas represent regions of data scatter. Even after adjusting for different modulus values, the data scatter is apparent. The data scatter increases significantly with stress level and is the most apparent at the highest stress level of 25 MPa. In addition, the scatter bands surrounding each stress level continuously expand during the creep period.

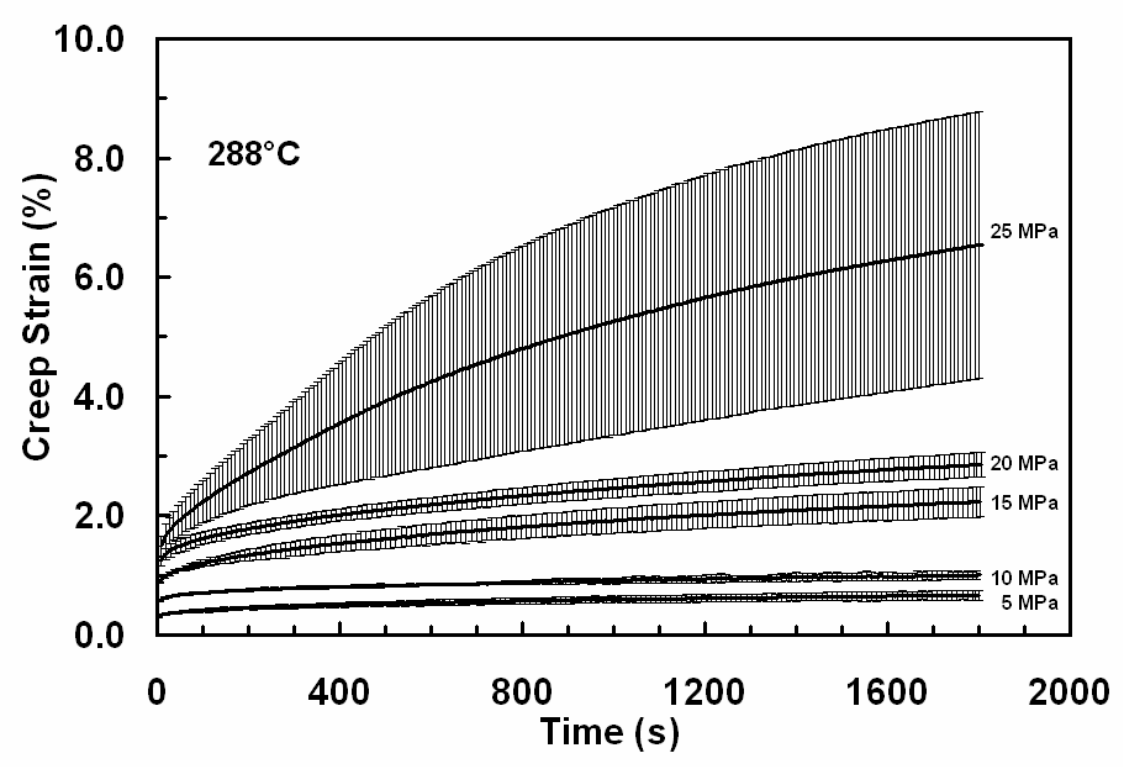

Figure 46: Creep strains vs. time curves and the associated data scatter

Determination of n, C, and D(0)

The first step in the characterization scheme is to define a reference recovery strain curve known as the master curve. The curve is found by comparing empirical recovery data to the predicted curve. In the linear range, assuming $a_\sigma = \frac{\Delta\varepsilon_1}{g_1} = 1$, Eq. 78 reduces to the following:

$$\varepsilon_r(t) = [(1+\lambda)^n - (\lambda)^n] \tag{81}$$

The variable n becomes the only unknown in this equation. It is determined by plotting the recovery strain, $\varepsilon_r(t)$, as a function of reduced time, λ, on a log-log plot for several

trial values of n . The shape of the recovery strain curve is then compared to empirical recovery data in the linear region.

For the PMR-15 neat resin, the stress levels of 5 and 10 MPa were determined to be in the linear region. Recovery duration following creep at the stress level of 5 MPa was 1.5 h and all specimens tested at this level recovered less than 70% of strain present at the onset of recovery. At the 10 MPa stress level, recovery duration was 5 h and the specimens recovered over 80% recovery of the initial strain, as shown in Figure 47. Specimen F-12 recovered 90% of initial strain and had the lowest permanent strain. For this reason, the value of n was determined using the recovery data for this specimen.

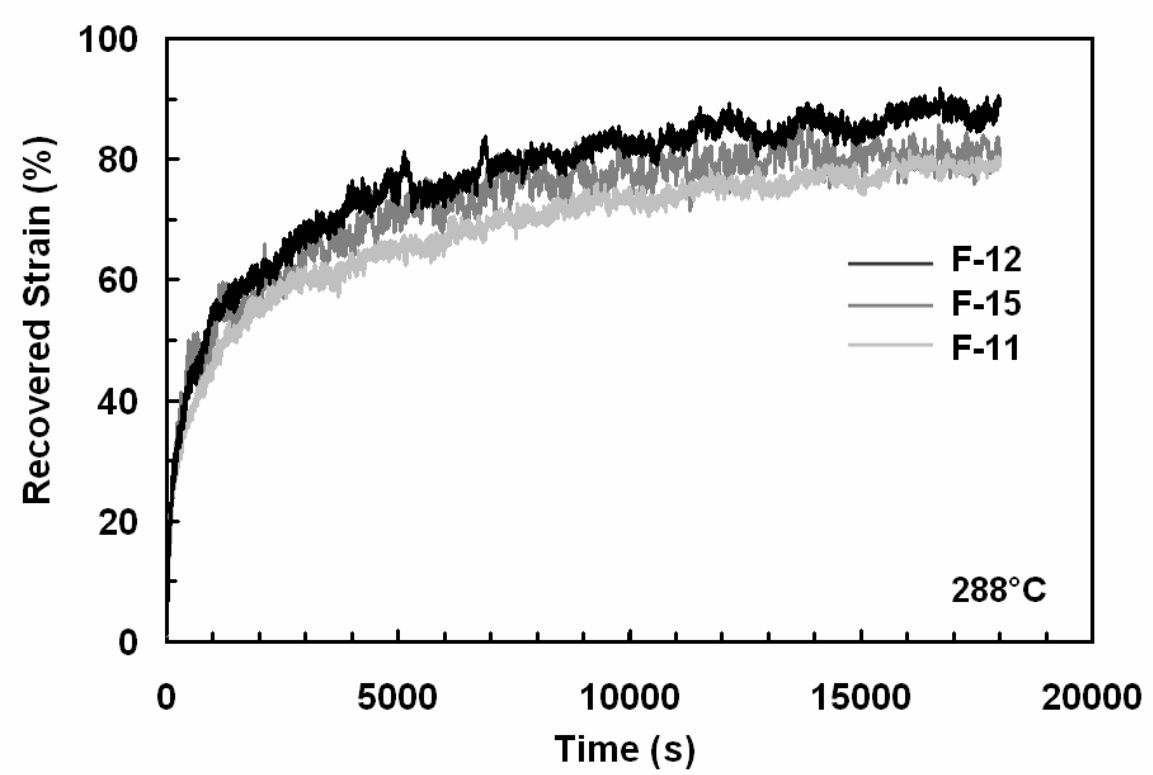

Figure 47: Recovery curves at zero stress following creep at 10 MPa. Recovered strain is presented as a percentage of the initial inelastic strain measured immediately after reaching zero stress.

As shown in Figure 48, the recovery strain at zero stress following creep at 10 MPa was plotted as a function of reduced time, λ, on a log-log plot. Predictions using Eq. 81 for several trial values of n ranging from 0 to 1 were plotted on the same graph and the predicted curves were compared to the empirical data. As a result, n=0.46 was determined to provide the best fit to experimental results.

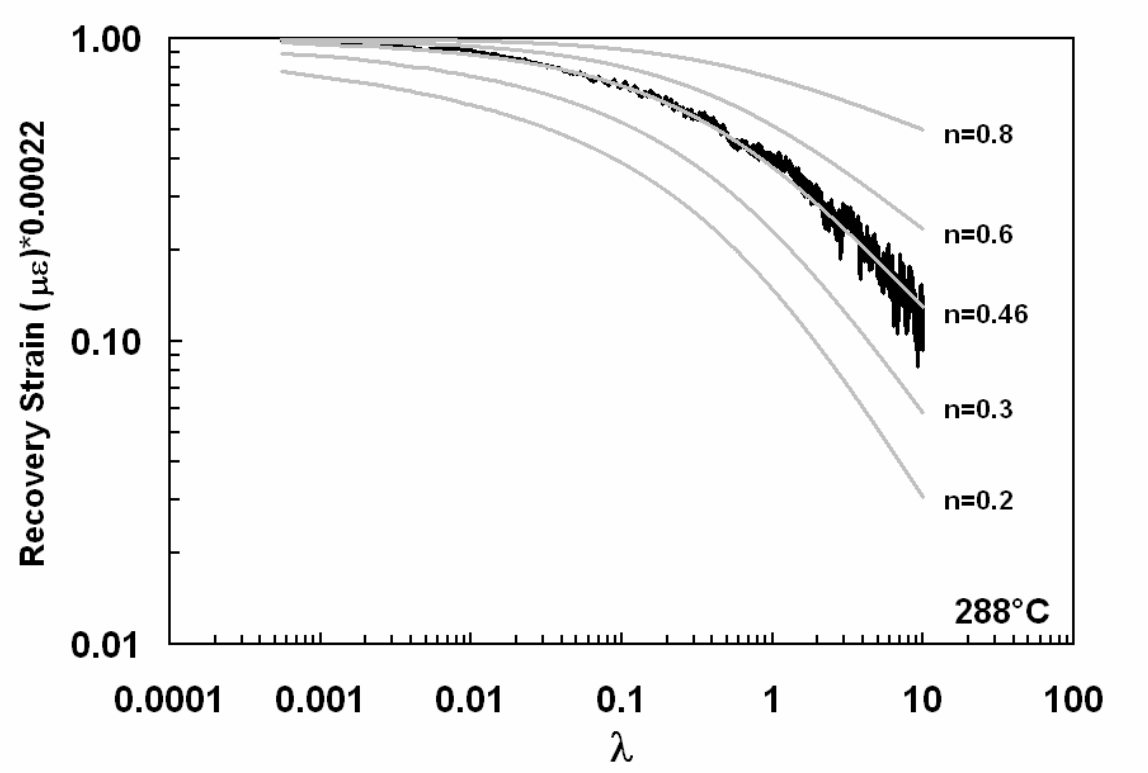

Figure 48: Recovery at zero stress following creep at 5 MPa plotted on a log-log scale for determination of constant n.

After the variable n was determined, two more constants were determined using empirical data from the creep portion of the test. Recalling that $g_0 = g_1 = g_2 = a_\sigma = 1$ in the linear range, the examination of Eq. 77 for a given creep stress level, σ_0, reveals that $D(0)$ and C are the only unknowns:

$$\varepsilon_c(t) = (D(0) + Ct^n)\sigma_0 \tag{82}$$

Consideration of the creep strain at two different times during the creep period, $t = t_a$ and $t = t_b$, where $0 < t_a < t_b < t_1$, results in the following expressions:

$$\varepsilon_c(t_a) = (D(0) + Ct_a{}^n)\sigma_0 \tag{83}$$

$$\varepsilon_c(t_b) = (D(0) + Ct_b{}^n)\sigma_0 \tag{84}$$

The difference of the creep strains at $\varepsilon_c(t_a)$ and $\varepsilon_c(t_b)$ becomes:

$$\varepsilon_c(t_b) - \varepsilon_c(t_a) = C\sigma_0(t_b{}^n - t_a{}^n) \tag{85}$$

This equation may be solved for the unknown constant *C* using the experimental creep data $\varepsilon_c(t_a)$ and $\varepsilon_c(t_b)$:

$$C = \frac{\varepsilon_c(t_b) - \varepsilon_c(t_a)}{\sigma_0(t_b^n - t_a^n)} \tag{86}$$

To provide the most accurate value, C is calculated by computing the average of all C values when t_a took on all times throughout the creep period and t_b was the time just prior to the end of the creep period. Using this method, the value of C was determined to be 10.01.

After the determination of C, it is possible to determine the initial linear viscoelastic creep compliance, $D(0)$, from Eq. 82 as follows:

$$D(0) = \frac{\varepsilon_c(t)}{\sigma_0} - Ct^n \tag{87}$$

Again, the average value of $D(0)$ was calculated for all values of t throughout the creep period and was determined to be 619.4.

After determining the material constants n, C, and D(0), it is possible to plot creep and recovery strains predicted by Eqs. 77 and 78 and compare the predicted strains to the

empirical data used to determine these constants. Once again, g_0, g_1, g_2, a_σ =1 in the linear range. The plots, shown in Figure 49 and Figure 50, provided verification that the constants were correctly determined.

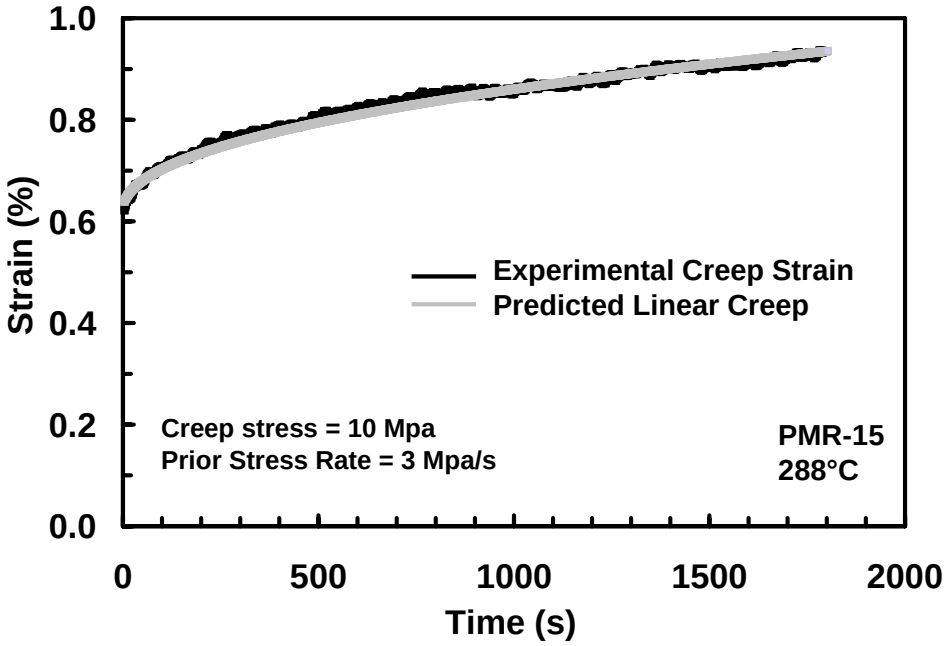

Figure 49: Creep strain as a function of time, experimental results used to determine material constants compared to predicted creep in the linear stress range

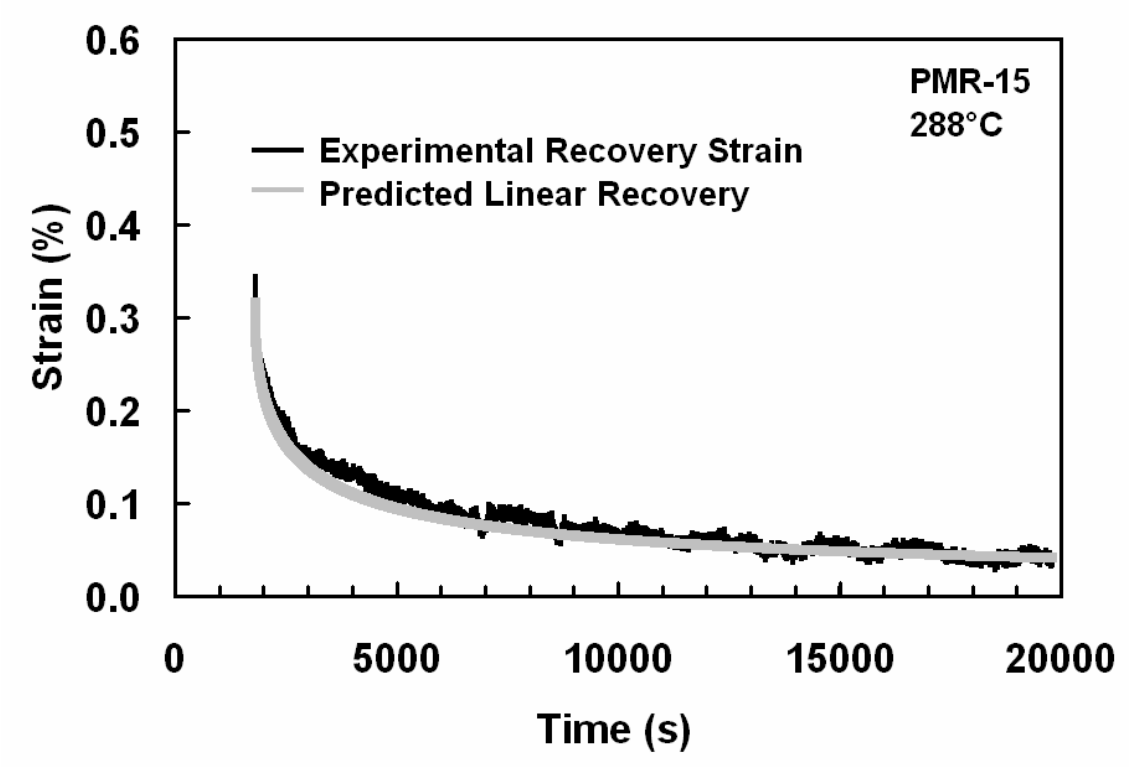

Figure 50: Recovery strain as a function of time, experimental results used to determine material constants compared to predicted recovery following creep in the linear stress range.

Determination of stress dependent constants

Next, the remaining material constants must be determined for stress levels beyond the linear range. The values for g_1 and a_σ are determined from the horizontal and vertical shifts, respectively, needed to match the master curve with the corresponding experimental recovery data at each stress level. Figure 51 shows a vertical shift, $\frac{\Delta\varepsilon_1}{g_1}$, of the master curve to match the experimental data. The upward shift corresponds to a value of $\frac{\Delta\varepsilon_1}{g_1}$ greater than one.

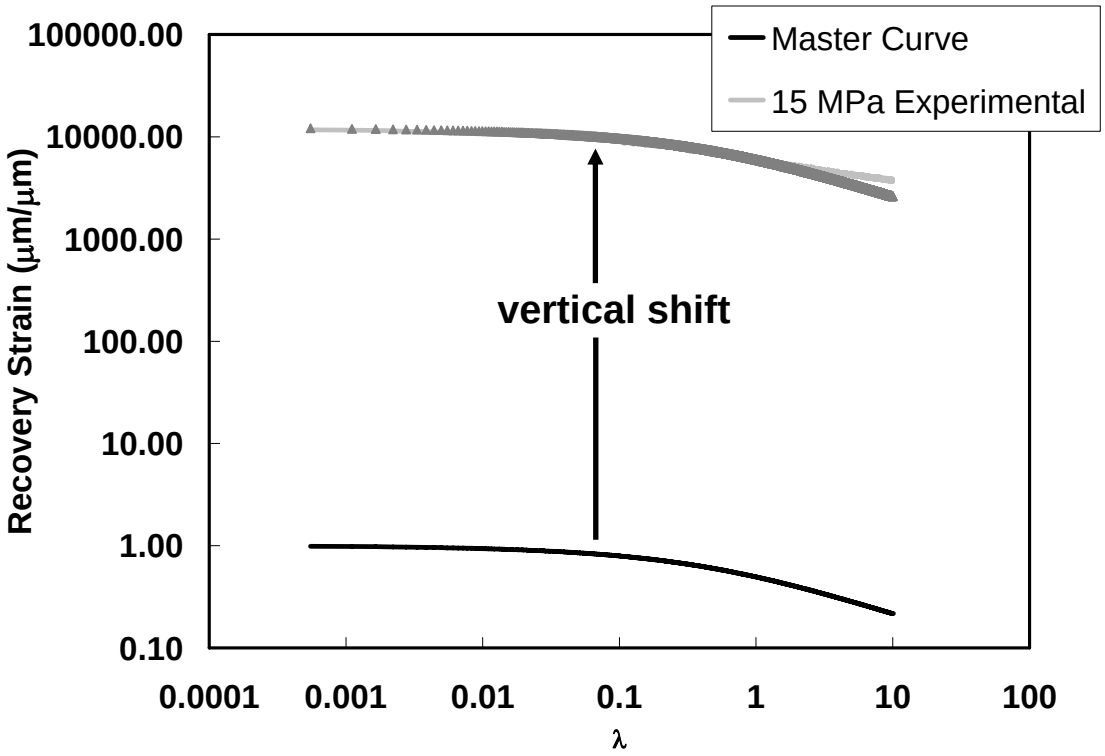

Figure 51: Vertical shift of master curve up to experimental recovery strain data following creep at 15 MPa.

The total amount of strain accumulated during the creep period, $\Delta\varepsilon_1$, is known from experimental data and is shown by the following relationship:

$$\Delta\varepsilon_1 = \varepsilon(t_1^-) - \varepsilon(t_0^+) \tag{88}$$

Therefore, the constant g_1 may be defined for each stress level as follows:

$$g_1 = \frac{\Delta\varepsilon_1(\sigma_0)}{vertical\_shift(\sigma_0)} \tag{89}$$

The constant g_1 is then plotted as a function of stress as shown in Figure 52. For values of stress within the linear range, g_1 is assumed to be one. However, a trend line is

applied to the values in the non-linear range in order to establish g_1 as a function of stress.

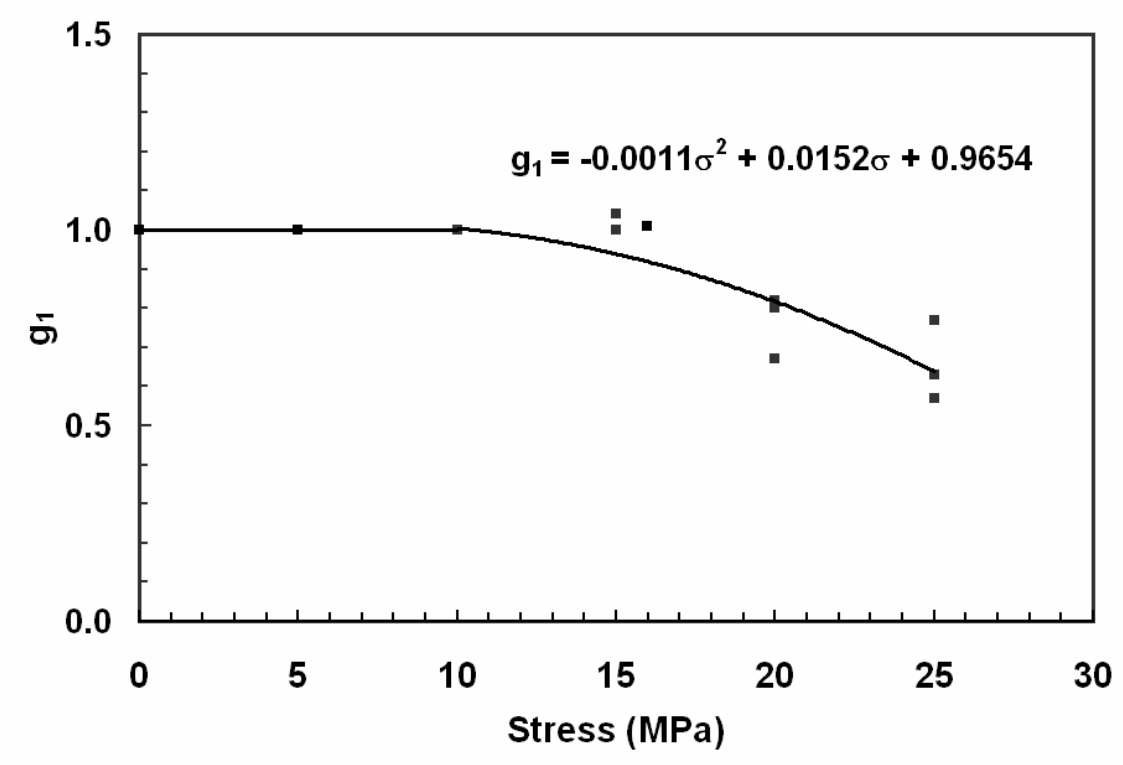

Figure 52: Material constant, g_1, as a function of stress

Similarly, a horizontal shift of the experimental data in Figure 51 to the left corresponds to a value of $a_\sigma < 1$. The value of a_σ was determined by calculating the differences in time between the vertically shifted master curve and the experimental recovery data for a given strain. The average was then calculated to determine the value of a_σ at each stress level. The constant a_σ is plotted as a function of stress in Figure 53.

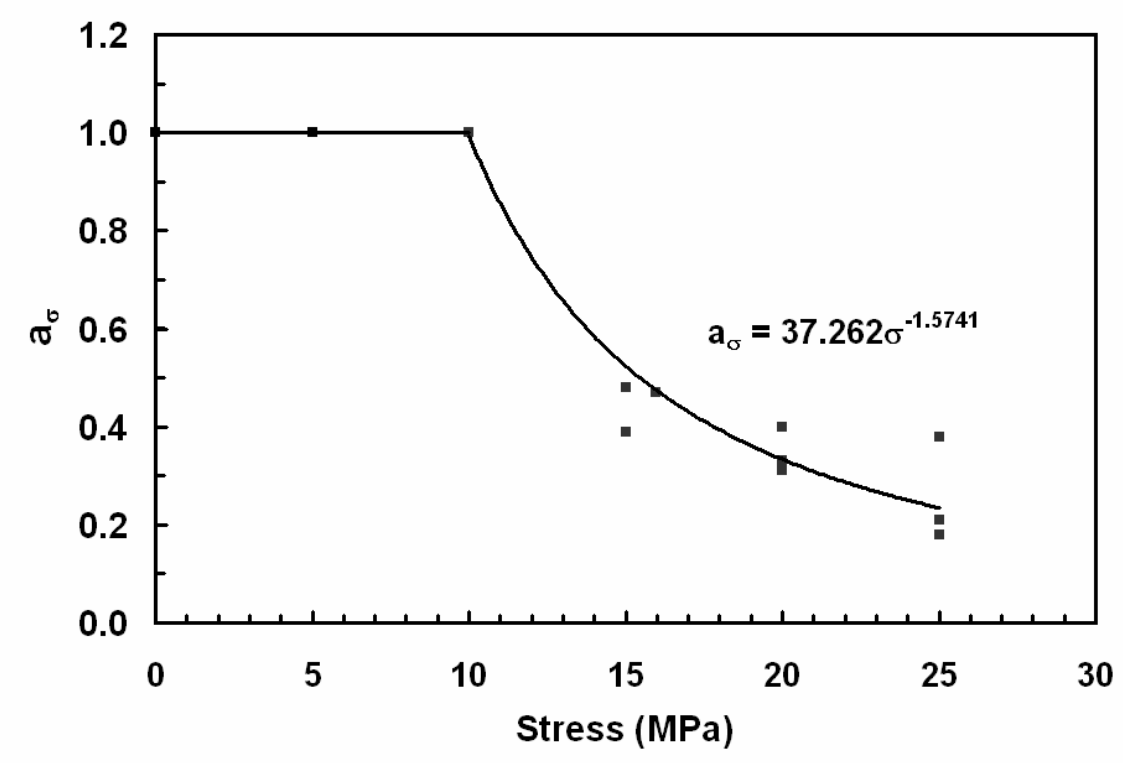

Figure 53: Material constant, a_σ, as a function of stress

The process used to determine the value of g_2 is similar to that used to previously determine the constant C. In the non-linear range, the difference of the creep strains at t_a and t_b becomes:

$$\varepsilon_c(t_b) - \varepsilon_c(t_a) = \frac{g_1 g_2 C}{a_0^n} \sigma_0 ({t_b}^n - {t_a}^n) \tag{90}$$

which may be solved for the quantity D_1 defined below:

$$D_1 = \frac{\varepsilon_c(t_b) - \varepsilon_c(t_a)}{\sigma_0 (t_b^n - t_a^n)} = \frac{g_1 g_2 C}{a_0^n} \tag{91}$$

D_1 was calculated by computing the average of values of D_1 when t_a took on all times throughout the creep period while t_b was the time just prior to the end of the creep period. After determination of D_1, it is now possible to solve Eq. 91 for g_2 as follows:

$$g_2 = \frac{D_1 a_0^n}{g_1 C} \tag{92}$$

As the instantaneous increase in strain resulting from a step increase in stress, ε_0, is known from experimental data the remaining unknown variable, g_0, may be found from Eq. 68:

$$g_0 = \frac{\varepsilon_0}{D(0)\sigma_0} \tag{93}$$

The material constants g_2 and g_0 are plotted as functions of stress in Figure 54 and Figure 55, respectively.

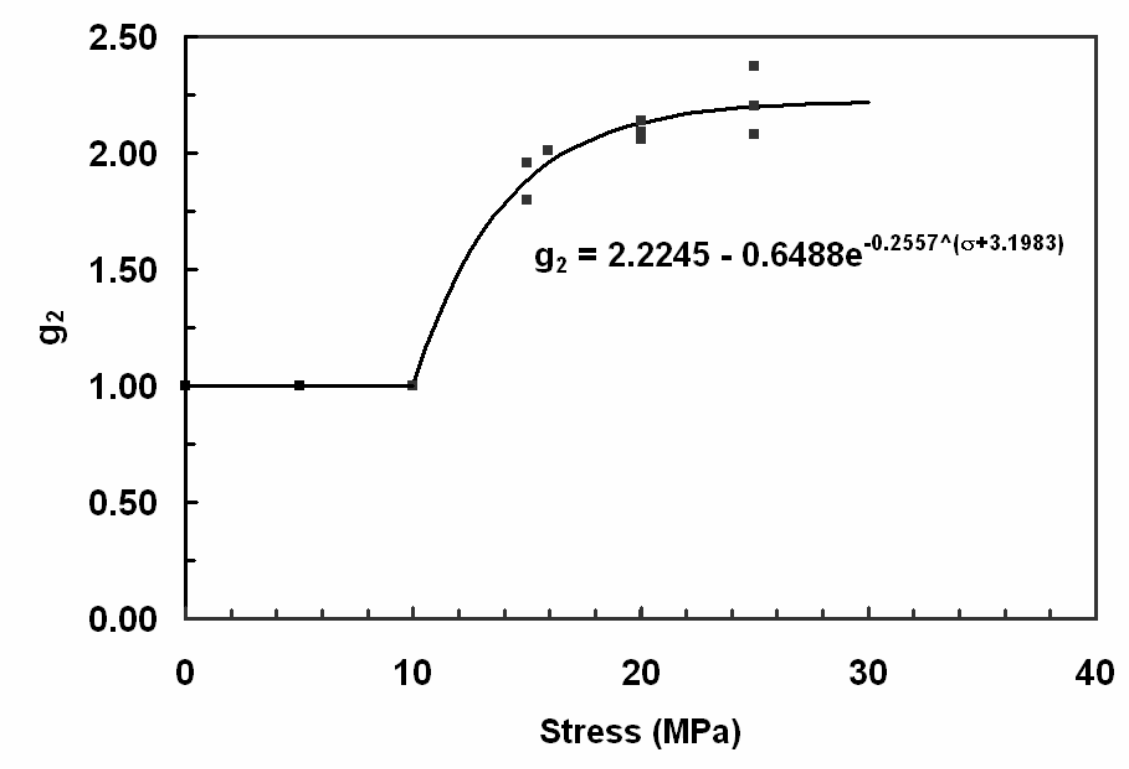

Figure 54: Material constant, g_2, as a function of stress

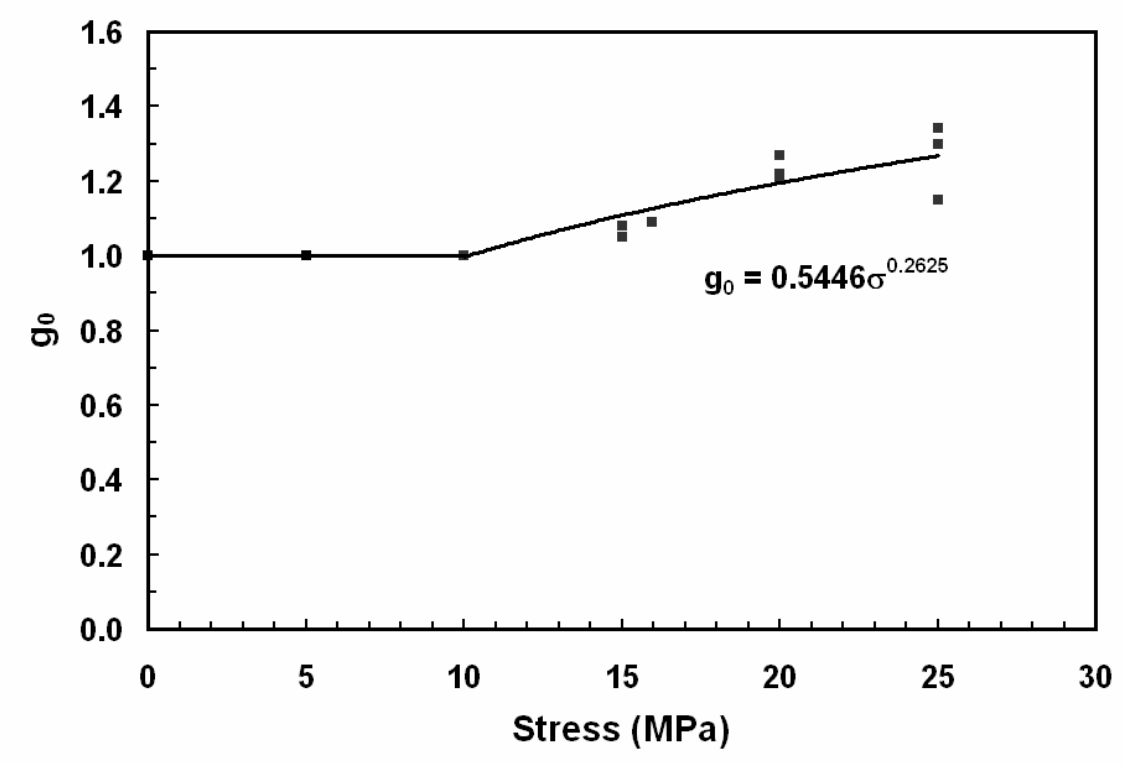

Figure 55: Material constant, g_0, as a function of stress

In summary, characterization of Schapery's model involved determination of the constants *n*, *D(0)*, and *C* which are independent of stress level. It also required determination of a_σ, $g_{0,}$ $g_{1,}$ and g_2 which depend on stress. While exact values for each constant may be determined from empirical data, the extension of this data to trends provides the ability to predict material behavior at stress levels other than those used for characterization of the model. For this characterization, all values of stress are in MPa, and strain is returned in units of microstrain.

Model Verification

The validity of the nonlinear viscoelastic model was tested against an assortment of loading histories. The specimens used for the model verification tests were cut from panel 2. The tests included monotonic loading and unloading under constant stress rates, a single step creep test followed by recovery, and a stepwise creep test followed by recovery. Each of these tests was carried out at stress rates of 1 MPa/s and 0.01 MPa/s. These tests were not used to determine the material constants and functions for the model.

The predictions were generated using a numerical integrator written to integrate Schapery's nonlinear viscoelastic model and calculate strain using stress as a function of time as input (25). It is useful to review the basic constitutive equations representing Schapery's model for a uniaxial case, as previously discussed:

$$\varepsilon(t) = g_0 D_0 \sigma(t) + g_1 \int_{0-}^{t} \Delta D(\psi - \psi') \frac{d}{d\tau}[g_2 \sigma(\tau)] \partial\tau \tag{94}$$

$$\psi(t) = \int_0^t \frac{dt'}{a_0[\sigma(t')]} \qquad \psi'(\tau) = \int_0^\tau \frac{dt'}{a_0[\sigma(t')]} \tag{95}$$

As a_σ is a function of stress only, as opposed to having additional time dependence, the expression of $(\psi - \psi')$ was reduced to $\frac{t-\tau}{a_\sigma(\sigma(\tau))}$. The elimination of this integral improved the computational time of the program. For each recorded time step, the integrator evaluated $\varepsilon(t)$ by integrating the convolution integral using a Runge Kutta fourth order method for numerical integration. This allowed the integral portion of Eq. 94 to become the following:

$$\sum_{\tau=0}^{t} \Delta A\left(\psi(t)-\psi(\tau)\right)\left(g_2(\sigma(\tau))\sigma(\tau)-g_2(\sigma(\tau-d\tau))\sigma(\tau-d\tau)\right) \quad (96)$$

The equations representing $\psi(t)$ were integrated prior to integrating the convolution. The functions g_0, g_1, g_2, and a_σ, were characterized as piecewise-continuous functions consisting of a region of linear viscoelastic behavior below 10 MPa, where the functions were evaluated as 1, and a nonlinear region where they became functions of stress. For the test conditions with a 1 MPa/s loading rate an integration time step of 0.1 s was used. For the 0.01 MPa/s rate, an integration time step of 1 s was used. The stress profiles were dependent on the loading condition and were input for each individual case. The integrator output the time, strain, and stress to a comma separated variable file for further processing at each recorded time.

Monotonic Loading and Unloading

The first test used for model verification was monotonic loading and unloading at a constant stress rate of 1 MPa/s. The comparison of experimental results to the predictions is presented in Figure 56. The model was capable of predicting behavior in the linear range, below 10 MPa, but predictions progressively drifted from the experimental data in the nonlinear range. A small "elbow" can be seen in the predicted response at the stress level where the material functions transition from linear to nonlinear behavior upon loading and unloading. The model over-predicted the total strain accumulated during loading as well as the strain removed during unloading. The model prediction does not follow the same unloading path; however, the prediction does run parallel to the experimental data during unloading in the linear range. Note that in

this particular case, the model was capable of predicting full recovery which was congruent with the actual material behavior. This was not surprising as only a small amount of strain was present upon unloading. It is important to note that the stress rate used in this test was of the same order of magnitude as that used in model characterization tests.

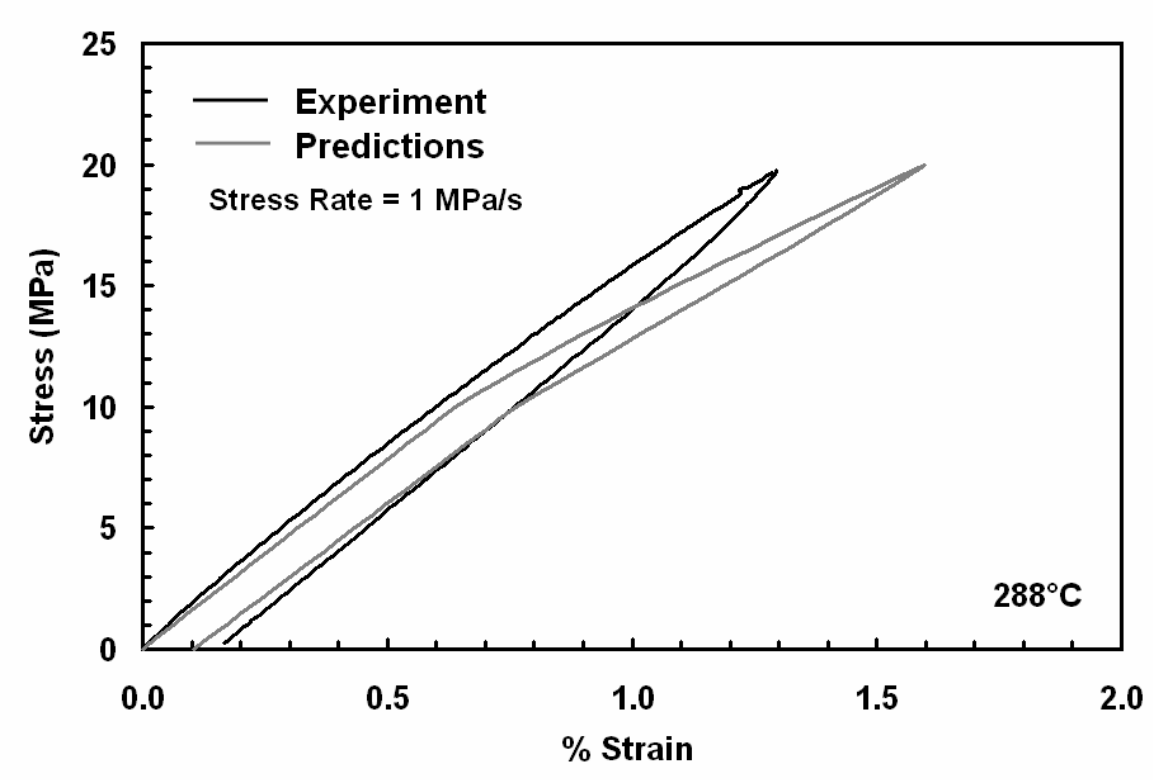

Figure 56: Loading and unloading at a constant stress rate of 1 MPa/s, experimental results compared to nonlinear viscoelastic model predictions

Comparison of the loading and unloading at a slower loading rate of 0.01 MPa/s is shown in Figure 57. In this case, the model did not predict the stress-strain behavior of PMR-15 accurately. The slower rate could not be accounted for and the strain during

loading is severely under predicted. The model predicts the "curved" unloading qualitatively, but quantitative predictions are inaccurate. The model predicted full recovery behavior, which was not achieved experimentally. The discrepancies between experimental and predictive data indicate the model's inability to account for a low stress rate of 0.01 MPa/s.

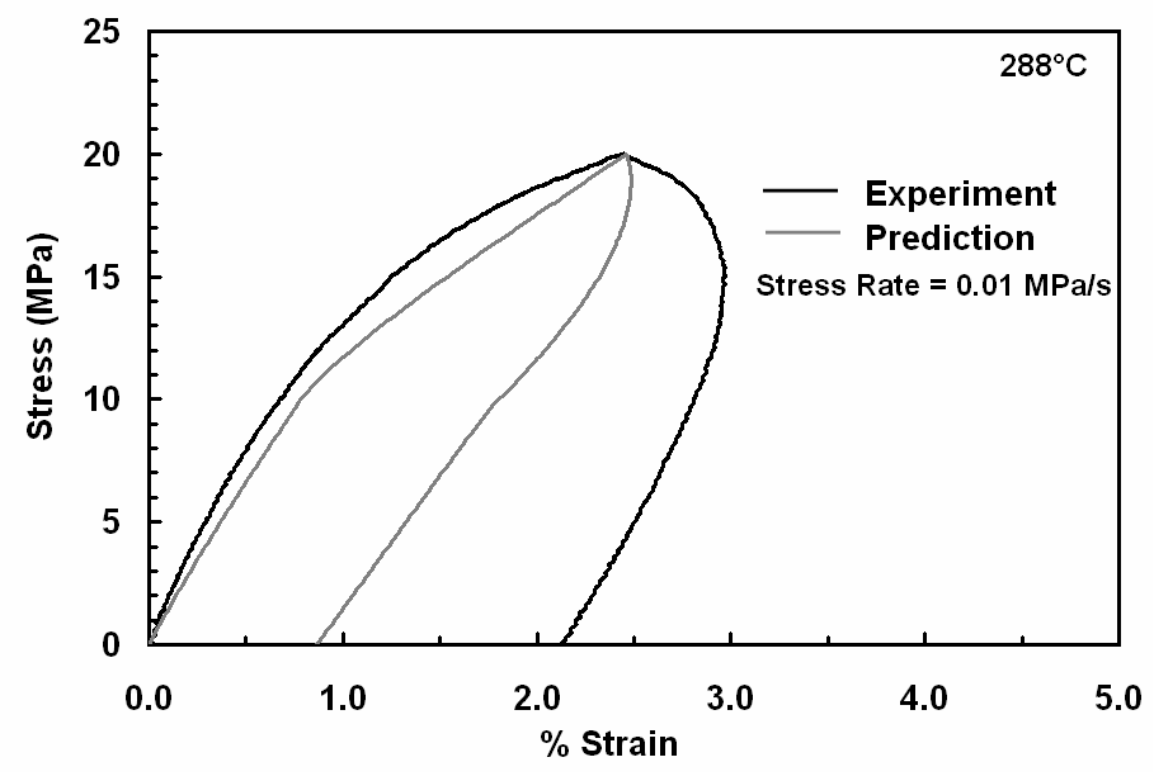

Figure 57: Loading and unloading at a constant stress rate of 0.01 MPa/s, experimental results compared to nonlinear viscoelastic model predictions

Creep Followed by Recovery

The next test used for model verification was a creep test followed by recovery. The predictions for the creep-recovery tests are shown in Figure 58 and Figure 59. During

creep, the model prediction follows the general shape of the experimental data but the model does not accurately predict the creep strain. The predicted strain departs from the experimental data after less than one hour of creep. While this creep test continued for 6 h, the tests used to determine the model parameters were limited to creep periods of 0.5 h. Extension of the data scatter bands, presented in Figure 46, to times greater than 1800 s (0.5 h) may indicate that the predictions of the nonlinear viscoelastic theory fall within the variance of the creep behavior of the material. Nonetheless, the model does not provide an accurate quantitative prediction for the long term creep behavior shown here.

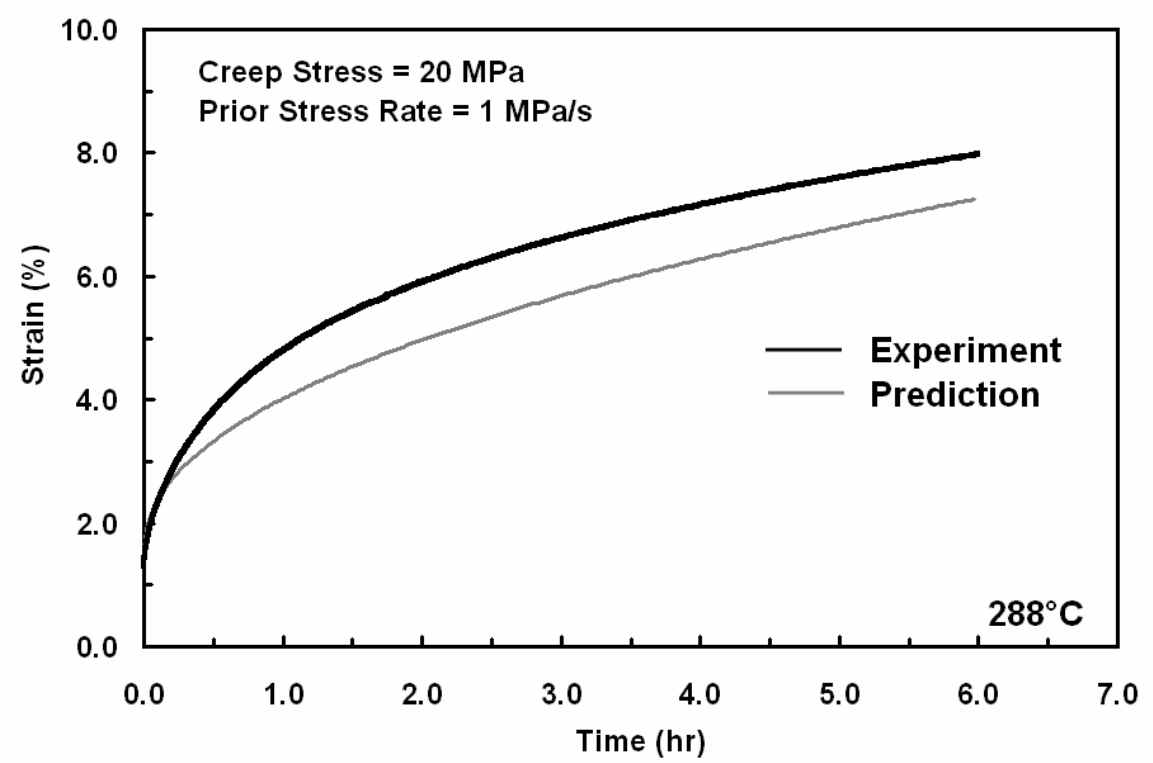

Figure 58: Creep at 20 MPa with a prior stress rate of 1 MPa/s, experimental results compared to viscoelastic model predictions.

The model over predicts the recovery strain following creep at 20 MPa (see Figure 59). While the experimental results reveal that recovery is nearly saturated after 12 h, the model predictions indicate that recovery is unsaturated. The model predicts a much lower permanent strain than that resulting from the experimental results.

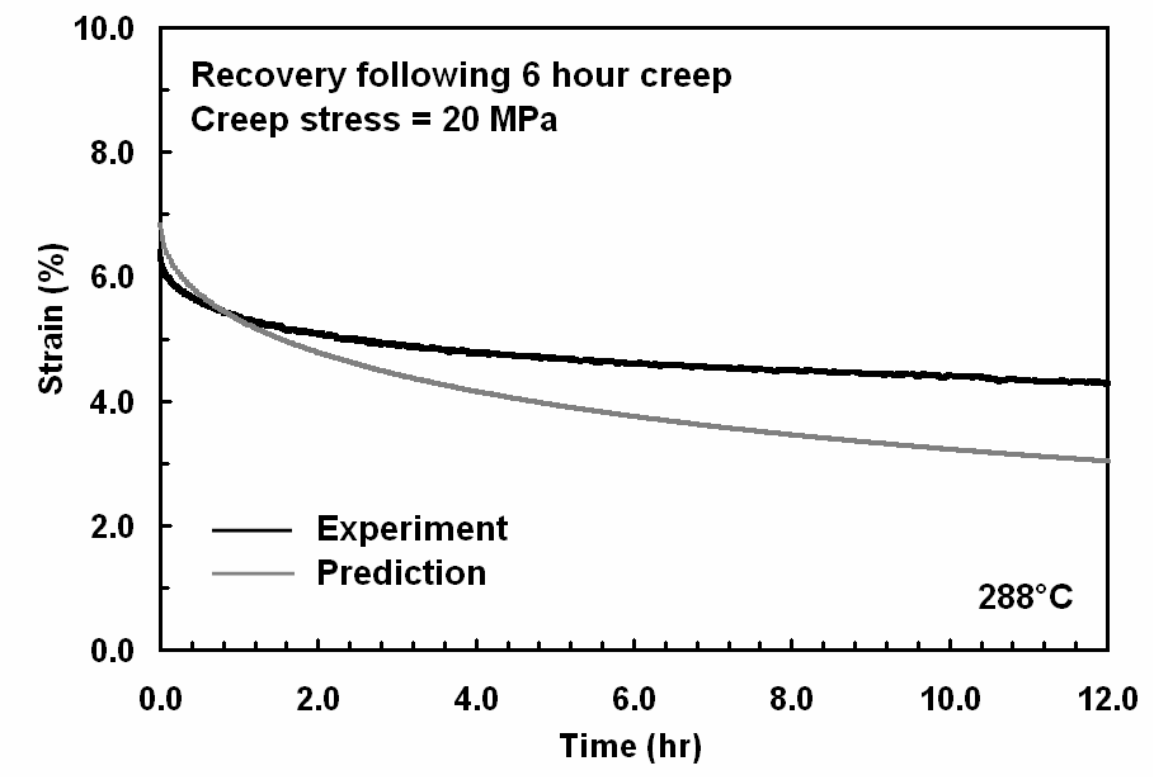

Figure 59: Recovery following creep at 20 MPa with a prior stress rate of 1 MPa/s, experimental results compared to viscoelastic model predictions

The model's ability to account for creep behavior following a much slower prior stress rate was also evaluated. Figure 60 displays the experimental results of the 20 MPa creep test preceded by a stress rate of 0.01 MPa/s together with the model predictions. The black dashed line represents the model prediction using the 0.01 MPa/s prior stress rate while the grey dashed line represents the prediction with the 1 MPa/s prior stress

rate. During the creep period the 1 MPa/s and 0.01 MPa/s predictions follow the same path. Again, the prior stress rate cannot be accounted for in the model. Therefore, predictions of material behaviors affected by prior stress rate are inaccurate.

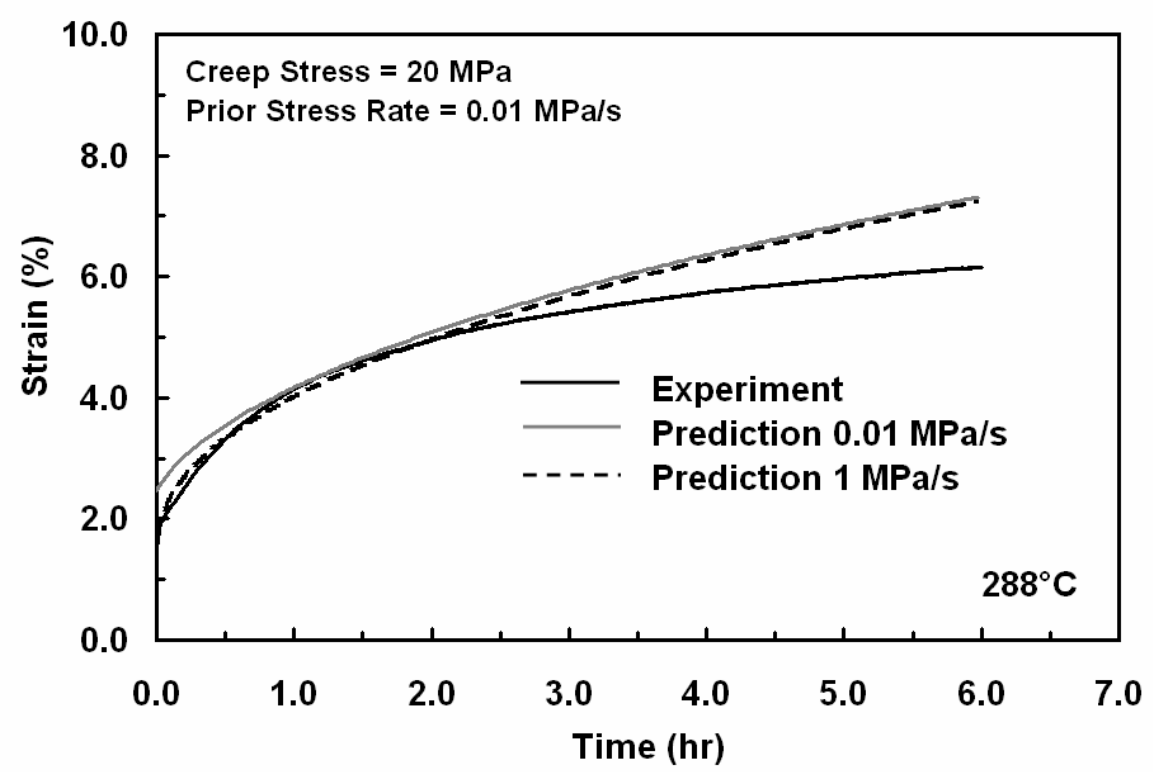

Figure 60: Creep at 20 MPa with a prior stress rate of 0.01 MPa/s, experimental results compared to viscoelastic model predictions.

Stepwise Creep Test

A stepwise creep test was also used for model verification. In this case, the predictions were compared to experimental data obtained with the stress rate of magnitude 1 MPa/s during loading and unloading. The specimen was loaded to 15 MPa, loaded to 20MPa, unloaded to 15 MPa, and unloaded to zero stress before recovering. A creep period of 1 h took place at each stress level. For this case, the equations in

Schapery's model were extended to include multiple steps as shown earlier in Eqs. 72-75. The experimental and predicted stress-strain curves are shown in Figure 61. While the amount of strain predicted during each creep period appears to be slightly different than the actual, the model generally performs fairly well in this case. A closer examination of the model's capabilities is presented in the following graphs.

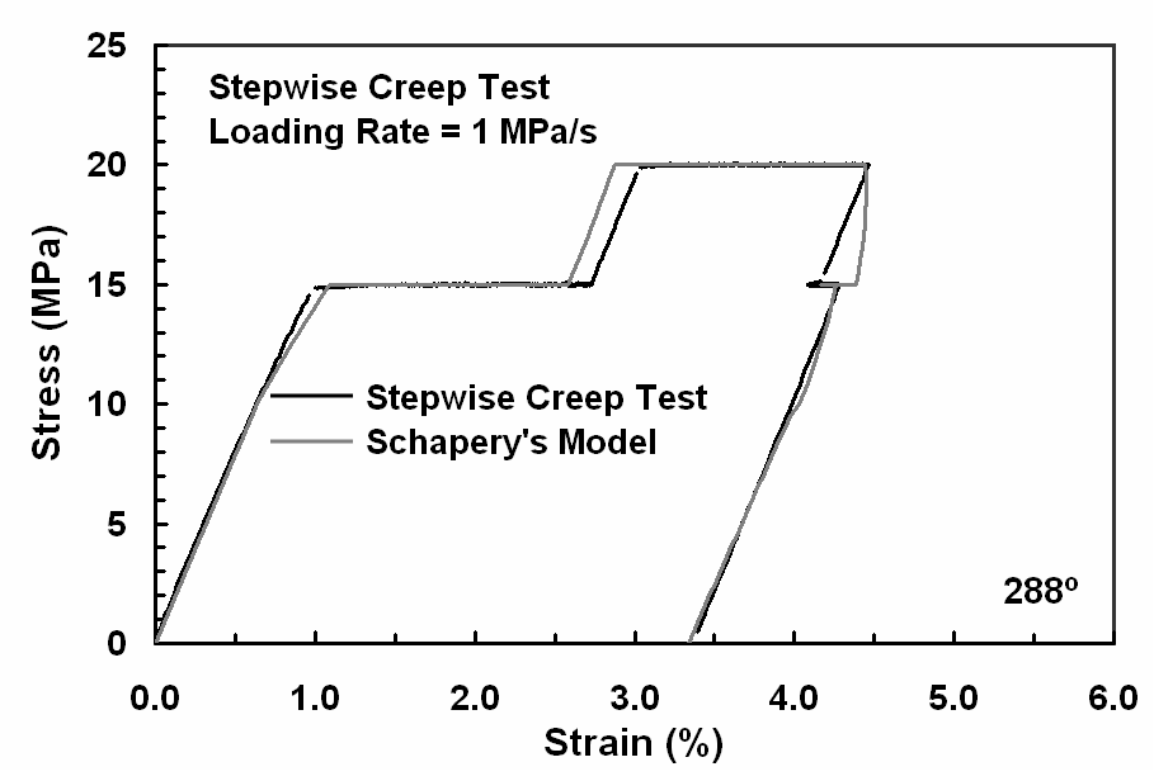

Figure 61: Stress-strain behavior of stepwise creep test, experimental results compared to viscoelastic model predictions

Figure 62 displays strain as a function of time for creep periods at 15 and 20 MPa. During both creep tests, the model predictions are similar to the experimental data. The model slightly under-predicts the creep strain value at 15 MPa but provides an accurate prediction of creep strain at 20 MPa. The effect of the stress profile input on the model's

predictive capabilities was evaluated. While the predictions shown in Figure 61 were made by inputting the stress profile actually implemented during testing, predictions using an instantaneous stress step input were also assessed. The dashed black line in Figure 62 represents the step input while the solid grey line represents the stress ramp up input. It is seen that the form of stress input has no effect on the model predictions.

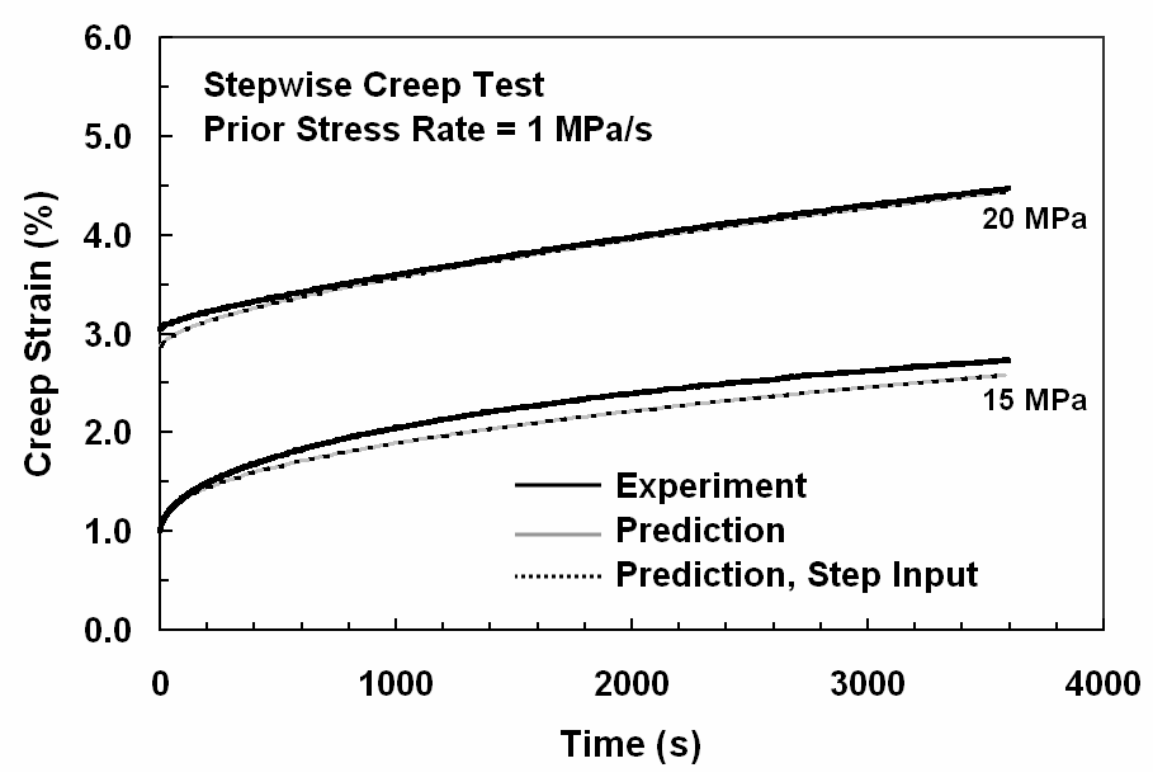

Figure 62: Creep behavior at 15 and 20 MPa on the loading path of the stepwise creep test, experimental results compared to viscoelastic model predictions

The model again performed well in predicting the strain as a function of time for the 15 MPa creep test during the unloading step (see Figure 63). It is extremely important to notice that not only does the model predict the negative creep behavior at the beginning of this creep period; it also predicts the creep strain rate reversal. The creep strain value

at the completion of this period was also accurate. A magnified view of the negative creep and creep rate reversal is shown in Figure 64. Although the model was not completely accurate quantitatively, qualitatively it was very powerful. The ability of the model to represent this aspect of the polymer behavior is apparent.

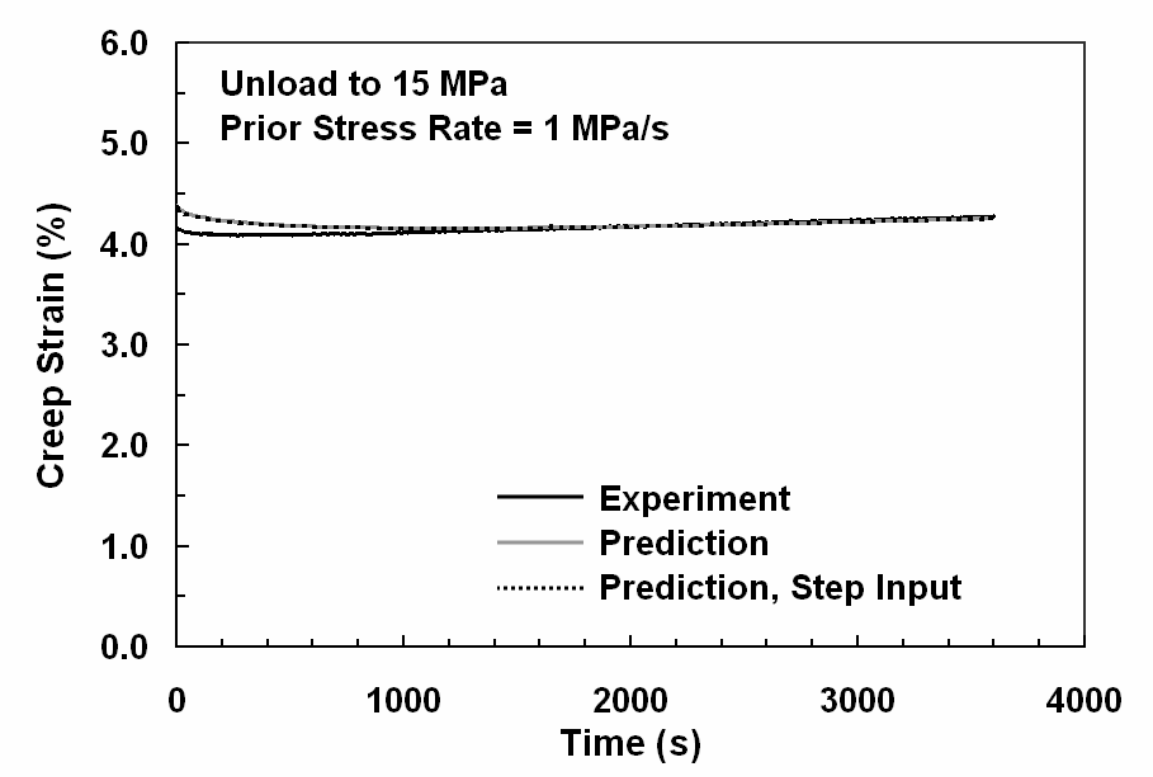

Figure 63: Creep behavior at 15 MPa on the unloading path of the stepwise creep test, experimental results compared to viscoelastic model predictions

Figure 64: Magnified view of creep behavior at 15 MPa on the unloading path of the stepwise creep test, experimental results compared to viscoelastic model predictions.

Finally, the predictions of recovery behavior (see Figure 65) were again unsuccessful. The model over predicts the amount of strain that was actually recovered

following the stepwise creep test. Similar model predictions were made of a stepwise creep test with loading rate magnitude of 0.01 MPa/s. These results are not presented as it has already been shown that the model cannot account for the effects of rate. The model predictions for the stepwise creep test conducted with the loading rate magnitude of 0.01 MPa/s were not accurate. Again, the model over-predicted the recovery strain.

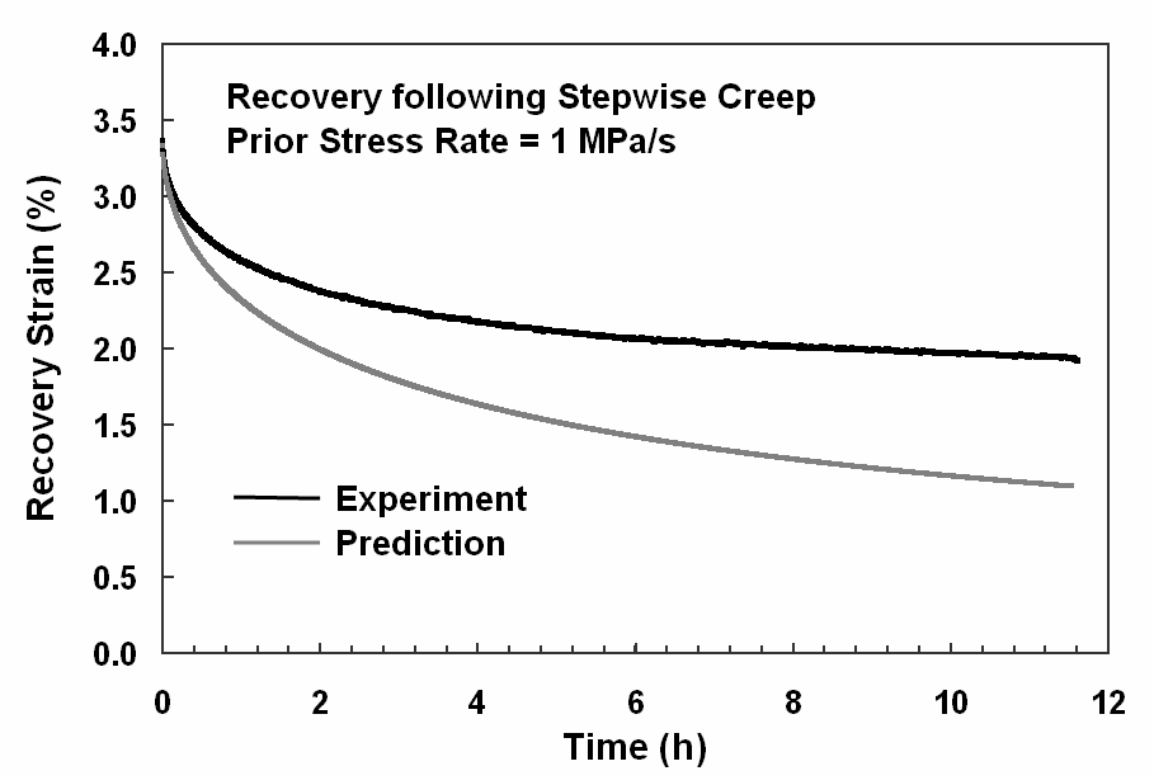

Figure 65: Recovery following stepwise creep with a prior stress rate magnitude of 1 MPa/s, experimental results compared to viscoelastic model predictions

Schapery's nonlinear viscoelastic model was capable of predicting creep behavior of PMR-15 neat resin at 288 ^{o}C with varying degrees of accuracy. The model was capable of accounting for prior loading history as demonstrated in the stepwise creep test. However, the model could not account for the effects of prior stress rate. One significant deficiency of the model was its inability to accurately predict the recovery behavior of

PMR-15 in all verification tests. This was likely due to the fact that the material did not exhibit full recovery in the linear range. This behavior introduced a permanent strain that is not accounted for in the model. Because this material does not achieve full recovery, even in the linear range, it is necessary to introduce permanent strain into the model formulation in order to accurately predict recovery behavior.

VI. Concluding Remarks

Conclusions

Results of the monotonic tensile tests revealed that the stress rate did not have a significant effect on the Young's modulus of PMR-15 at 288 ^{o}C. However, the failure strains were influenced by rate. As the stress rate increased by two orders of magnitude, the failure strain increased from 3.65 % to 6.13%. The results of the creep and recovery tests conducted on PMR-15 at 288^{o}C indicated that the creep response was dependent on the prior stress rate, with creep strain accumulation increasing with increasing prior stress rate. The magnitude of the percent change in strain recovered at zero stress also increased with increasing magnitude of prior loading rate. Observations made concerning the monotonic loading and unloading of the material revealed the effect of stress rate. The stress rate had a considerable effect on the stress-strain behavior, with curved unloading becoming pronounced at the slower stress rate.

The effect of prior loading history on the behavior of PMR-15 was studied by subjecting the material to a stepwise creep test. For the loading rate of 1 MPa/s, the amount of creep strain decreased as creep stress increased from 15 to 20 MPa. Negative creep followed by reversal to positive creep was observed in the creep test at 15 MPa conducted on the unloading path. The magnitude of the negative creep strain was smaller than that of the positive creep periods observed during loading. At the slower stress rate of 0.01 MPa/s, only positive creep was observed during each creep period. The third creep period imposed at 15 MPa during unloading produced the smallest creep strain.

Comparison of creep strains accumulated during a stepwise creep test to those accumulated during creep preceded by uninterrupted loading indicate that the prior stress history affects the creep behavior. Dependency on prior stress history was also evident in the recovery behavior following each of these test histories.

The material functions and constants in Schapery's model were determined for PMR-15 at 288 ^{o}C. Verification of the model was accomplished by comparing model predictions to results of various deformation experiments. Schapery's nonlinear viscoelastic model was capable of predicting the behavior of PMR-15 with varying degrees of accuracy. Predictions were most accurate when the stress rate was of the same order of magnitude of that used in the characterization tests. The predictions of monotonic loading and unloading behavior showed considerable hysteresis at higher stress levels. These results also produced over prediction of the maximum strain obtained during the loading period. Comparisons of model predictions to creep data revealed that the model qualitatively predicted the experimental data but did not accurately predict the creep strain. The model failed to provide an accurate quantitative prediction of the long term creep response. The model performed fairly well in predicting the behavior of PMR-15 during a stepwise creep test with creep periods of one hour. The model predicted negative creep and creep rate reversal in the creep test conducted during unloading. Finally, the model was unable to predict the recovery behavior of PMR-15. This was likely due to the large permanent strain measured even in the linear range of the material.

Recommendations

Future modeling efforts of the behavior of PMR-15 neat resin may involve enhancements of Schapery's Model or an alternative constitutive model. The inclusion of a permanent strain function into Schapery's model framework may provide a more realistic description of the material's recovery behavior and result in increased accuracy of the model predictions. Another model which shows great potential for describing polymeric behavior is the viscoplasticity theory based on overstress (VBO). This model is particularly attractive for modeling the deformation behavior of PMR-15 as it does not require the assignment of a linear range or a purely elastic region.

The deformation of a material is often dependent on external parameters such as temperature, prior aging, or exposure to various environments. The incorporation of additional variables of this nature into constitutive model formulations would greatly extend predictive capabilities. Furthermore, upon development of a predictive model that is fully capable of describing the behavior of the neat resin at hand, modeling efforts must be extended to represent the behavior of composite materials to be used in aerospace applications.

Bibliography

1. Aklonis, John J. and William J. MacKnight. *Introduction to Polymer Viscoelascticity.* 2nd edition. John Wiley and Sons, 1983.

2. Balconis, John, G. *Some Aspects of the Mechanical Response of BMI-5250-4 Neat Resin at 191 °C.* Air Force Institute of Technology, Wright-Patterson AFB OH, March 2006.

3. Brinson, Catherine L. and others. *Going to Extremes Meeting the Emerging Demand for Polymer Matrix Composites.* Washington DC, The National Academies Press, 2005.

4. Cytec Engineered Materials. "CYCOM 2237 Polyimide." http://www.cytec.com/business/EngineeredMaterials/Datasheets/CYCOM2237.pdf.

5. Daniel, Isaac M. and Ori Ishai. *Engineering Mechanics of Composite Materials.* Oxford University Press, 1994.

6. "DMBZ Polyimides Provide an Alternative to PMR-15 for High-Temperature Applications", NASA/Lewis Research Center, 2005.

7. Elahi, M. and Y.J. Weitsman. *On the Mechanical Response of P4 Chopped Glass/Urethane Resin Composite: Data and Model.* Contract DEAC05-96OR22464. Oak Ridge TN: Lockheed Martin Energy Research Corp, October 1999.

8. Findley, William N. and others. *Creep and Relaxation of Nonlinear Viscoelastic Materials.* North Holland Publishing Company, 1976.

9. Green, John A.S. and others. *New Materials for Next Generation Commercial Transports*. Washington DC, The National Academies Press, 1996.

10. Jerina, K.L., R.A. Schapery, R.W. Tung, and B.A Sanders. "Viscoelastic Characterization of a Random Fiber Composite Material Employing Micromechanics", *Short Fiber Reinforced Composite Materials, ASTM STP 772*, B.A. Sanders, Ed., American Society for Testing Materials, 1982, pp.225-250.

11. Khan, Fazeel. *The Deformation Behavior of Solid Polymers and Modeling with the Viscoplasticity Theory Based on Overstress.* PhD dissertation. Renesselaer Polytechnic Institute. Troy NY, 2002.

12. Krempl, Erhard and Christine Bordonaro. "A State Variable Model for High Strength Polymers." *Polymer Engineering and Science*, 35: 310-316 (February 1995).

13. Lou, Y.C and R.A Schapery. "Viscoelastic Characterization of a Nonlinear Fiber-Reinforced Plastic." *J. Composite Materials*, 5:208-234 (April 1971).

14. Lovell, P. A. and R.J. Young. *Introduction to Polymers* (2nd edition). Chapman and Hall Publishing, 1991.

15. Marais, C. and G. Villoutreix, "Analysis and Modeling of the Creep Behavior of the Thermostable PMR-15 Polyimide", *Journal of Applied Polymer Science*, 69: 1983-1991, 1998.

16. MTS Systems Corporation. *Model 793.00 System Software: UserInformation and Software Reference.* MTS Systems Corporation, 2001.

17. Odegard, G. and M. Kumosa, "Elastic-plastic and failure properties of a unidirectional carbon/PMR-15 composite at room and elevated temperatures," *Composite Science and Technology*, 60:2979-2988, 2000.

18. Peretz, D. and Weitsman Y.J. "Nonlinear Viscoelastic Characterization of FM-73 Adhesive," *Journal of Rheology*. 26: 245-261. John Wiley & Son, Inc, 1982.

19. Pipkin, A.C, and T.G. Rogers. "A Non-Linear Integral Representation for Viscoelastic Behavior", *J. Mech. Phys. Solids:* 16:59-72 (1968).

20. Polyimide Composites. Aeronautics Learning Laboratory for Science, Technology, and Research. NASA All Star Network, 2004. 6 July 2006. http://www.allstar.fiu.edu/AERO/polycomp.htm

21. Riande, Evaristo and others. *Polymer Viscoelasticity: Stress and Strain in Practice.* Marcel Dekker, Inc, 2000.

22. Ruggles-Wrenn, M.B. Class Notes, Introduction to Viscoelasticity and Viscoplasticity. Air Force Institute of Technology, Wright- Patterson AFB OH, May 2006.

23. Schapery, R.A. Nonlinear viscoelastic solids. *International Journal of Solids and Structures.* Vol. 37: 366 (2000).

24. Schapery, R.A. On the Characterization of Nonlinear Viscoelastic Materials. *Polymer Engineering and Science.* Vol. 9, No.4: 295-310 (July 1969).

25. Schinder, Aaron. Schapery's Nonlinear Viscoelastic Model Matlab Code. Air Force Institute of Technology, Wright- Patterson AFB OH, July 2006.

26. Smith, L.V. and Y.J. Weitsman. The Visco-Damage Mechanical Response of Swirl-Mat Composites. *International Journal of Fracture.* 97:301- 319 (1999).

27. Tjuji, Lewis C., Hugh L. McManus, Kenneth J. Bowels, "Mechanical Properties of Degraded PMR-15 Resin", *NASA/Lewis Research Center,* TM—1998-208487.

28. Ward, I.M, and J. Sweeney. *An Introduction to the Mechanical Properties of Solid Polymers.* John Wiley & Sons, Ltd, 2004.

29. Westberry, Candice, M. *Rate Dependence and Short-Term CreepBehavior of PMR-15 Neat Resin at 23 and 288 °C.* Air Force Institute of Technology, Wright-Patterson AFB OH, September 2005.

30. Xie, W., W.P. Pan, K.C. Chuang,, "Thermal Degradation Study of Polymerization of Monomeric Reactants (PMR) Polyimides", *Journal of Thermal Analysis and Calorimetry*, 74: 477-485, 2001.

REPORT DOCUMENTATION PAGE

Form Approved
OMB No. 074-0188

1. REPORT DATE *(DD-MM-YYYY)*	**2. REPORT TYPE**	**3. DATES COVERED** *(From – To)*
14-09-2006	**Master's Thesis**	Sep 2005 – Sep 2006

4. TITLE AND SUBTITLE

Some Aspects of the Mechanical Response of PMR-15 Neat Resin at 288 °C; Experiment and Modeling

5a. CONTRACT NUMBER

5b. GRANT NUMBER

5c. PROGRAM ELEMENT NUMBER

6. AUTHOR(S)

Falcone, Christina, M., 2nd Lt, USAF

5d. PROJECT NUMBER
2005-158, 2005-025

5e. TASK NUMBER

5f. WORK UNIT NUMBER

7. PERFORMING ORGANIZATION NAMES(S) AND ADDRESS(S)
Air Force Institute of Technology
Graduate School of Engineering and Management (AFIT/EN)
2950 Hobson Way
WPAFB OH 45433-7765

8. PERFORMING ORGANIZATION REPORT NUMBER

AFIT/GAE/ENY/06-S03

9. SPONSORING/MONITORING AGENCY NAME(S) AND ADDRESS(ES)

AFOSR/NL
Attn: Dr. Charles Y-C Lee
875 Randolph St.
Arlington, VA 22203-1954 Comm No: (703)696-7799

AFRL/MLBCM
Attn: Greg Schoeppner
2941 P Street
WPAFB, OH 45433, (937)255-9072

10. SPONSOR/MONITOR'S ACRONYM(S)

11. SPONSOR/MONITOR'S REPORT NUMBER(S)

12. DISTRIBUTION/AVAILABILITY STATEMENT
APPROVED FOR PUBLIC RELEASE; DISTRIBUTION UNLIMITED.

13. SUPPLEMENTARY NOTES

14. ABSTRACT

The mechanical response of PMR-15 neat resin was investigated at 288°C. Monotonic loading/unloading tests performed at several constant stress rates revealed considerable rate dependence, especially on the unloading path. Effect of prior stress rate on creep behavior was evaluated in creep tests preceded by uninterrupted loading to a target stress. Creep response was dependent on the prior stress rate. Effect of loading history was studied in stepwise creep tests, where specimens were subjected to a constant stress rate loading followed by unloading to zero stress with intermittent creep periods during both loading and unloading. Comparison of creep strains accumulated during a stepwise creep test to those accumulated during creep preceded by uninterrupted loading indicate that the prior stress history affects the creep behavior.

A nonlinear viscoelastic model (Schapery's formulation) was characterized using creep and recovery tests. The model was verified by comparing the predictions with experimental results obtained in monotonic loading/unloading, single-step, and multi-step creep tests. The model qualitatively predicted creep response to single- and multi-step creep tests, including negative creep and creep rate reversal during unloading. However, predictions were not quantitatively accurate. The model was unable to accurately predict the recovery behavior and could not account for rate effects.

15. SUBJECT TERMS
polymer, PMR-15, creep, recovery, prior stress rate, prior loading history, nonlinear viscoelastic theory

16. SECURITY CLASSIFICATION OF:			**17. LIMITATION OF ABSTRACT**	**18. NUMBER OF PAGES**	**19a. NAME OF RESPONSIBLE PERSON**
REPORT	**ABSTRACT**	**c. THIS PAGE**			Dr. Marina B. Ruggles-Wrenn
U	**U**	**U**	**UU**	136	**19b. TELEPHONE NUMBER** *(Include area code)* 785-3636, ext 4641; email: @afit.edu

Standard Form 298 (Rev: 898)
Prescribed by ANSI Std. Z39-18